FE-2028-15

KINETICS AND MECHANISM OF DESULFURIZATION AND DENITROGENATION OF COAL-DERIVED LIQUIDS

Thirteenth Quarterly Report for June 21—September 20, 1978

By
Bruce C. Gates
James R. Katzer
Jon H. Olson
Harold Kwart
Alvin B. Stiles

March 16, 1979
(Date Published)

Work Performed Under Contract No. EX-76-C-01-2028

Departments of Chemical Engineering & Chemistry
University of Delaware
Newark, Delaware

U. S. DEPARTMENT OF ENERGY

DISCLAIMER

NOTICE

FE-2028-15
Distribution Category UC-90d

KINETICS AND MECHANISM OF DESULFURIZATION AND DENITROGENATION OF COAL-DERIVED LIQUIDS

Thirteenth Quarterly Report for Period

June 21, 1978 to September 20, 1978

Prepared by:

Bruce C. Gates, James R. Katzer
Jon H. Olson, Harold Kwart, and Alvin B. Stiles

Departments of Chemical Engineering and Chemistry
University of Delaware
Newark, Delaware 19711

Date Published

March 16, 1979

Prepared for

Fossil Energy
Department of Energy
Washington, D.C.

Under Contract No. E(49-18)-2028

TABLE OF CONTENTS

	Page
I. ABSTRACT	1
II. OBJECTIVES AND SCOPE	2
III. SUMMARY OF PROGRESS TO DATE	4
Time Plan and Milestone Chart	10
Cumulative Expenditures	12
IV. DETAILED DESCRIPTION OF TECHNICAL PROGRESS	13
A. Catalytic Hydrodesulfurization (HDS)	13
1. Experimental	13
2. Analytical	15
3. Results and Discussion	15
i. Catalyst stability	16
ii. Hydrogen dependence of DBT HDS from differential rate data	18
B. Biphenyl Hydrogenation	27
C. Catalytic Hydrodenitrogenation	31
a. Singe component studies	31
Hydrogenation of naphthalene	36
Hydrodenitrogenation of indole	40
Reaction network for HDN of indole	44
Hydrodesulfurization of dibenzothiophene	44
Summary	52
b. Binary interactions	54
Hydrogenation of naphthalene in the presence of quinoline	54
Hydrodenitrogenation of Quinoline in the presence of naphthalene	73
HDN of indole in the presence of quinoline	73
HDN of quinoline in the presence of indole	80
HDS of DBT in the presence of quinoline	80
Summary	90
D. Adsorption of Quinoline on Catalyst Under Reaction Conditions	92
Procedure	92
Reaction Network Modeling	95
Quinoline Network	95
Quinoline-Indole Network	97
Types of lumps in literature	100
APPENDIX	101
V. PUBLICATIONS	126
VI. PERSONNEL	127

LIST OF FIGURES

		Page
Figure 1	Reproducibility of initial conversion from three separate experimental runs. DBT Concentration: 1.24 mole percent; catalyst loading; 65 mg HDS 16A; Temperature: 300°C; Weight hourly space velocity: 13 gmol/h gcat.	19
Figure 2	Long-term stabilization of catalytic activity at constant temperature, pressure and concentration. DBT Concentrations: 1.24 mole %; Temperature: 300°C; Pressure; 1400 psig; Weight hourly space velocity: 13 gmol/h gm cat	20
Figure 3	Catalytic activity as a function of time on stream with and without H_2S in the feed. Differential rates measured at standard conditions of: 1.24 mole % DBT; 300°C, and 1400 psig total pressure	21
Figure 4	Effect of hydrogen pressure on DBT hydrodesulfurization rate. Curve is hydrogen saturation kinetic model fit to data	22
Figure 5	Effect of hydrogen pressure on DBT hydrodesulfurization rate at 275°C. Curves represent fit and confidence limits of fit from hydrogen saturation kinetic model	23
Figure 6	Effect of hydrogen pressure on DBT hydrodesulfurization rate at 300°C. Curves represent fit and confidence limits of fit from hydrogen saturation kinetic model	24
Figure 7	Effect of hydrogen pressure on DBT hydrodesulfurization rate at 325°C. Curves represent fit and confidence limits of fit from hydrogen saturation kinetic model	25
Figure 8	Differential conversion plot.	28
Figure 9	Effect of CS_2 concentrate	29
Figure 10	Effect of H_2 Sat. Press.	30
Figure 11	Reaction network for hydrodenitrogenation of quinoline.	34
Figure 12	HDN of 0.5 wt % Q: □ = quinoline + 1,2,3,4-tetrahydroquinoline; x = total nitrogen.	35
Figure 13	Hydrogenation of 5 wt % naphthalene	38
Figure 14	Reaction network for hydrogenation of naphthalene . . .	39

		Page
Figure 15	Hydrodenitrogenation of indole	42
Figure 16	Hydrodenitrogenation of indole	43
Figure 17	Reaction network for hydrodenitrogenation of indole.	45
Figure 18	HDN of indole.	46
Figure 19	HDS OF dibenzothiophene.	48
Figure 20	HDS of DBT	49
Figure 21	HDS of DBT	50
Figure 22	HDS of DBT (0.7 wt %).	51
Figure 23	Reaction network for HDS of DBT.	53
Figure 24	Naphthalene hydrogenation (with 0.2 wt % quinoline).	55
Figure 25	Hydrogonation of naphthalene (with 0.5 wt % quinoline)	56
Figure 26	Hydrogenation of naphthalene (with 2.0 wt % quinoline)	57
Figure 27	Naphthalene hydrogenation (with 0.2 wt % quinoline)	58
Figure 28	Naphthalene hydrogenation (with 0.2 wt % quinoline)	59
Figure 29	Naphthalene hydrogenation (with 0.5 wt % quinoline)	60
Figure 30	Naphthalene hydrogenation (with 0.5 wt % quinoline)	61
Figure 31	Inhibition of naphthalene hydrogenation by quinoline, Region I.	64
Figure 32	Inhibition of naphthalene hydrogenation by quinoline, Region I.	65
Figure 33	Inhibition of naphthalene hydrogenation by quinoline, Region I	66

		Page
Figure 34	Inhibition of naphthalene hydrogenation by quinoline, Region II	67
Figure 35	Inhibition of naphthalene hydrogenation by q quinoline, Region II	68
Figure 36	Inhibition of naphthalene hydrogenation by quinoline, Region II	69
Figure 37	Quinoline HDN at standard conditions	70
Figure 38	Quinoline HDN at standard conditions	71
Figure 39	Quinoline HDN at standard conditions	72
Figure 40	Effect of quinoline concentration on HDN of quinoline	74
Figure 41	Effect of quinoline concentration on HDN of quinoline	75
Figure 42	Effect of quinoline concentration on HDN of quinoline	76
Figure 43	Effect of quinoline concentration on HDN of quinoline	77
Figure 44	Effect of quinoline concentration on HDN of quinoline	78
Figure 45	Effect of quinoline concentration on HDN of quinoline	79
Figure 46	HDS of 0.7 wt % dibenzothiophene (with 0.5 wt % quinoline).=	81
Figure 47	HDS of 0.7 wt % DBT (with 2 wt % quinoline).	82
Figure 48	HDS of 0.7 wt % DBT (with 2 wt % quinoline).	83
Figure 49	Effect of quinoline on HDS of DBT (0.7 wt %) first order k for disappearance of dibenzothiophene.	85
Figure 50	Effect of quinoline on HDS of DBT (0.7 wt %) first order k for disappearance of dibenzothiophene.	86
Figure 51	Effect of quinoline on HDS of DBT (0.7 wt %) first order k for disappearance of dibenzothiophene.	87

Page

Figure 52 Effect of quinoline on HDS of DBT (0.7 wt %) first order k for disappearance of dibenzothiophene 88

Figure 53 Effect of quinoline on HDS of DBT (0.7 wt %) first order k for disappearance of dibenzothiophene 89

Figure 54 Effect of quinoline on HDS of DBT (0.7 wt %): $k_{(DBT \quad Biphenyl)}$ estimated from data points in Region I 91

Figure 55 HDN of quinoline (.05 wt %) Total nitrogen before and after catalyst injection. 93

LIST OF TABLES

Page

Table 1 Standard Reaction Conditions for Interaction Studies. 32

ABSTRACT

Studies of competing hydroprocessing reactions catalyzed by Ni-Mo/γ-Al_2O_3 and involving quinoline, indole, dibenzothiophene, and naphthalene in n-hexadecane show that marked interactions exist. The naphthalene hydrogenation rate is markedly reduced by the presence of quinoline; whereas the reactivity of quinoline is virtually unchanged by the presence of naphthalene. Similarly the rate of hydrodenitrogenation of indole, a non-basic nitrogen-containing compound, is strongly reduced by the presence of quinoline, whereas the rate of hydrodenitrogenation of quinoline, a basic nitrogen-containing compound, is unaffected by the presence of indole. The hydrogenation reactions in the dibenzothiophene reaction network are inhibited as severely as indicated by the reduction in their pseudo first-order-rate constants as are the hydrogenation reactions for naphthalene. Thus the hydrogenation rate is reduced 30-fold by increasing the initial quinoline concentration from 0.0 to 0.5 wt % in naphthalene hydrogenation and in dibenzothiophene hydrodesulfurization. The rate of direct sulfur removal is reduced by only 3-fold by increasing the quinoline concentration from 0.0 to 0.5 wt %. These results clearly show that the rate expressions for the hydrotreating reactions are of the form

$$\text{Rate} = \frac{k_i\, C_i\, P_{H_2}^{n}}{[1+K_j C_j + K_Q C_Q]\, F(H_2)}$$

II. OBJECTIVES AND SCOPE

The major objectives of this research are as follows:

i) to develop high-pressure liquid-phase microreactors for operation in pulse and steady-state modes to allow determination of quantitative reaction kinetics and catalytic activities in experiments with small quantities of reactants and catalyst.

ii) To determine reaction networks, reaction kinetics, and relative reactivities for catalytic hydrodesulfurization of multi-ring aromatic sulfur-containing compounds found in coal-derived liquids.

iii) To determine reaction networks, reaction kinetics, and relative reactivities for catalytic hydrodenitrogenation of multi-ring aromatic nitrogen-containing compounds found in coal-derived liquids.

iv) To obtain quantitative data characterizing the chemical and physical properties of aged hydroprocessing catalysts used in coal liquefaction processes and to establish the mechanisms of deactivation of these hydroprocessing catalysts.

v) To develop reaction engineering models for predicting the behavior of coal-to-oil processing and of catalytic hydroprocessing of coal-derived liquids and to suggest methods for improved operation of hydrodesulfurization and hydrodenitrogenation processes.

vi) In summary, to recommend improvements in processes for the catalytic hydroprocessing of coal-derived liquids.

SCOPE

A unique high-pressure, liquid-phase microreactor is being developed for pulse (transient) and steady-state modes of operation for kinetic measurements to achieve objectives ii) through iv). The relative reactivities of the important types of multi-ring aromatic compounds containing sulfur and nitrogen are being measured under industrially important conditions (300-450°C and 500-4000 psi). The reaction networks and kinetics of several of the least-reactive multi-ring aromatic sulfur-containing and nitrogen-containing compounds commonly present in coal-derived liquids will be determined. Catalyst deactivation is an important aspect of the commercial scale upgrading of coal-derived liquids. Accordingly, the chemical and physical properties of commercially aged coal-processing catalysts are being determined to provide an understanding of catalyst deactivation; these efforts can lead to improved catalysts or procedures to minimize the problem. To make the results of this and related research most useful to DOE, reaction engineering models of coal-to-coal processing in trickle-bed and slurry-bed catalytic reactors including deactivation will be developed to predict conditions for optimum operation of these processes. Based on the integrated result of all of the above work, recommendations will be made to DOE for improved catalytic hydrodesulfurization and hydrodenitrogenation processing.

III. SUMMARY OF PROGRESS TO DATE

This summary is organized to parallel the task statements of the contract. A milestone chart is provided at the end of this section.

Microreactor Development

Three continuous-flow, liquid-phase, high-pressure microreactors have been built and operated under this contract. The work in this report confirms the success of these microreactors; the data from the batch autoclave runs are effectively identical to data from the flow microreactors. This task has been completed.

Catalytic Hydrodesulfurization

The hydrodesulfurization of dibenzothiophene (DBT) has been examined with a high-pressure microreactor and in batch, stirred-autoclave experiments. The range of data show that the reaction network is slightly more complex than the direct reduction of dibenzothiophene (DBT) to hydrocarbon products; the network is the following at 300°C and 100 atm where the rate constants for units of m^3/kg of catalyst·s:

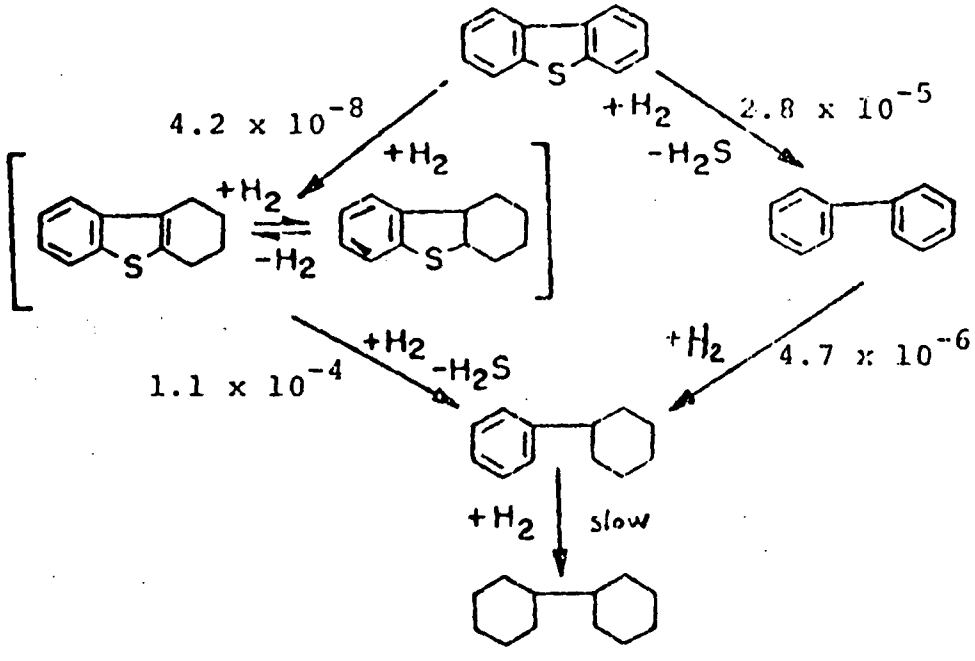

The relative rates of hydrodesulfurization of a variety of the important sulfur-containing compounds in coal-derived liquids have been determined. The compounds include methyl-substituted dibenzothiophenes, which evidently are among the least reactive compounds in hydrodesulfurization. The relative rate constants for the various reactants are the following: dibenzothiophene (DBT), 1; 4-MeDBT, 0.16; 4,6-diMeDBT, 0.10; 3,7-diMeDBT, 1.7; and 2,8-diMeDBT, 2.6. These results are largely explained by steric and inductive effects. Groups located β to the sulfur

atom restrict its interaction with a surface anion vacancy and lower the reactivity. Inductive effects explain the higher reactivities of the compounds having methyl substituents where they exert no steric influence. The reactivities of the compounds have been determined with individual sulfur-containing compounds and with pairs of these compounds. The reactivities of these compounds are influenced by competitive adsorption determined by the previously mentioned steric and inductive effects.

More detailed study of the hydrodesulfurization of 4,6-dimethyl-dibenzothiophene, which is the least reactive sulfur-containing compound found so far, shows that the reaction network is similar to that of dibenzothiophene but that hydrogenation of the aromatic ring is more pronounced than for dibenzothiophene.

Results from batch-autoclave reactor studies on the hydrodesulfurization of multi-ring sulfur-compounds (with sulfided Co-Mo/γ-Al_2O_3, 300°C and 70 ± 2 atm of H_2) show that the reactivity decreases from 1-ring to 3-ring compounds and then it increases for the 4-ring compound. Thus the three-ring sulfur-compound, dibenzothiophene and its methyl derivatives are the least reactive compounds studied so far. The first-order rate constants for the hydrodesulfurization of these compounds are given below:

Reactant	Pseudo first-order rate Constant, cm^3/g cat h
thiophene	5000
benzothiophene	2900
dibenzothiophene	200
benzonaphthothiophene	600
7,8,9,10-tetrahydrobenzo-naphthothiophene	280

Three different catalysts, namely Co-Mo/γ-Al_2O_3, Ni-Mo/ -Al_2O_3 and Ni-W/Al_2O_3 have been tested for the hydrodesulfurization of dibenzothiophene. The activities of these catalysts have been found to decrease in the order: Ni-Mo > Ni-W ≥ Co-Mo.

A new "three-point" adsorption of thiophenic compounds has been suggested to be important in the surface-catalyzed hydrodesulfurization mechanism. The new mechanism accounts for the observed substituent effects and the effects of the number of rings in the reactant; it also accounts for results of H-D exchange studies reported in the literature.

Catalytic Hydrodenitrogenation

The hydrodenitrogenation of quinoline has been studied to yield a nearly complete identification of the reaction network and partial identification of the rate parameters in this network. The network is as follows:

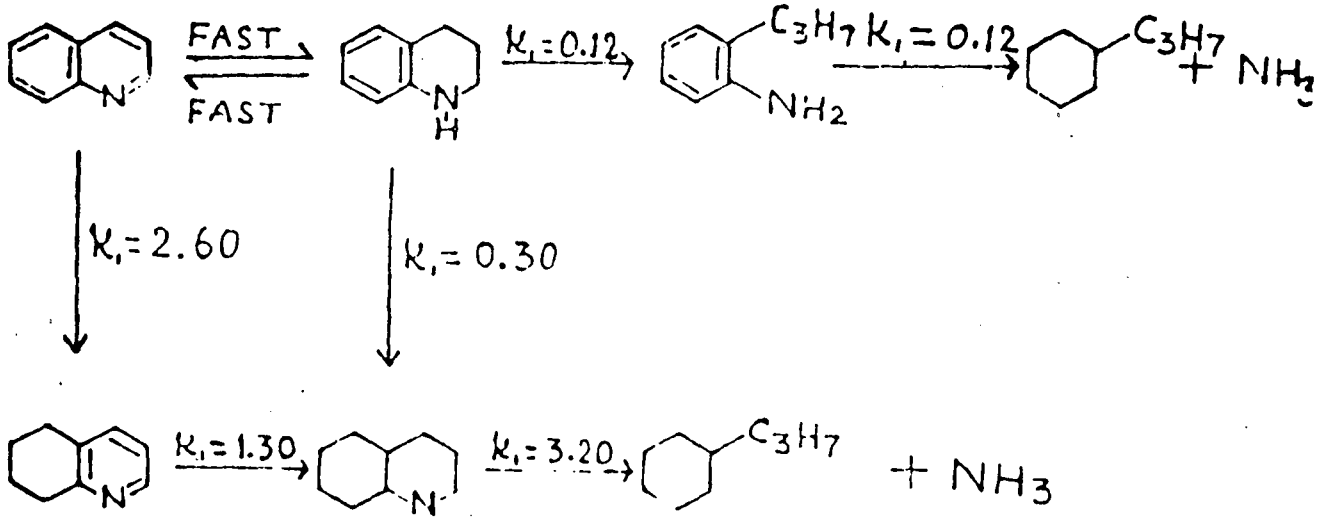

This network shows that usually both the benzene and pyridine rings are saturated before the C-N bond in the (now) piperidine ring is broken. Thus, the hydrodenitrogenation of quinoline requires a large consumption of hydrogen before the nitrogen atom is removed from the hydrocarbon structure. The lack of selectivity encountered in hydrodenitrogenation stands in sharp contrast to the high selectivity in hydrodesulfurization.

The total rate of hydrodenitrogenation shows a maximum with respect to hydrogen partial pressure. This is because the pseudo first-order rate constants for the C-N bond scission reactions are reduced by increasing hydrogen pressure, the rate constants for the hydrogenation reactions, which increase with hydrogen pressure at lower hydrogen pressures, approach a maximum with increasing hydrogen pressure at the high hydrogen pressures, and because high hydrogen pressure shifts the quinoline $\rightleftarrows$ 1,2,3,4-tetrahydroquinoline strongly to 1,2,3,4-tetrahydroquinoline which is not as reactive as quinoline for further reaction.

In the hydrodenitrogenation of acridine, a large amount of hydrogenation precedes nitrogen removal also, and the carbon-nitrogen bond breaking reactions are relatively slow. In the presence of Co-Mo/γ-Al_2O_3, heteroaromatic ring hydrogenation is favored, and with Ni-Mo/γ-Al_2O_3, aromatic ring hydrogenation is favored. For both acridine and quinoline, little effect of replacing Co with Ni in the catalyst could be detected in the nitrogen removal reactions, although Ni-Mo/γ-Al_2O_3 is roughly twice as active for the hydrogenation reactions as Co-Mo/γ-Al_2O_3.

The hydrodenitrogenation of carbazole has been examined under conditions similar to those used for acridine. Both carbazole disappearance and total nitrogen removal can be represented as first-order reactions. Tetrahydrocarbazole is the major intermediate compound present in the product. Both cis-hexahydrocarbazole and octahydrocarbazole are minor reaction products. Reactivity of carbazole is slightly less than that of quinoline, and acridine is the least reactive.

Experiments have been carried out to characterize hydrodenitrogenation of the substituted quinolines 2,6-, 2,7- and 2,8-dimethylquinoline. The conditions used were similar to those used for quinoline hydrodenitrogenation, and reaction products identified were analogous to those observed in the quinoline reaction network. The reactivity of these compounds to hydrodenitrogenation is comparable to that of quinoline to hydrodenitrogenation.

The reaction network for the hydrodenitrogenation of acridine (in White Oil) catalyzed by Ni-Mo/ -Al_2O_3 catalyst is as given below:

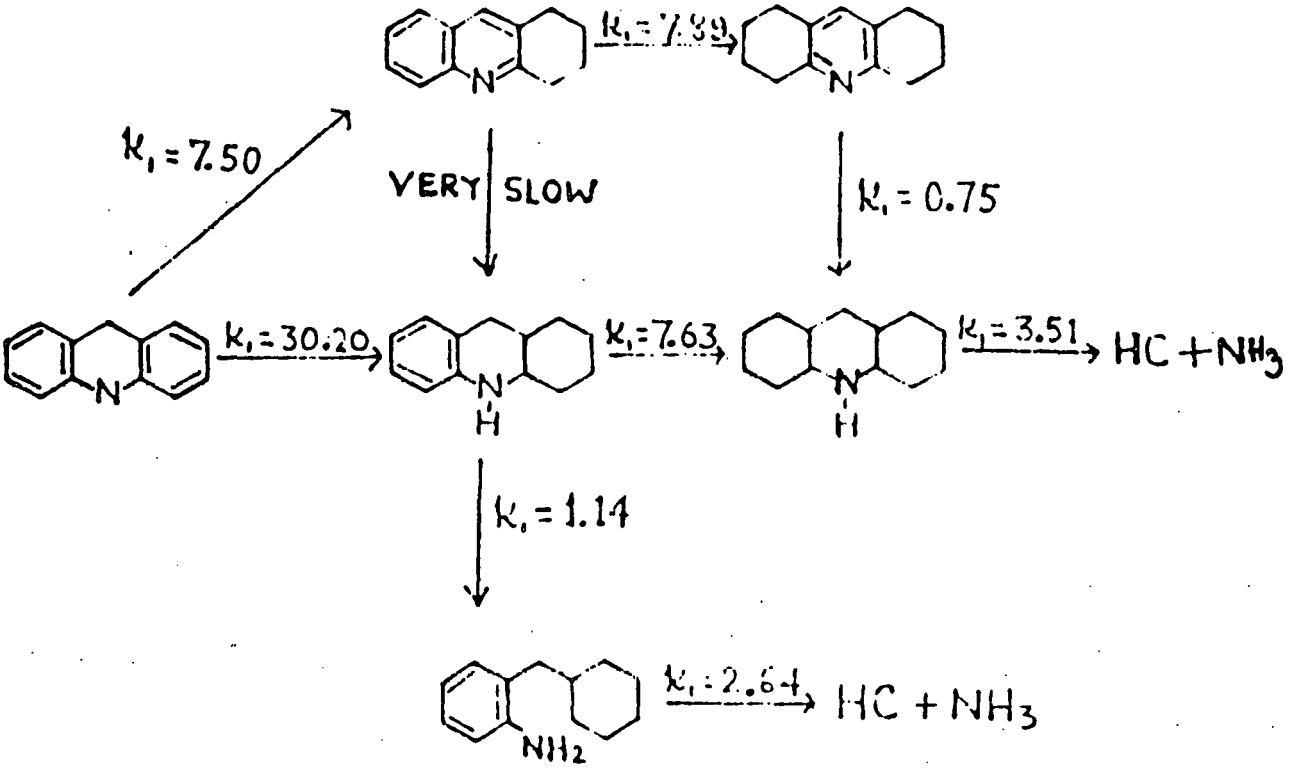

The pseudo first-order rate constants for 367°C and 136 atm are given associated with the reactions on the figure.

The pseudo first-order rate constants for hydrodenitrogenation (total nitrogen removal) of multi-ring nitrogen-containing aromatic compounds containing up to five rings at 367°C and 136 atm catalyzed by Ni-Mo/γ-Al_2O_3 fall in the following order:

Reactant	Pseudo first-order rate constant for total nitrogen removal, min^{-1}
Dibenz[c,h]acridine	3.79
Quinoline	2.52
Carbazole	2.43
Acridine	1.62
Benz[c]acridine	1.54
Benz[a]acridine	1.08

Studies of competing hydroprocessing reactions catalyzed by Ni-Mo/γ-Al_2O_3 and involving quinoline, indole, dibenzothiophene, and naphthalene in n-hexadecane show that marked interactions exist. The naphthalene hydrogenation rate is markedly reduced by the presence of quinoline; whereas the reactivity of quinoline is virtually unchanged by the presence of naphthalene. Similarly the rate of hydrodenitrogenation of indole, a non-basic nitrogen-containing compound, is strongly reduced by the presence of quinoline, whereas the rate of hydrodenitrogenation of quinoline, a basic nitrogen-containing compound, is unaffected by the presence of indole. The hydrogenation reactions in the dibenzothiophene reaction network are inhibited as severely as indicated by the reduction in their pseudo first-order rate constants as are the hydrogenation reactions for naphthalene. Thus the hydrogenation rate is reduced 30-fold by increasing the initial quinoline concentration from 0.0 to 0.5 wt % in naphthalene hydrogenation and in dibenzothiophene hydrodesulfurization. The rate of direct sulfur removal is reduced by only 3-fold by increasing the quinoline concentration from 0.0 to 0.5 wt %. These results clearly show that the rate expressions for the hydrotreating reactions are of the form

$$\text{Rate} = \frac{k_i C_i P_{H_2}^n}{[1+K_j C_j K_Q C_Q] F(H_2)}$$

Catalyst Deactivation

A variety of physical techniques have been used to identify the aging process for catalysts used in the synthetic liquid fuel processes. Catalyst samples from three processes have been examined: a proprietary fixed-bed process, Synthoil, and H-Coal^R. The spent fixed-bed catalysts show the formation of an external crust which appears to be formed by columnar grain growth combined with the deposition of coal mineral matter, particularly clays and rutile. This external crust is absent from the H-Coal^R catalyst. The interior of the catalyst is altered by several

processes: coking, reactive deposition of mineral matter, passive deposition of mineral matter, and crack enhancement. These four processes are found in catalysts from all three processes. Coking fills the micropore volume of the catalyst. Reactive deposition of mineral matter penetrates about 200 μm from the outer surface into the interior of the catalyst. The concentration profile is approximately exponentially decreasing from the exterior surface. Passive cementing occurs within 50 μm of the surface unless the irregular concentration profiles. Finally, grain growth can occur inside the catalyst near the surface and tends to increase these cracks. When the surface cracks become a significant portion of the pore volume, passive deposition can penetrate further into the interior of the catalyst.

The activity of aged catalyst from the H-Coal^R process has been measured in batch experiments with dibenzothiophene and with quinoline. The activity was reduced 20-fold for hydrodesulfurization of dibenzothiophene and five-fold for hydrodenitrogenation of quinoline. Burning off of carbonaceous deposits increased the activity of the aged catalyst only three-fold for dibenzothiophene hydrodesulfurization, which implies that irreversibly deposited inorganic matter was responsible for most of the loss of catalytic activity.

Microreactor Engineering

The use of moments as a tool in interpreting pulse data from microreactors has been extended to fairly complex reaction networks. This work is now complete. The complex data from quinoline and acridine reactions have been reduced to rate parameters by extension of nonlinear regression analysis. Reaction engineering concerned with coal hydroprocessing is now underway.

TIME PLAN* AND MILESTONE CHART**

Year 0	1	2	3
ACCOMPLISHMENT			
A. APPARATUS CONSTRUCTION			
1st High Pressure Microreactor Completed	month 6 100%		
2nd High-Pressure Microreactor Completed	month 10		
Batch Reactors Completed	month 4		
B. MICROREACTOR STUDIES OF HDS & HDN			
Definition of reaction procedures and operating conditions	month 8		
Choice of HDN Catalyst	100% month 8		
Reaction Studies For:			
Benzothiophene	month 6 month 12	Started 90% month 18	100%
Quinoline			100%
Dibenzothiophene	month 12		95%
Carbazole	10%	50%	100%
Naphthobenzothiophene	Synthesis Underway	month 18 month 24	Started 95%
Acridine		85% month 24 month 28	100% month 30
Higher molecular weight and methyl-substituted nitrogen and sulfur compounds	Synthesis Underway month 12 75%	month 28 month 30	100% 100%
Reaction Kinetics Reaction Networks and Inhibitor Studies of Least Reactive Sulfur and Nitrogen Compounds		75% month 18 month 24 month 28	85% month 30 90%
HDS-HDN: Simultaneously, Effect of Inhibitors	month 16	Started 20%	50% 60% month 36

TIME PLAN* AND MILESTONE CHART** (Continued)

Year 0	1	2	3
C. CATALYST DEACTIVATION			
SYNTHOIL CATALYST:			
Physical Properties	month 6 100%		
Chemical Properties	month 6	month 16 75%	80%
Other Deactivated Catalysts	90% month 10	month 24	80%
Catalyst Deactivation Studies	50%	month 14 70%	100% month 30
D. REACTION ENGINEERING			
Reactor Models for Pulse and Flow Microreactors	75%	month 14 90%	95% 100%
Process Reaction Engineering	5%	month 14 15%	30% 70% month 36

*Time Plan and Milestone Chart as Presented in Proposal.

**Hatching indicates that activity indicated is under active investigation; number in hatch region indicates the percentage completed; crosshatching indicates that the task has been completed.

CUMULATIVE EXPENDITURES*

Quarter	Personnel	Travel	Supplies & Expenses	Occupancy & Maintenance	Equipment	Information Processing	Transfers (Overhead)
First	$ 5,807	$ 28	$ 4,674	$ 6,110	$ 610	$ --	$ --
Second	20,740	528	10,007	9,208	17,978	--	10,202
Third	37,396	1,152	19,582	10,108	30,704	--	20,035
Fourth	53,418	1,152	25,735	10,634	34,930	97	38,710
Fifth	91,593	1,521	37,291	13,755	50,614	154	75,839
Sixth	112,666	2,458	42,341	13,920	54,013	375	93,287
Seventh	132,669	3,140	51.589	14,396	54,013	1,180	113,830
Eighth	146,146	3,814	56,488	14,600	52.295	1,868	123,576
Ninth	167,884	5,119	54,778	16,325	54,977	2,044	117,681
Tenth	192,658	6,113	70,579	18,010	54,977	2,248	134,895
Eleventh	224,941	6,113	76,733	19,635	54,977	2,369	161,208
Twelfth	261,759	7,349	95,041	24,159	57,778	2,454	186,267
Thirteenth							
Fourteenth							

IV. DETAILED DESCRIPTION OF TECHNICAL PROGRESS

A. Catalytic Hydrodesulfurization (HDS)

Third High-Pressure Flow Microreactor - Dibenzothiophene HDS Kinetics

1. Experimental

With the objective of obtaining satisfactory rate data for dibenzothiophene (DBT) hydrodesulfurization (HDS), experimental conditions have been refined to permit continuous operation of the flow reactor with varying temperature, pressure and concentration without irreversible loss of catalyst activity. These refinements include (1) increased concentration of dibenzothiophene (DBT), 2) increased catalyst loading, and 3) addition of H_2S to reaction mixture. The standard experimental conditions for rate measurements are:

- Catalyst: HDS 16A; mass: 40 mg; particle size, 149-178 μm
- DBT Concentration: 1.24 mole % DBT in n-hexadecane (before adding H_2 and H_2S
- Hydrogen Pressure: 1400 psig
- H_2S Concentration: 0.73 mole % in n-hexadecane
- Temperature: 300°C
- Total Reactor Pressure: 2550 psig.

This standard set of conditions serve as a reference point during the course of one experimental run to verify constant catalyst activity. At the standard conditions flow rate was varied to determine range of conversions corresponding to a differential reactor model.

Operating in the differential conversion regime, rates of reaction were measured for a range of hydrogen saturation pressures at each of three temperatures. DBT and H_2S concentrations were held constant. The temperature and hydrogen pressure range examined were 275, 300 and 325°C, and 35 to 157 atm. The temperature range was selected to agree with previous work at 300°C. Higher or lower temperatures were not possible without changing the catalyst loading, i.e., starting a new experimental run. The hydrogen pressure was restricted to the available gas cylinder pressure. Continuation of this work will measure rates for various reactant and product concentrations.

Addition of H_2S to the reaction mixture was accomplished by pressurizing the saturation vessel to a calculated pressure with an H_2S in H_2 gas mixture prior to bringing the total pressure to the desired valve with pure hydrogen. Calculation of the desired pressure of the H_2S/H_2 gas mixture was based on solubility data reported by Tremper and Prausnitz (1976) for the H_2S-hexadecane systems. Reported as a Henry's constant good at infinite dilution, extrapolation to high total pressures was made using the Krickersky-Kasarnovsky equation (see Prausnitz (1969), p. 356) for Henry's constant, and the Lee-Eilar-Edmister equation of etat (see Reid et al.(1977)) for the fugacity coefficient of H_2S in the presence of H_2 at high pressures. These corrections should be reasonable for the H_2S-H_2-n-hexadecane systems and the calculated H_2S concentrations are within a few percent of the correct values.

To keep the H_2S/H_2 saturation vessel at the desired pressure, a mixture of the same mole fraction H_2S as in the saturating vessel was prepared in a similar run in a 500 cm^7 cylinder at about 2400 to 2800 psig. From this cylinder the saturation vessel was repressurized as needed. The reactor set up was modified as necessary to provide gas mixing capabilities.

2. Analytical

Essentially all reactor sample analysis has been accomplished using the Antek Gas Chromatography equipped with an FID detector and a 3.5 meter 1/8" O.D. stainless steel column packed with 3% SP2100-DB (Supelco methyl silicone stationary phase with base sites deactivated) on 100-120 mesh Supelcoport. Disappearance of the dibenzothiophene and appearance of 1,2,3,4-tetrahydro DBT, biphenyl and cyclohexylbenzene were all quantified from the analysis. Interference from solvent cracking was very small compared to analysis reported in the 10th Quarterly Report.

3. Results and Discussion

With the objective of measuring dibenzothiophene reaction rates under a wide range of temperatures, pressures and concentrations, it was essential to first determine whether and under what circumstances the catalyst would maintain activity throughout the variety of conditions and length of time necessary to get a consistent set of rate data. Once catalyst stability is established, sufficient rate data must be collected to adequately reflect the kinetics dependence upon dibenzothiophene, hydrogen and product concentrations as well as temperature. During the

present quarter catalyst stability was achieved and a set of data reflecting rate dependence upon hydrogen pressure was obtained.

[i] Catalyst Stability

In the 10th Quarterly Report the first experiments with H_2S added to the feed were reported with the conclusion that H_2S might aid in maintaining catalyst activity besides simply inhibiting the desulfurization rate. In a separate publication (Broderick et al. (1978)) the stabilizing and activating effect of higher H_2S/H_2 ratios was substantiated. In all of this work the DBT concentration was 0.12 wt % and the highest concentration of H_2S was 0.0067 mole fraction. Further experiments in the same concentration ranges served to confirm the qualitative effect of H_2S, but showed a loss of catalyst activity with time even with 0.010 mole fraction H_2S in the feed.

Since a need for even more sulfur in the catalyst environment was suggested by the above results, and improved quantification of the DBT in the analysis was desirable, the DBT concentration was increased to 1.01 wt %, the hydrogen pressure to 96 atm and the catalyst loading correspondingly to 65 mg. Under identical operating conditions, several repeat experiments showed nicely reproducible conversion levels (see Fig. 1) and constant activity for up to 85 hr at constant flow rate. An extended experiment depicted in Fig. 2 in which flow rate was changed to allow periods of low conversion revealed that the catalyst activity (measured as a pseudo-first-order rate constant) dropped and then leveled out remaining nearly constant after 200 hr. Given this indication of catalyst stability, an experimental run was begun without

H_2S in the feed to measure rates in the differential regime. DBT conversions level out after 100 hr and a systematic variation of DBT concentration, H_2 saturation pressure and temperature was begun. Each rate was measured by solluting and analyzing four samples at two space velocities. Throughout the course of the experiment it was noted that at either high DBT concentrations, high conversions, or high temperature, catalyst activity remained high or increased. In contrast, at either low DBT concentrations, low conversions, low temperature, or high hydrogen pressure, catalyst activity dropped and could be only partially regained at more activating conditions. The plot in Fig. 3 of reaction rate at the standard conditions measured every 200 to 300 hr demonstrates the zig-zag decrease in catalytic activity which results from changing between activating and deactivating conditions. With an overall drop in rate of 30 percent from the point at 350 hr to the point at 330 hr, the set of data produced cannot be considered sufficiently consistent to be useful in differenting between kinetic models and in determining rate parameters.

As a final step to stabilize the catalyst a constant level of H_2S was added to the feed mixture as described in the experimental section (B.1). The standard conditions for checking the activity of the catalyst are also given in section B.1. An initial survey of catalyst stability at various H_2S levels indicated that a mole fraction of 0.001 was too low. At 0.0073 mole fraction H_2S the catalyst was stable for over 1600 hr (see Fig. 3). Even with H_2S present, minor activity variations are noticeable. Effect on the rate data of these variations is minimized by randomly alternating between activating and deactivating conditions.

[ii] Hydrogen Dependence of DBT HDS from Differential Rate Data

While maintaining constant pressure in the reactor the hydrogen saturation pressure was varied randomly from 35 to 157 atm (500 to 2300 psig) at three separate temperatures. In Fig. 4 rate data at all three temperatures are plotted showing a non-linear rate dependence on hydrogen pressure. A preliminary fit of the data to a saturation form of kinetics, i.e., rate = $\frac{k\ K_{H_2}\ P_{H_2}}{(1+K_{H_2}\ P_{H_2})}$ results in the curves through the data shown in Fig. 4. While this kinetic model shows a reasonable visual fit to the set of data, it is not the only possible model and no effort has been made as of yet to discriminate between models on statistical grounds.

Figures 5, 6, and 7 show the data at each of the three temperatures separately along with the 95 percent confidence limits on the fitted model. Comparison of such limits represent one means of comparing and discriminating kinetic models. They also reveal the greater degree of data reaction at the lowest temperature. Collection of rate data will continue until all important parameters have been investigated after which final model discrimination will be performed.

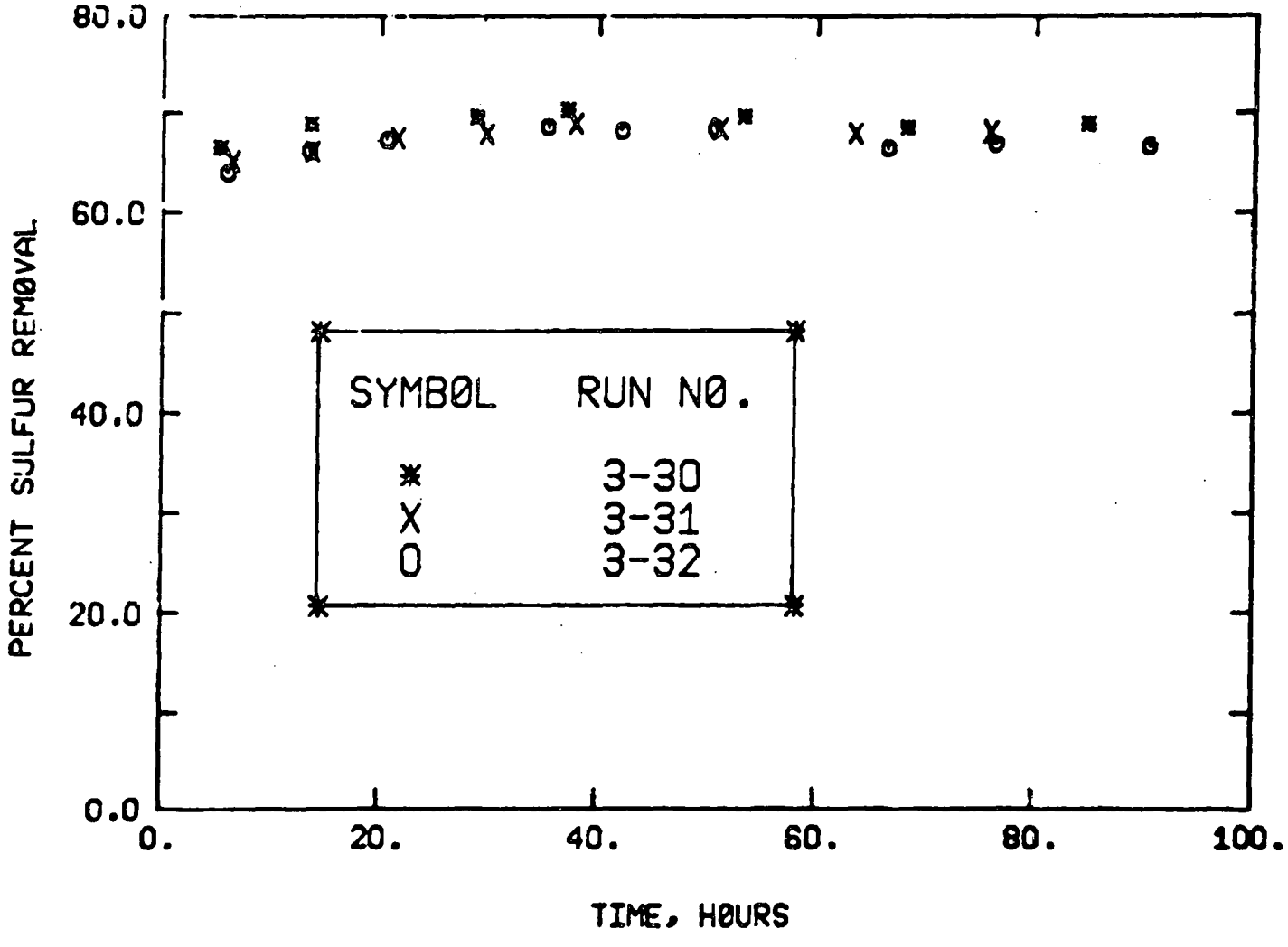

Fig. 1. Reproducibility of initial conversion from three separate experimental runs. DBT Concentration: 1.24 mole percent; Catalyst Loading: 65 mg HDS 16A, Temperature: 300°C; Weight hourly space velocity: 13 gmol/h gcat.

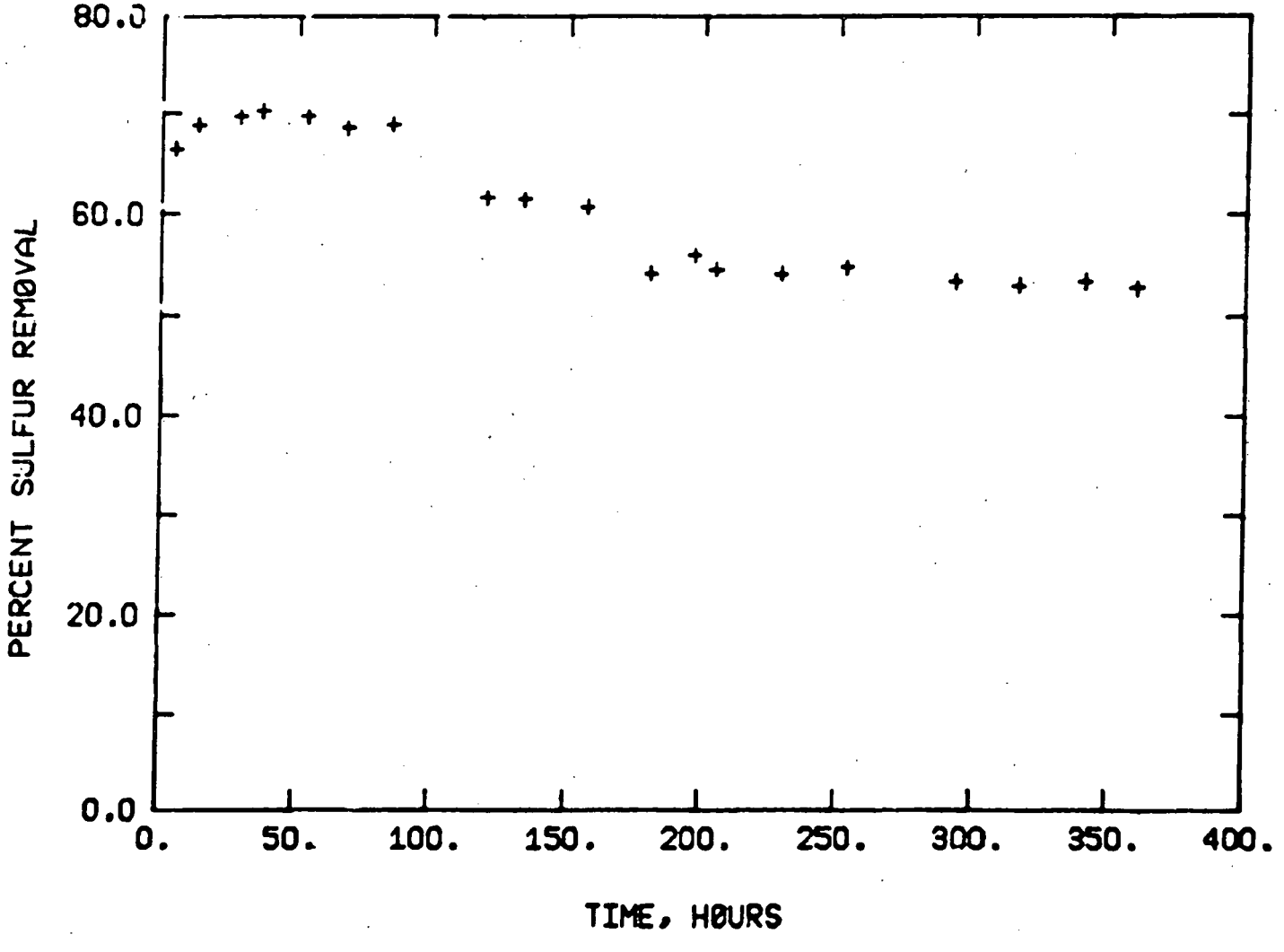

Fig. 2. Long-term stabilization of catalytic activity at constant temperature, pressure and concentration. DBT Concentrations: 1.24 mole %; Temperature: 300°C; Pressure: 1400 psig; Weight hourly space velocity: 13 gmol/h gm cat.

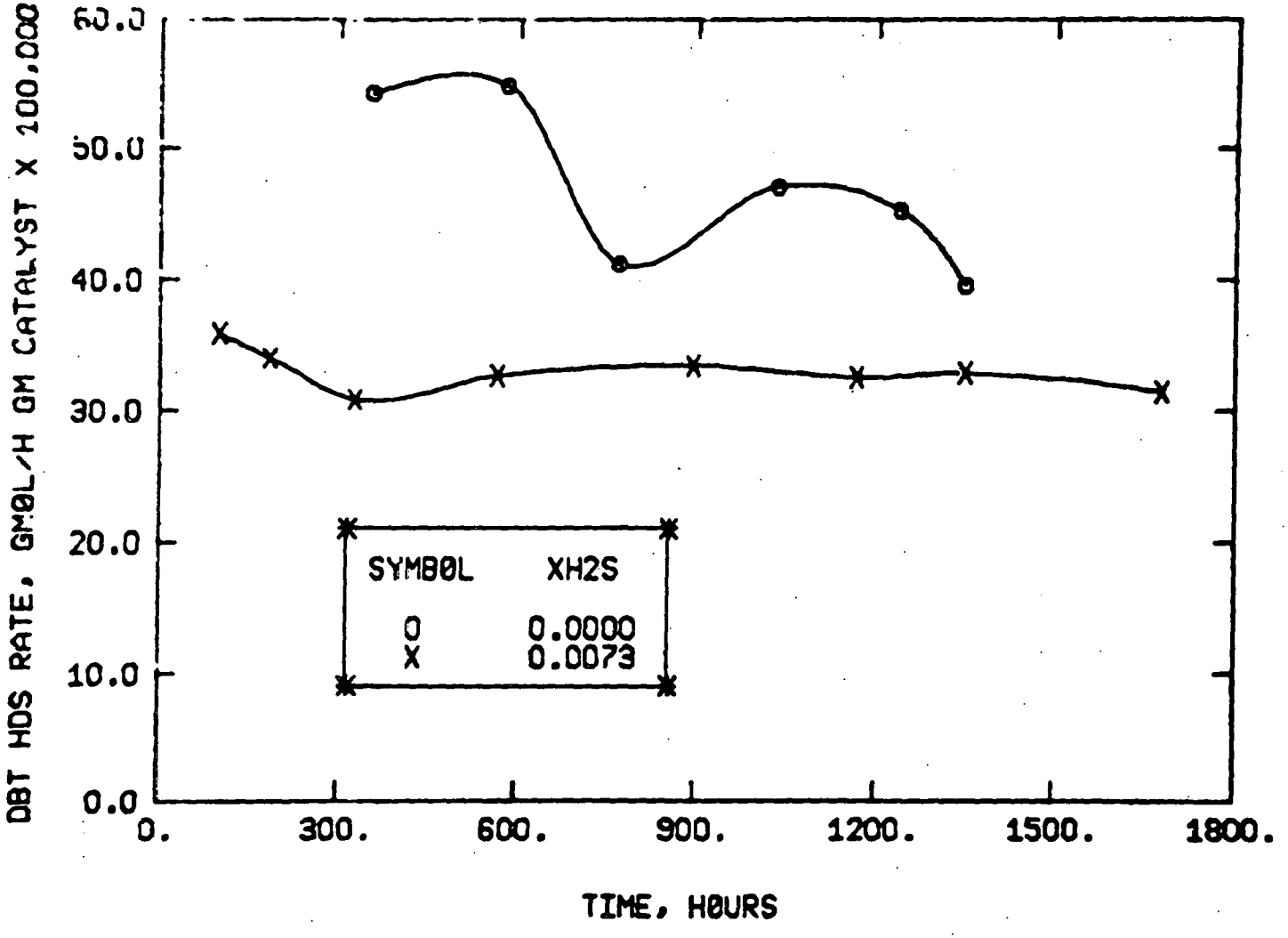

Fig. 3. Catalytic activity as a function of time on stream with and without H_2S in the feed. Differential rates measured at standard conditions of: 1.24 mole % DBT; 300°C, and 1400 psig total pressure.

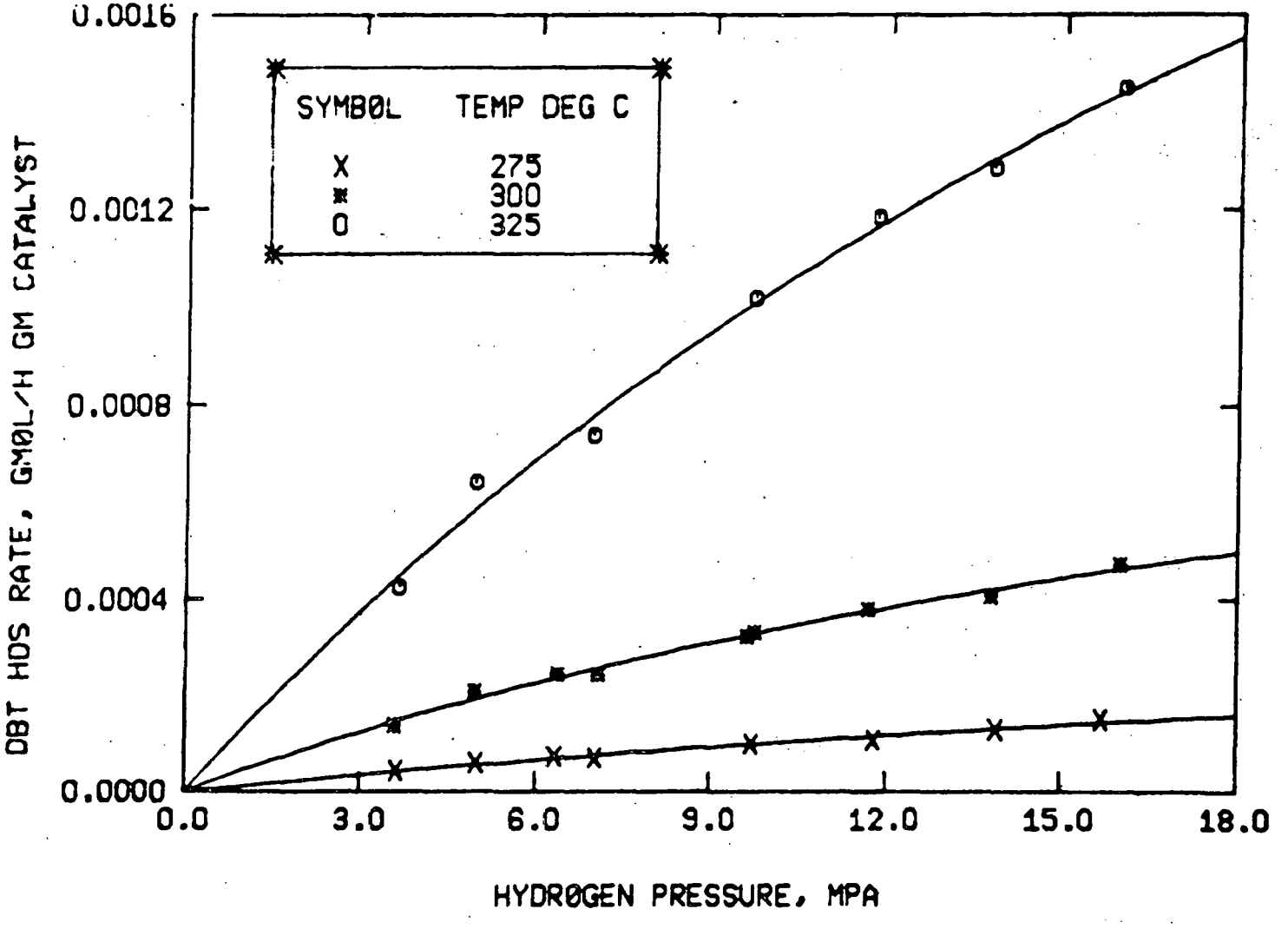

Fig. 4. Effect of hydrogen pressure on DBT hydrodesulfurization rate. Curve is hydrogen saturation kinetic model fit to data.

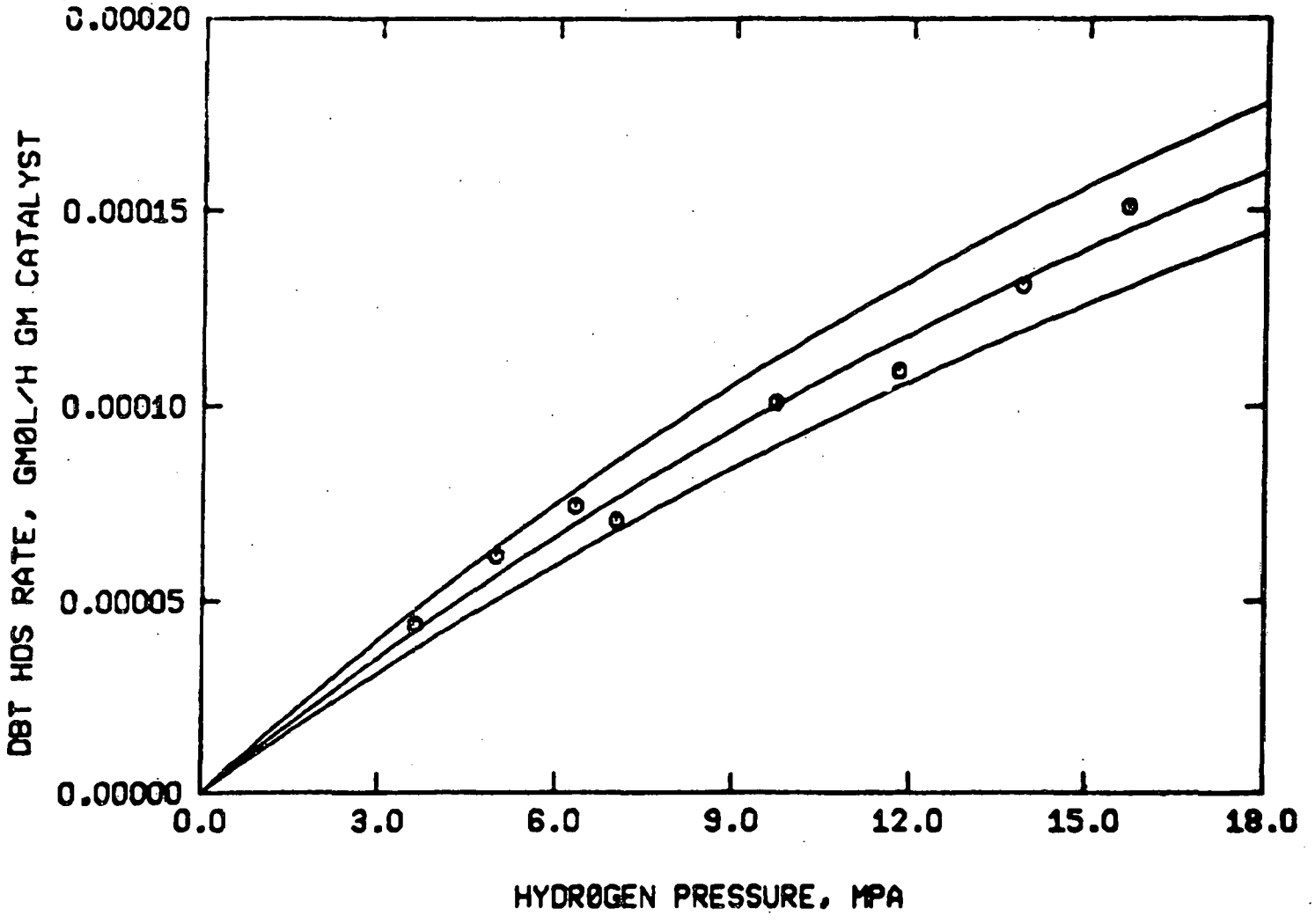

Fig. 5. Effect of hydrogen pressure on DBT hydrodesulfurization rate at 275°C. Curves represent fit and confidence limits of fit from hydrogen saturation kinetic model.

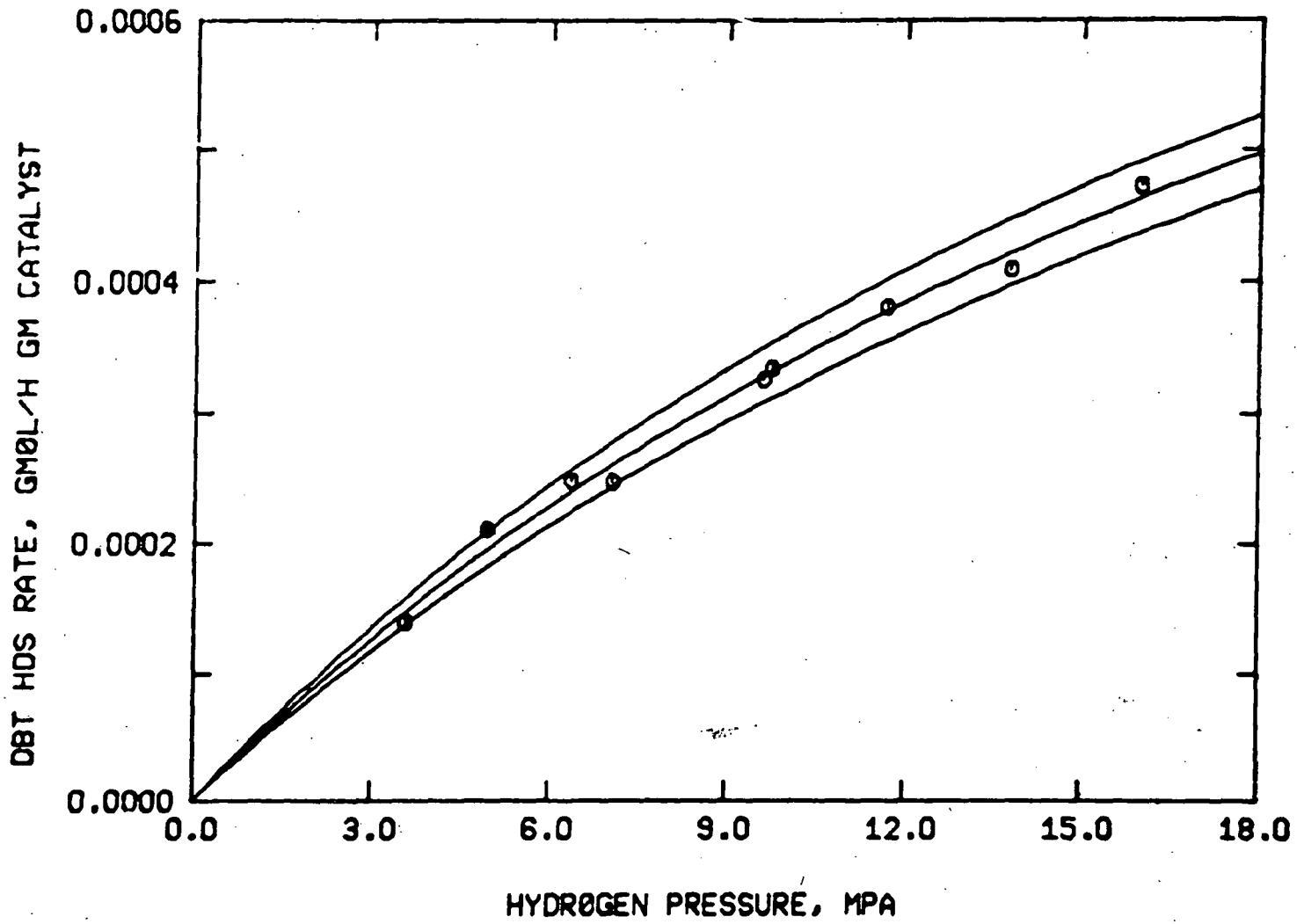

Fig. 6. Effect of hydrogen pressure on DBT hydrodesulfurization rate at 300°C. Curves represent fit and confidence limits of fit from hydrogen saturation kinetic model.

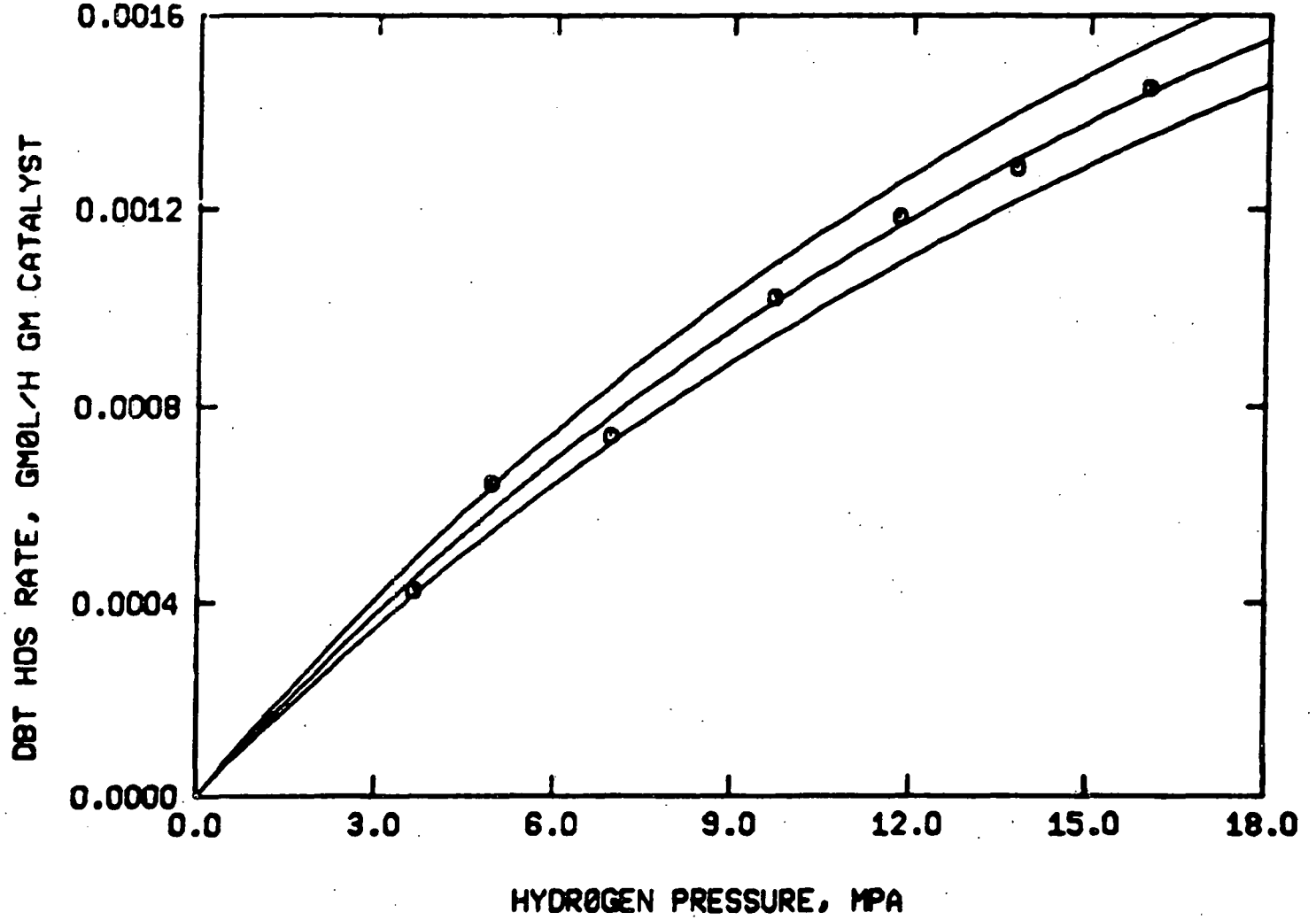

Fig. 7. Effect of hydrogen pressure on DBT hydrodesulfurization rate at 325°C. Curves represent fit and confidence limits of fit from hydrogen saturation kinetic model.

References

Tremper, K. K., and Prausnitz, J. P., J. Chem. Eng. Data 21 (3), 295 (1976).

Reid, R. C., Prausnitz, J. M., Sherwood, T. K., The Properties of Gases and Liquids, Third Ed., McGraw-Hill, New York, (1977).

Prausnitz, J. M., Molecular Thermodynamics of Third-Phase Equilibria, Prentice-Hall, Inc., Englewood Cliffs, N.J., (1969).

Broderick, D. H., Schuit, G. C. A., and Gates, B. C., "The Sulfided Co-Mo/γ-Al_2O_3 Catalyst," J. Catalysis 54, 94 (1978).

B. Biphenyl Hydrogenation

Fig. 8 shows the differential conversion plot for the biphenyl hydrogenation reaction. Plot is linear up to quite a high conversion level and then starts bending over. From the slope of this graph we can determine the rate of the reaction.

Fig. 9 shows the effect of conc. of CS_2 (which is needed to maintain the activity of the catalyst) on the rate of hydrogenation at three different temperatures.

Fig. 10 shows the effect of H_2 sat. press. on the rate of hydrogenation at four different temperatures.

Experiments are in progress to determine the full non-linear rate expression for the biphenyl hydrogenation reaction.

Differential Conversion Plot

Fig. 8

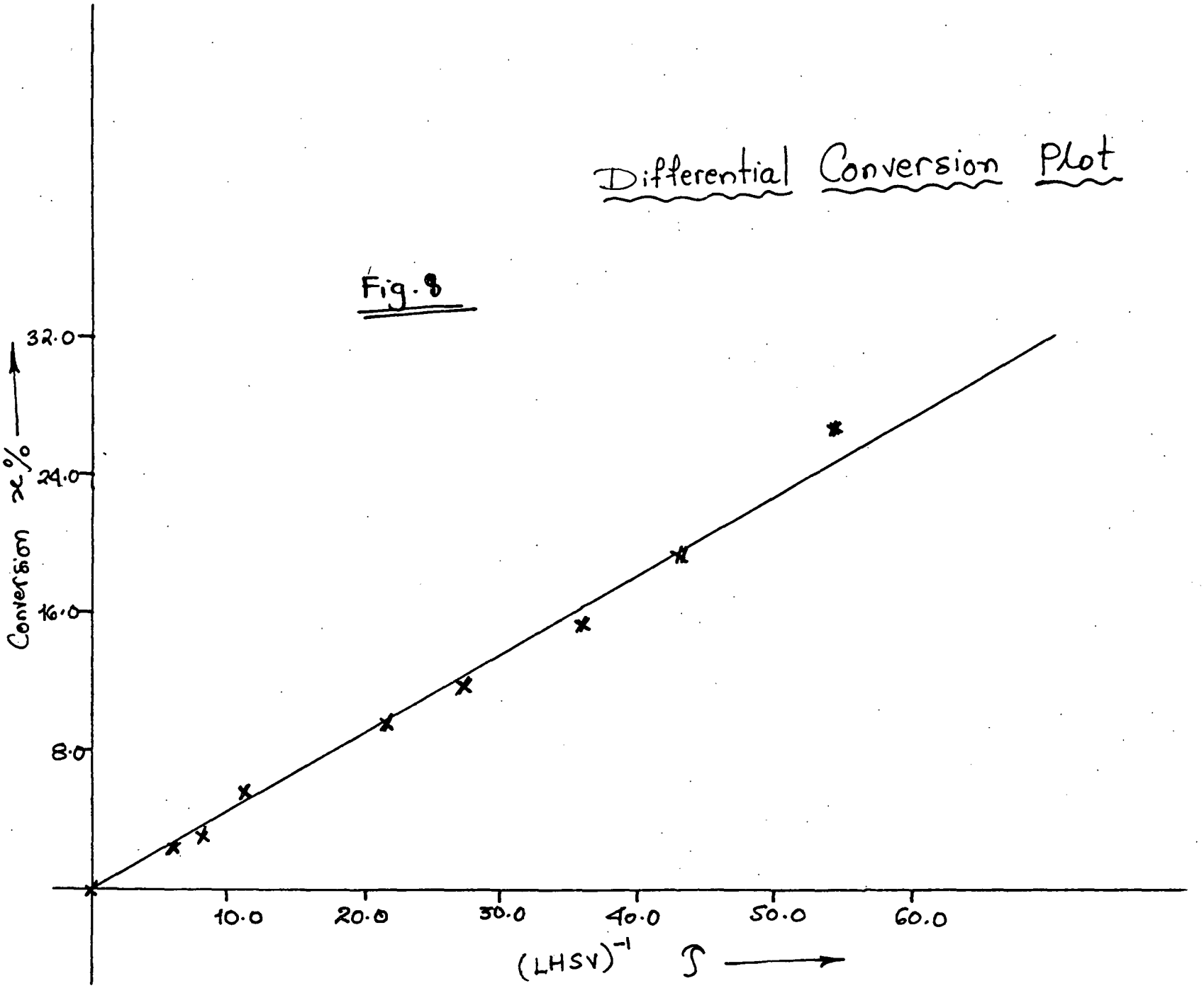

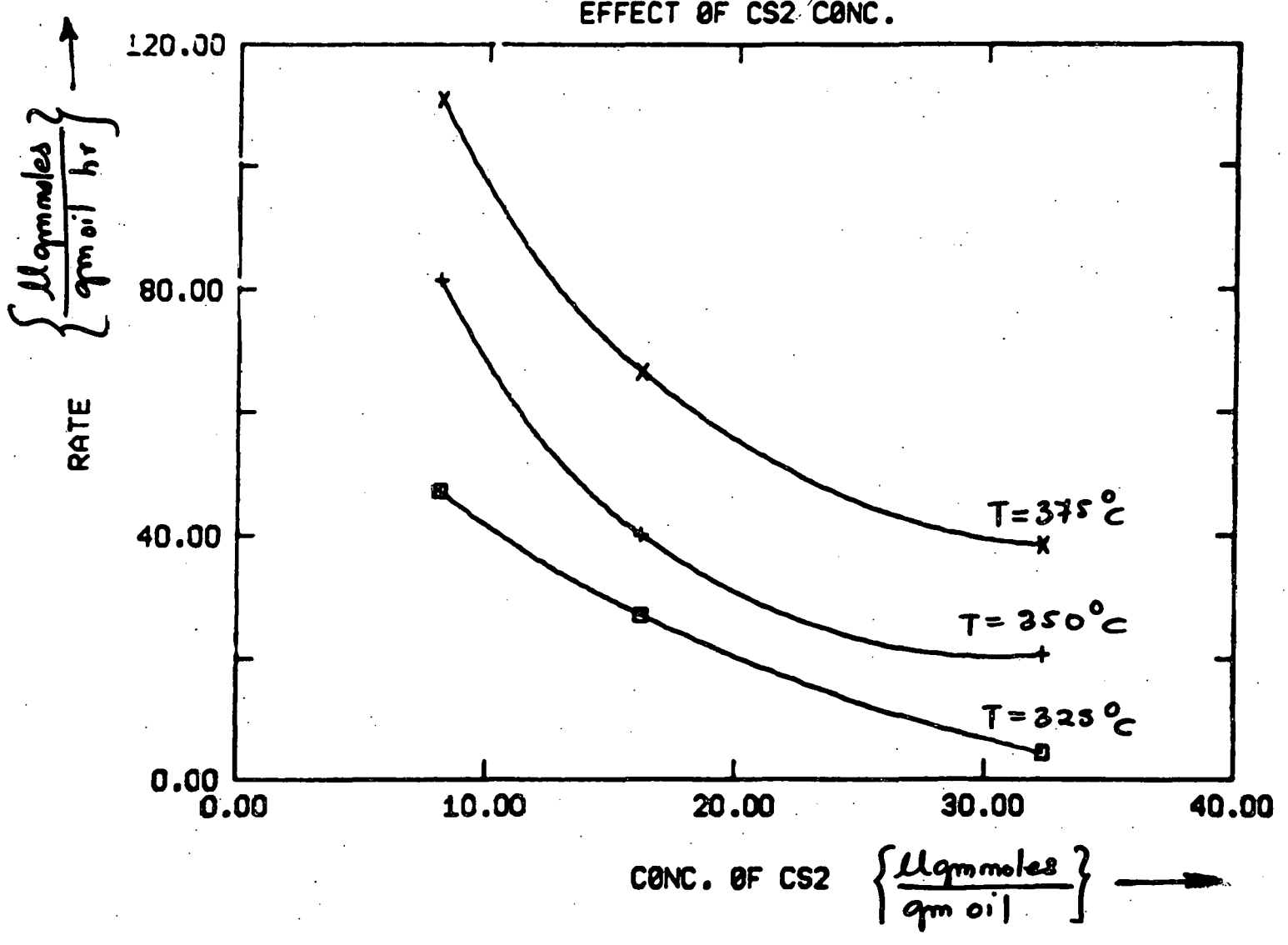
EFFECT OF CS2 CONC.
120.00
80.00
40.00
0.00
RATE {μgmmoles / gm oil hr} →
0.00
10.00
20.00
30.00
40.00
CONC. OF CS2 {μgmmoles / gm oil} →
T=375°C
T=350°C
T=325°C

FIG. 9

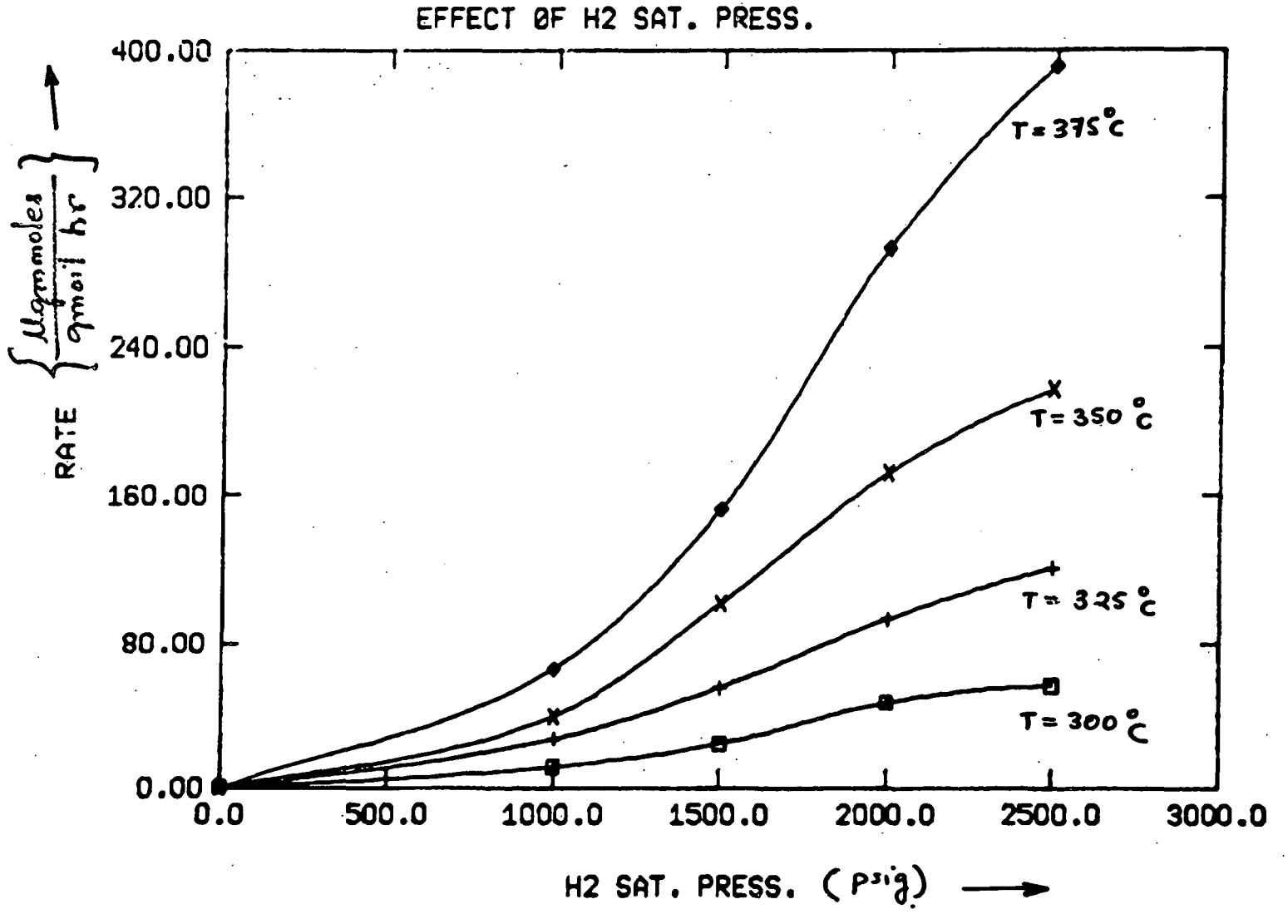
EFFECT OF H2 SAT. PRESS.
RATE {μgmmoles / gmoil hr} →
400.00
320.00
240.00
160.00
80.00
0.00
0.0
500.0
1000.0
1500.0
2000.0
2500.0
3000.0
T = 375°C
T = 350°C
T = 325°C
T = 300°C
H2 SAT. PRESS. (Psig) →

FIG. 10

C. Catalytic Hydrodenitrogenation

This report covers all the hydrodenitrogenation experiments that have been conducted since the last report. The report is presented in a logical sequence giving all the results from these experiments. Brief discussion of the results are presented at the end of each section. However, no attempt has been made to discuss the results in greater detail. This will be done in the Final Progress report.

All of the experiments reported in this report were carried out in the 1 liter stirred batch autoclave reactor. High-pressure liquid-phase catalytic hydroprocessing reactions were carried out for the following binary systems:

(1) A basic nitrogen-containing compound and an aromatic compound: quinoline and naphthalene.

(2) A basic and a non-basic nitrogen-containing compound: quinoline and indole.

(3) A basic nitrogen-containing compound and a sulfur-containing compound: quinoline and dibenzothiophene.

Reaction conditions used for all of the experiments were identical except that initial concentrations of the reactants were varied. Reaction conditions are listed in Table 1..

a) Singe Component Studies

Hydrodenitrogenation of quinoline

A quinoline hydrodenitrogenation run (run #1020) was carried out under standard conditions with initial quinoline concentration of

TABLE 1

STANDARD REACTION CONDITIONS FOR INTERACTION STUDIES

Temperature:	350^{o} ($\pm 1^{o}C$)
Pressure:	34 (± 1) atm
Catalyst:	Ni-Mo/γ-Al_2O_3 (HDS-9A) presulfided at $400^{o}C$ for 2 hr in the stream of 10% H_2S/H_2 @ ~100 cm^3/min
Conc. of catalyst:	0.5 wt %
Solvent:	n-hexadecane
CS_2:	0.05 wt %
Stirring speed:	1500 rpm
Reactants:	Quinoline 15×10^{-6} - 160×10^{-6} gmole/g oil (0.2-2.0 wt %)
	Naphthalene ~35×10^{-5} gmole/g oil (5 wt %)
	Indole ~35×10^{-5} gmole/g oil (0.5 wt %)
	Dibenzothiophene ~35×10^{-6} gmole /g oil (0.7 wt)

(Reactions were carried out with one or two of the above)

35×10^{-6} gmole/g oil (0.5 wt %). Reaction products were found to be 1,2,3,4-tetrahydroquinoline, 5,6,7,8-tetrahydroquinoline, trans- and cis-decahydroquinolines, o-propylaniline, n-propylcyclohexane and n-propylbenzene. Typical product concentrations vs. time for the nitrogen-containing compounds is presented in Figs. 11-13. Under hydrodenitrogenation conditions, quinoline rapidly hydrogenated to 1,2,3,4-tetrahydroquinoline in what appeared to be equillibrium concentrations. The trans-isomer of decahydroquinoline was predominant and the relative concentrations of the two isomers remained constant at a value of ~5.0 throughout most of the run. For simplicity in kinetic analysis, the concentrations of two isomers of decahydroquinoline were lumped together in all of the experiments. The shapes of the time-concentration profiles for 5,6,7,8-tetrahydroquinoline and the lumped group of decahydroquinolines were those expected commonly for reaction intermediates in the course of a batch reactor run. The concentration of o-propylaniline built up relatively rapidly and declined at a slower rate from its maximum value.

This behavior of reaction intermediates is similar to that reported by Shih et al. (1977) and Reiff (1977). A reaction network which adequately describes hydrodenitrogenation of quinoline is presented in Fig. 14 as reported by Shih et al. (1977). All the intermediate reactions are assumed to follow pseudo-first-order behavior.

Since this experiment was carried out in n-hexadecane, sample analysis was performed using flame ionization detector. Two major hydrocarbon products were observed in liquid samples as described

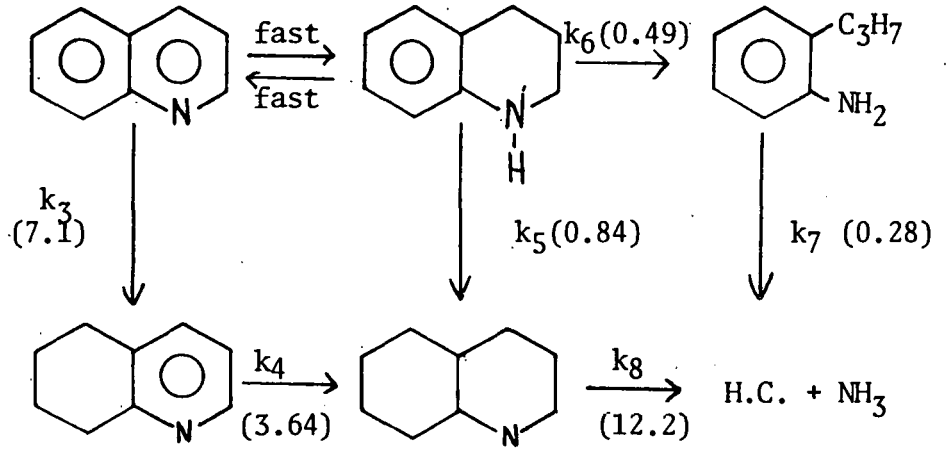

Figure 11. Reaction network for hydrodenitrogenation of quinoline.

Numbers in brackets are estimated pseudo first-order rate constants (g oil/gcat-min) for HDN of 0.5 wt % quinoline at standard conditions. Table 1 gives standard conditions.

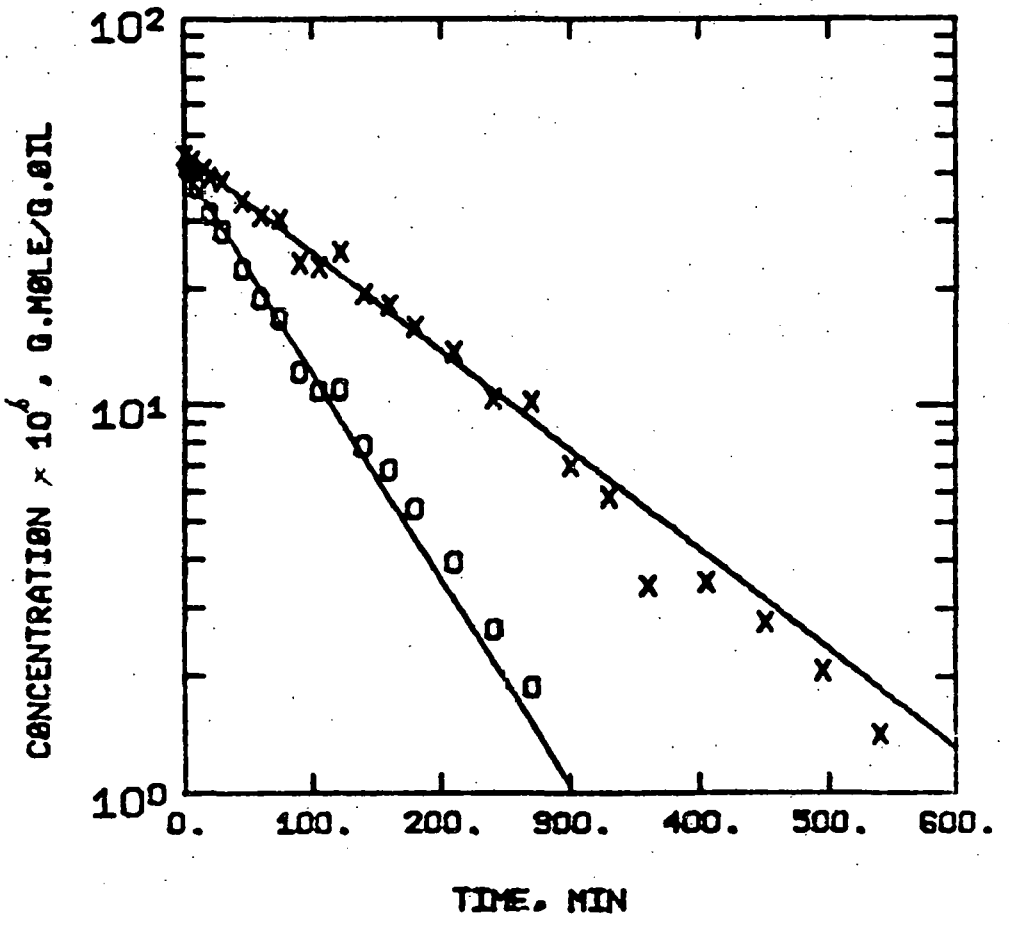

Figure 12. HDN of 0.5 wt % Q:

□ = quinoline + 1,2,3,4-tetrahydroquinoline
x = total nitrogen

earlier. Normal-propylcyclohexane was the major hydrocarbon product although small quantities of n-propylbenzene were always observed. No attempts were made to include these hydrocarbon products in the reaction network due to uncertainties of reaction paths and complexities in the resulting networks.

The rate of total nitrogen removal and the rate of disappearance of the lumped group of quinoline and 1,2,3,4-tetrahydroquinoline could be well represented by pseudo first-order kinetics as shown in Fig. 15. It can be seen that the rate of total nitrogen removal increased toward the end of the run (at high conversions). This will be discussed later in Chapter V.

Kinetic analysis was carried out using the method described by Himelblau, Jones and Bischoff (1967); the kinetic rate constants in the reactions in the network are presented in Fig. 14. In Figs. 11-13 the points represent experimental data and solid lines represent numerical solution of the set of simultaneous differential equations describing the reaction network with the best-fit values of the pseudo first-order rate constants.

Hydrogenation of Naphthalene

Naphthalene hydrogenation in the absence of quinoline was carried out under standard conditions (Table 1). The initial concentration of naphthalene used was 35×10^{-5} gmole/g oil (5 wt %).

Naphthalene was rapidly hydrogenated to 1,2,3,4-tetrahydronaphthalene (tetralin). Tetralin was further hydrogenated to trans-

and cis-decahydronaphthalene (decalin). All the products were identified by using GC analysis of authentic compounds, by comparing retention times with those of pure compounds. Time-concentration profiles for the reaction products are presented in Fig. 16. As can be observed from Fig. 6, formation of trans-decalin was favored over that of cis-decalin and the relative amounts of the two isomers remained constant. No other hydrocarbon product was detected.

Response factors for naphthalene and its hydrogenation products differed by ~10%, these differences were taken into account in calculating the concentrations from chromatogram peak areas. (Sample-splitting during sample injection in capillary column was reproducible within ±6%. To reduce the scatter in the data, a perfect mass balance was assumed in calculating concentrations of various products. This assumption was later verified by the use of internal standard technique which is independent of injection techniques and irreproducibilities in sample-splitting.)

From Fig. 16, a reaction network for naphthalene hydrogenation can be described as given in Figure 17.

Dehydrogenation of decalin to tetralin is possible but it could not be concluded from the experimental data. ((A reaction network in Fig. 17 with parallel paths for formation of two isomers of decalin correctly predicts constant ratio of concentrations of the two isomers observed experimentally; however, equillibrium (fast reversible reactions) between two isomers of decalin cannot be ruled out. The energy difference

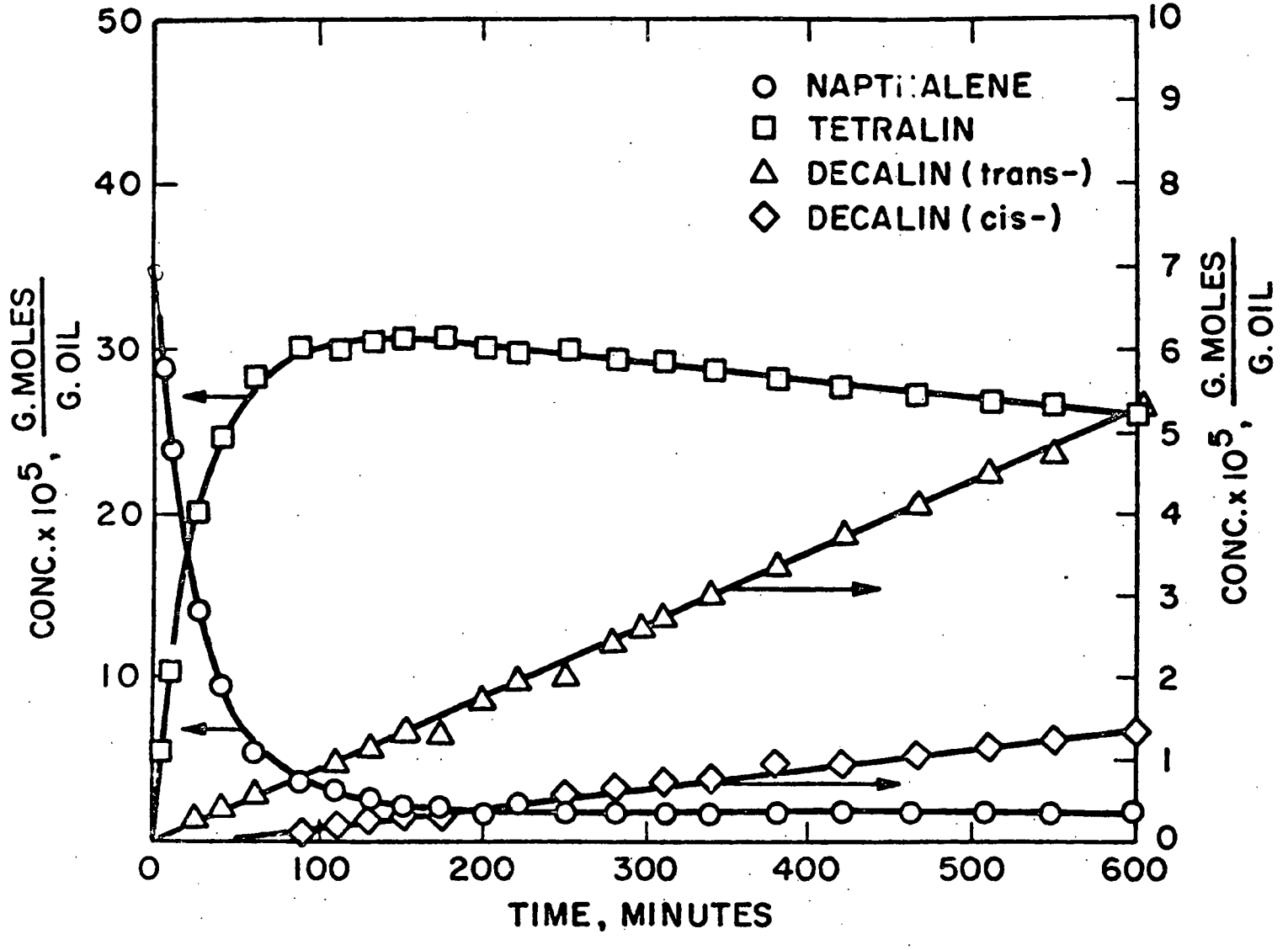

Figure 13. Hydrogenation of 5 wt % naphthalene.

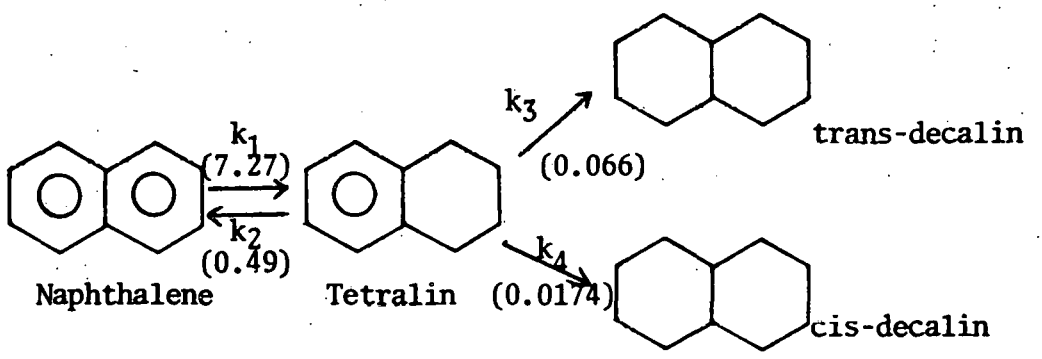

Figure 14. Reaction network for hydrogenation of naphthalene.

Numbers in brackets are estimated pseudo first-order rate parameters for hydrogenation of 5 wt % naphthalene at standard conditions.

between the two forms of decalin is approximately 2.4 kcal (Emmett, and it is likely that such isomerization could occur readily. On the other hand, it has been reported that during vapor phase catalytic dehydrogenation studies over Pt/Al_2O_3 cis-decalin isomerizes to trans-decalin but not vice-versa. Since detailed mechanistic aspects were beyond the scope of this work all kinetic parameters were estimated on the basis of reaction network in Fig. 22. Kinetic analysis for Run #1017 was also carried out on the basis of the following network:

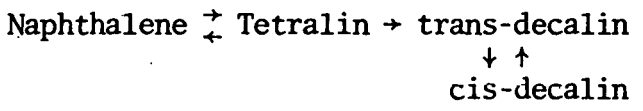

Rate parameters from this network predicted distribution equally well.))

Solid lines in Fig. 17 represent model predictions from estimated rate parameters which are shown in Fig. 32. The predictions from the model are in good agreement with experimental data.

Estimation of parameters for this set of data was also carried out using a standard non-linear least-squares (NLLS) routine (Marquardt, 1963). The rate parameters estimated by the method of Himmelblau, Jones and Bischoff (1967) and those estimated by NLLS were in very good agreement (better than 3%).

Hydrodenitrogenation of Indole

Indole hydrodenitrogenation was carried out n-hexadecane under standard conditions with an initial indole concentration of 0.5 wt %. Indoline and o-ethylaniline were found to be nitrogen-containing reaction

intermediates. Ethylbenzene and ethylcyclohexane were observed to be ultimate products of HDN of indole. Besides 2,3-dihydroindole (indolin), no other hydrogenated indole was observed as product. This is attributed to the fact that once the benzene ring in indole is hydrogenated, the resulting intermediate hydrodenitrogenates very rapidly.

Ethylcyclohexane was the predominant hydrocarbon product from HDN of indole. Figs. 18 and 19 show the concentration profiles of indole and its reaction products as a function of time. The concentrations of the two hydrocarbon products were lumped together. Under hydrodenitrogenation conditions indole was rapidly converted to 2,3-dihydroindole in what appeared to be equillibrium concentrations. By comparison of products from indole HDN with those of quinoline HDN and from literature evidence (Aboul Abeit et al., 1973; Stern, W. E., 1977) a preliminary reaction network for indole HDN can be proposed as follows:

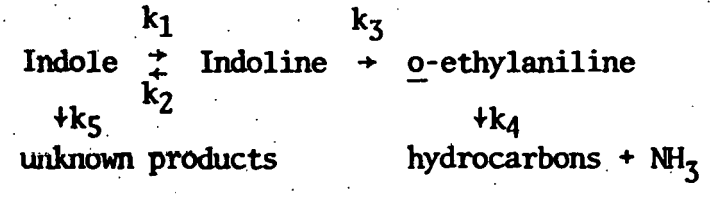

Rate parameter k_5 was included in the above reaction network. This was deemed necessary to account for some loss in mass balance (sum of the concentrations of reactant and products) in the initial period of the experiment. The reason for the loss in mass balance is not quite clear but it can be attributed to some polymerization reactions and formation of high molecular weight compounds. Such phenomena have been reported (Hartung et al., 1961; Flinn et al., 1963) to occur during

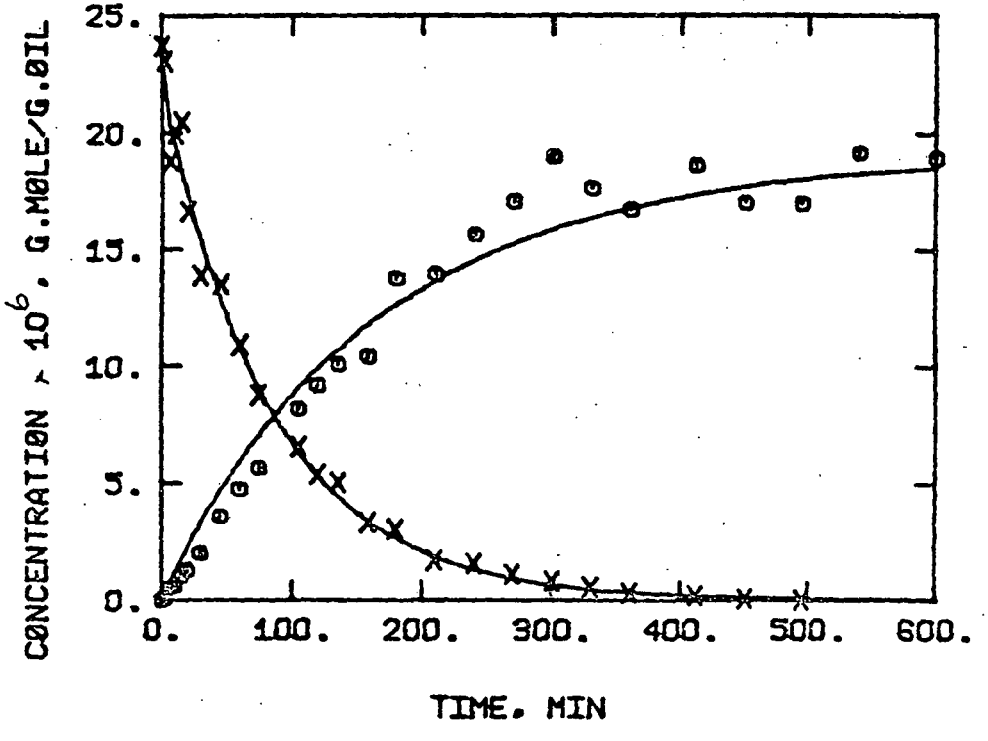

Figure 15. Hydrodenitrogenation of indole.

x = indole
▣ = ethylbenzene + ethylcyclohexane

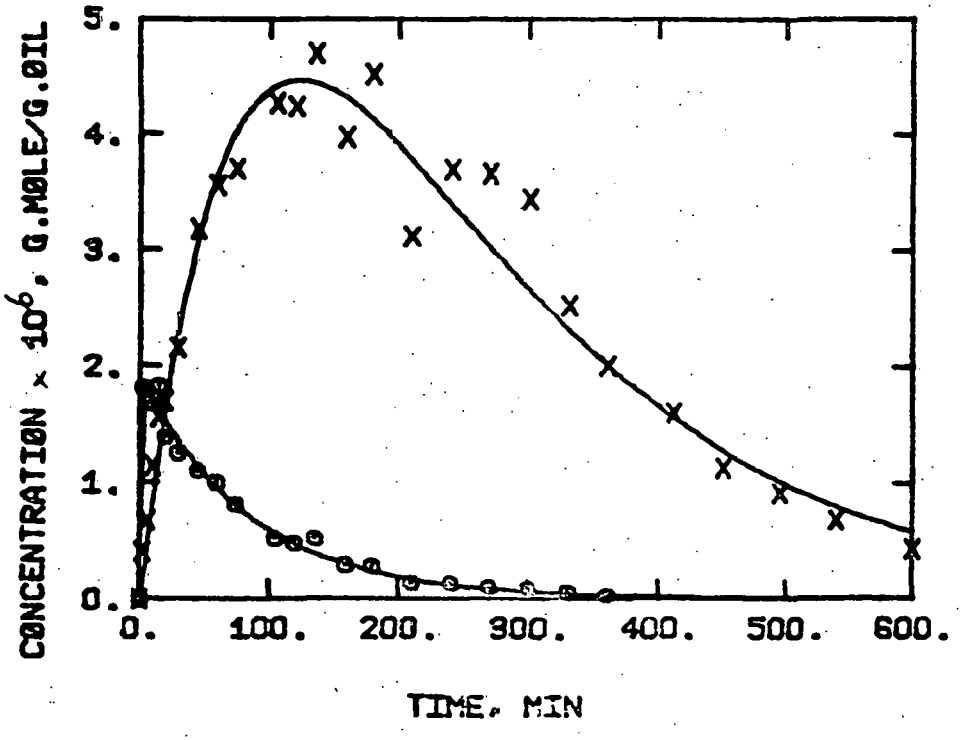

Figure 16. Hydrodenitrogenation of indole.
■ = indolin
x = o-ethylaniline

hydrodenitrogenation of indole.

Even with the reaction step k_5 added to the network, the model could not describe the behavior of reaction system satisfactorily. The rate of HDN of o-ethylaniline was found to be too slow to account for rapid formation of nitrogen-free hydrocarbons. This was not surprising since anilines are refractory to HDN. Such was the case for HDN of o-propylaniline in quinoline reaction network and of o-butylanilines in methylquinolines' reaction networks.

From the above observations it was concluded that there had to be some other route for HDN. It was thought that indole can be hydrodenitrogenated through reaction intermediates containing hydrogenated benzene ring. Since such intermediates can be unstable under the conditions of the reaction, one may not be able to observe them in reaction samples and the reaction network given in Fig. 35 was thought more appropriate.

Reaction network for HDN of indole

The rate of total nitrogen removal and the disappearance of the lumped group of indole and indoline followed pseudo first-order kinetics as shown in Fig. 21. The rate parameters for HDN of indole are shown in Fig. 20. Figures 18 and 19 show the agreement between the experimental data and model predictions.

Hydrodesulfurization of dibenzothiophene

HDS of DBT was carried out under standard conditions. The initial concentration of DBT was 4×10^{-5} gmole/g oil (0.7 wt %).

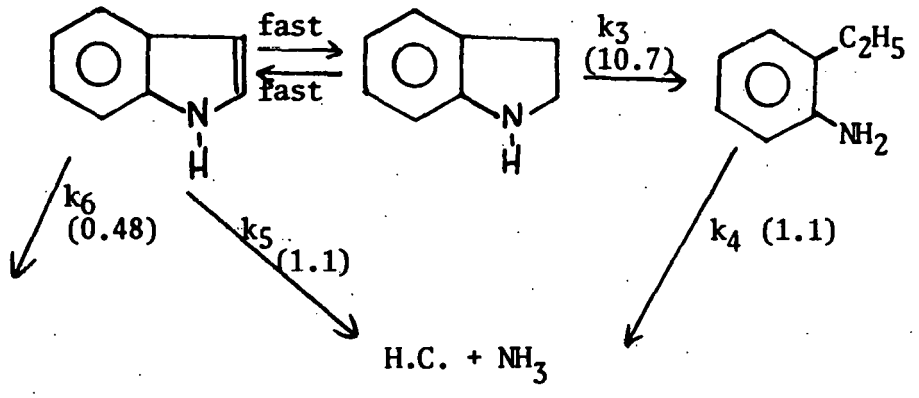

Figure 17. Reaction network for hydrodenitrogenation of indole.

Numbers in brackets are pseudo first-order rate parameters for hydrodenitrogenation of 0.5 wt % indole at standard conditions.

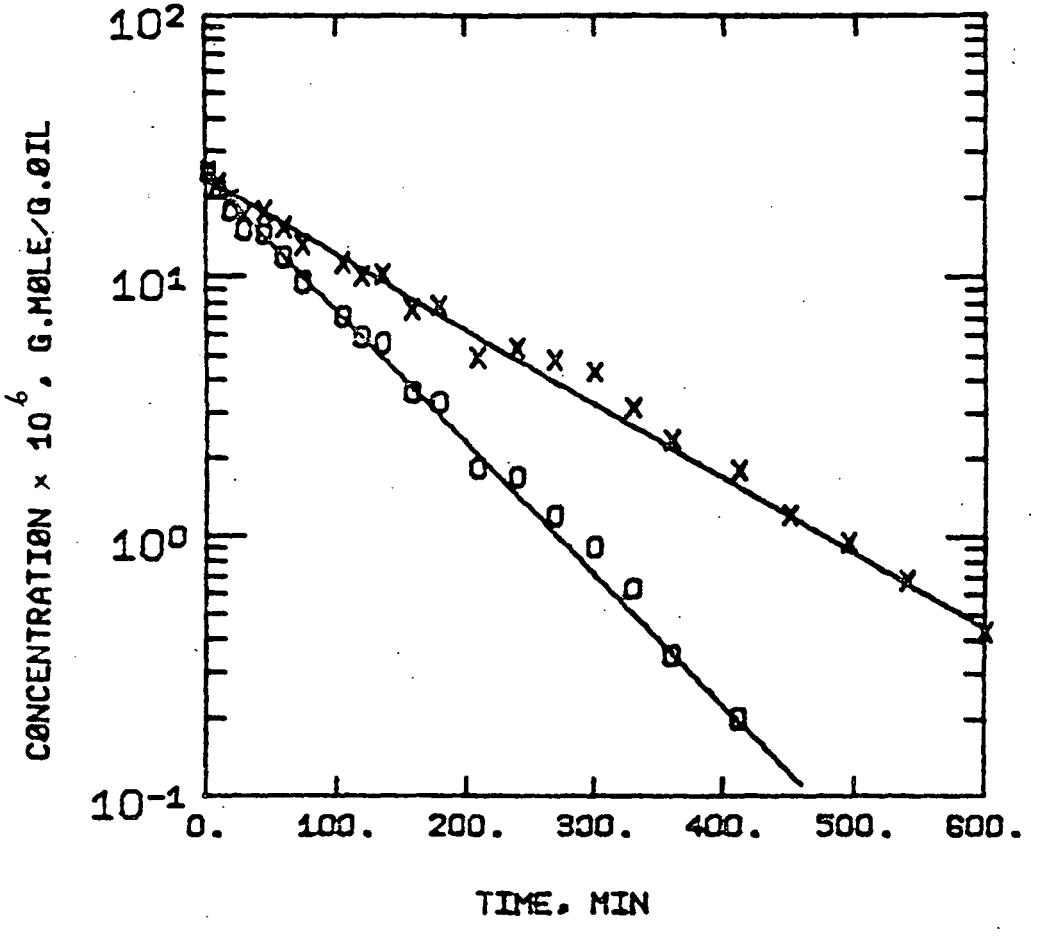

Figure 18. HDN of indole.
x = total nitrogen
□ = indole + indoline

Biphenyl was the most important product of the HDS reaction. Under the reaction conditions, biphenyl was hydrogenated to cyclohexylbenzene which was further hydrogenated to bicyclohexyl. Trace amounts of two sulfur-containing reaction intermediates, tetrahydrodibenzothiophene and hexahydrodibenzothiophene, were also found. The ratio of the concentrations of these two sulfur-containing reaction intermediates remained constant.

Tetrahydrodibenzothiophene was favored under the reaction conditions. Product distribution for the experiment is presented in Figs. 22, 23, and 24.

Since the tetrahydro- and hexahydro dibenzothiophene remained in equillibrium and their concentrations were small they were lumped together for the purpose of kinetic analysis. Cyclohexylbenzene and bicyclohexyl were difficult to separate chromatographically, and since reaction between the two was not important, they also were lumped together. The separation of the two hydrocarbons took approximately 4 hr of gas chromatographic time (column temperature 125°C) and only a few samples were separately analyzed in this manner to estimate the rate of hydrogenation of cyclohexylbenzene to bicyclohexyl.

Disappearance of dibenzothiophene followed pseudo first-order rate behavior as can be seen from Fig. 25. As in the case of indole hydrodenitrogenation, the sum of the concentrations of reactant and products (s) declined during the initial period of the experiment. In fact, the value of s declined continuously to about 80% of its initial value until all sulfur compounds were reacted after which it

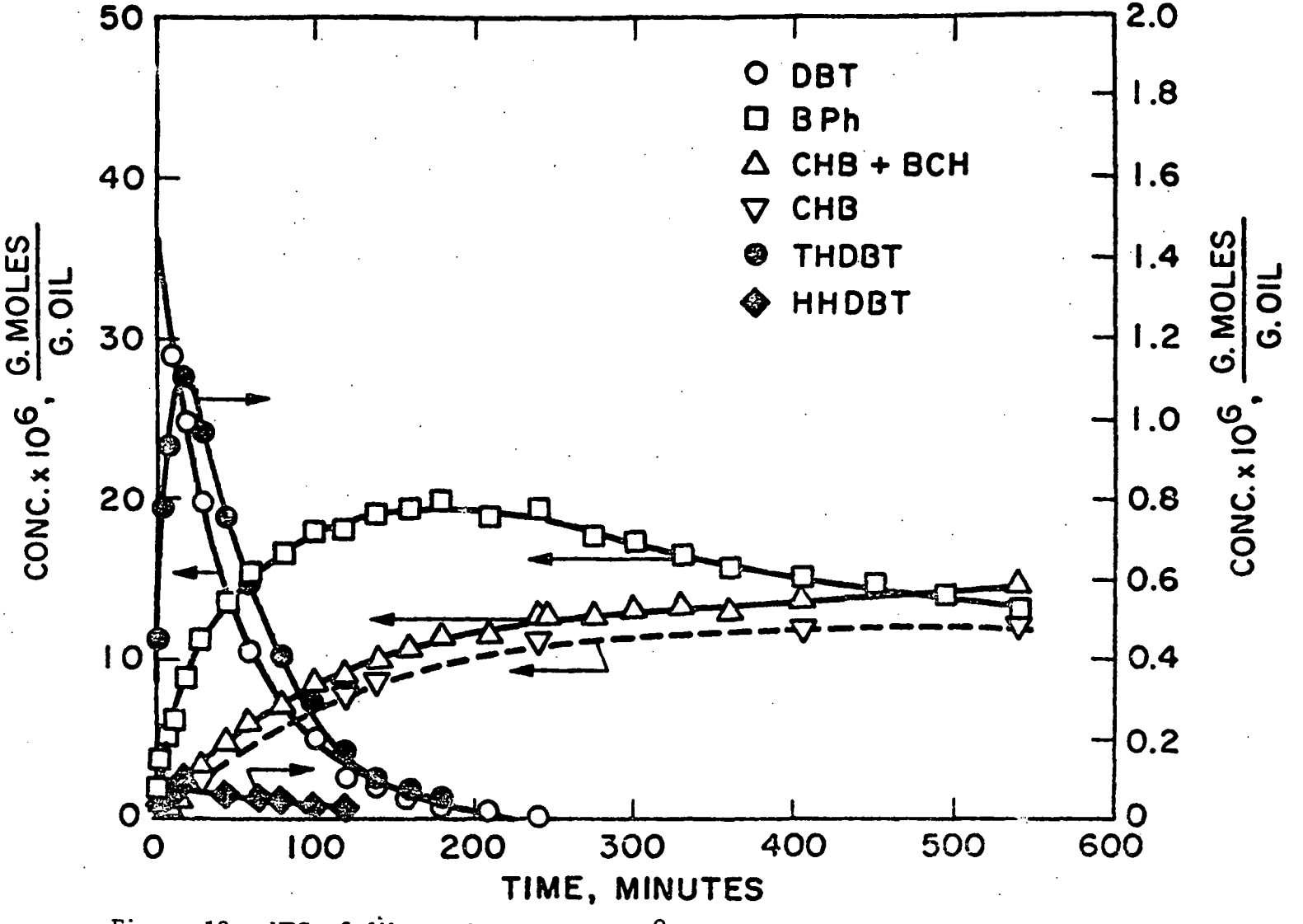

Figure 19. HDS of dibenzothiophene: 342°C, 34 atm, Ni-Mo/γ-Al_2O_3, DBT only.

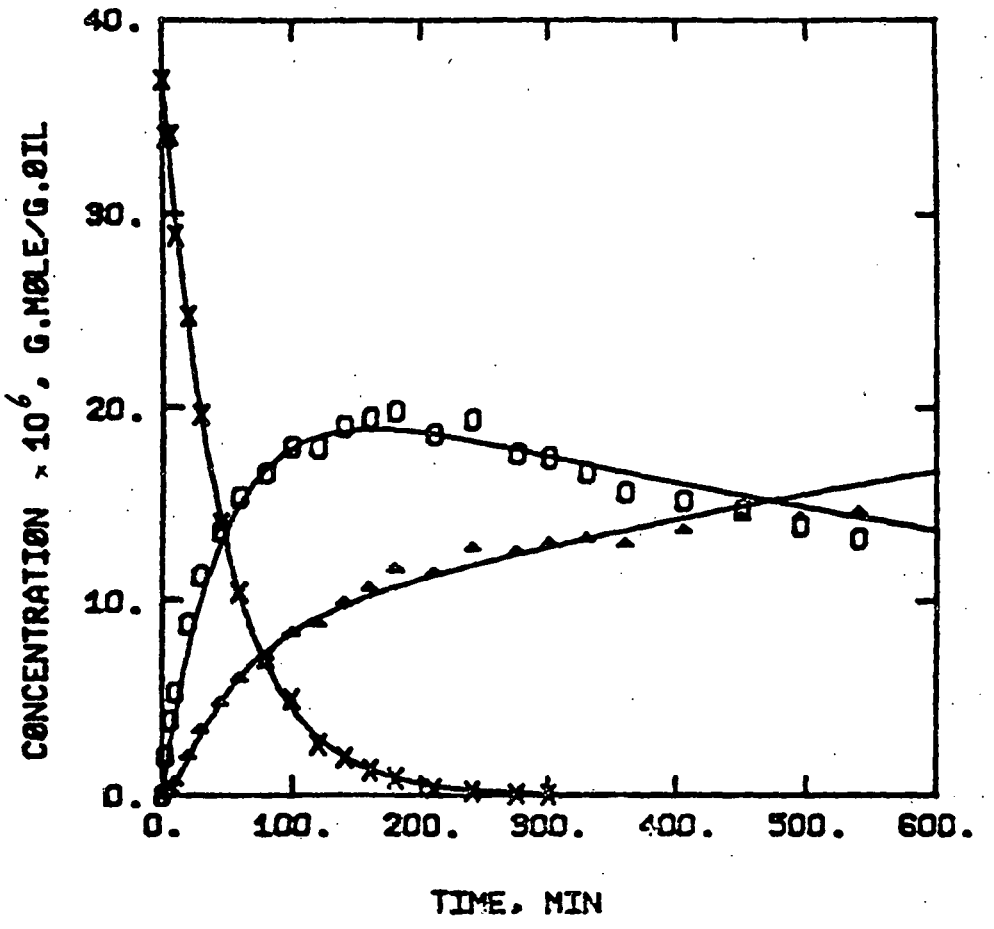

Figure 20. HDS of DBT:
x = DBT
O = biphenyl
▲ = cyclohexylbenzene + bicyclohexyl

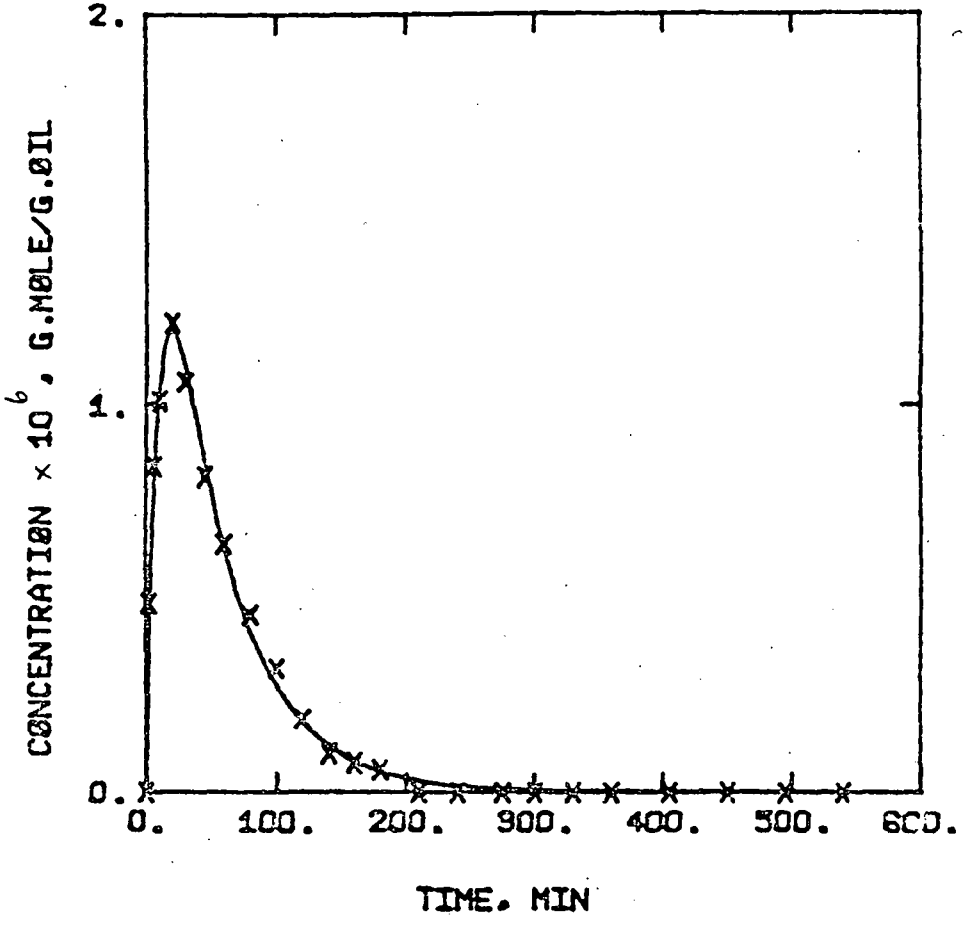

Figure 21. HDS of DBT: x = tetrahydro- + hexahydro-dibenzothiophene

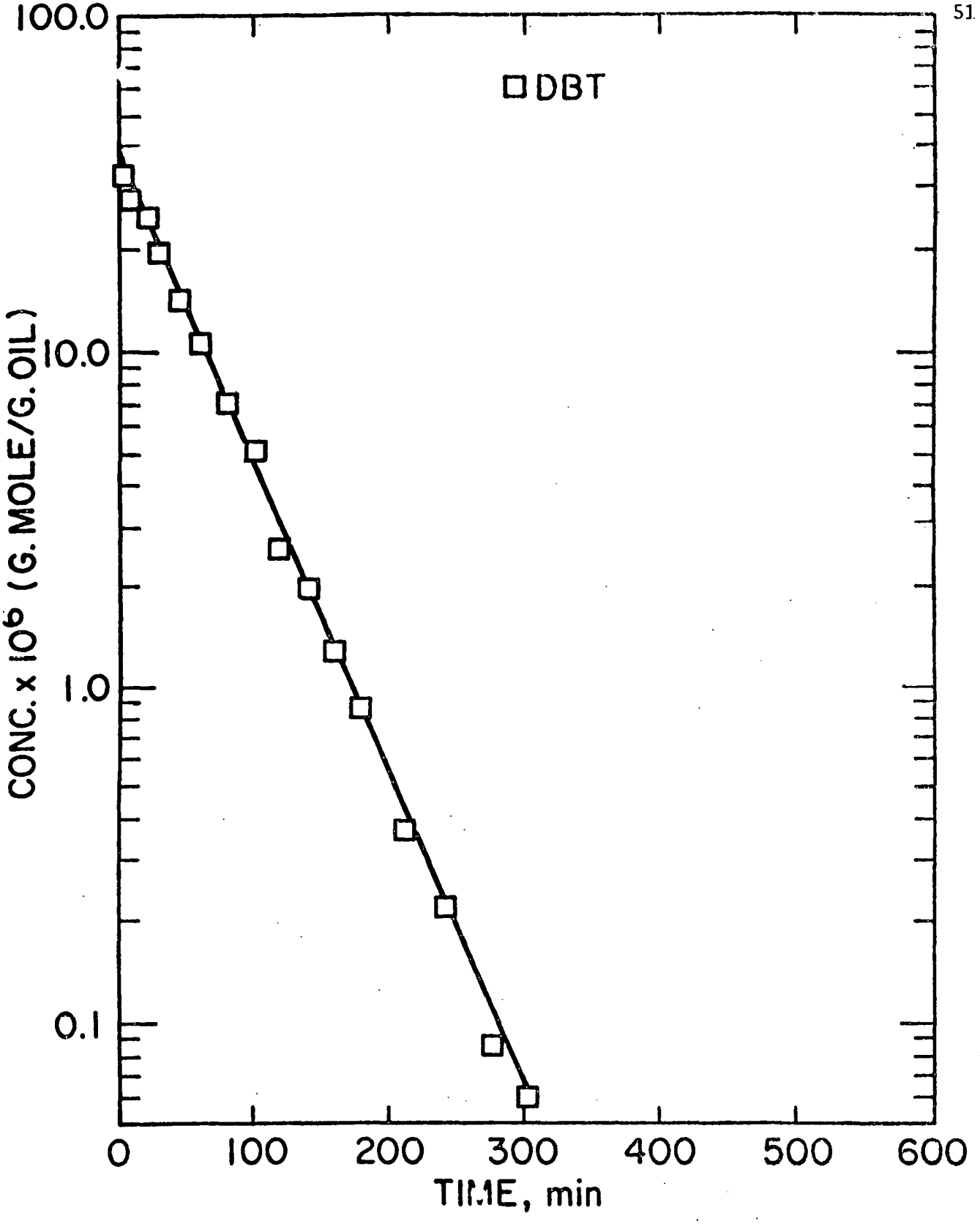

Figure 22. HDS of DBT (0.7 wt %).

remained constant within experimental error. This behavior was again attributed to formation of high molecular weight compounds.

Based on the above information and based on dibenzothiophene reaction network studies on presulfided Co-Mo/ -Al_2O_3 in our laboratory (Broderick et al.,), the reaction network was proposed (Fig. 26). All reactions in the network were assumed to follow pseudo first-order kinetics.

The rate constant for hydrogenation of cyclohexylbenzene to bicyclohexyl could not be evaluated directly due to lack of sufficient data. However, an estimate of the rate parameter was obtained using the following procedure.

Concentrations of cyclohexylbenzene and bicyclohexyl were measured experimentally at six values of reaction time. Smooth curves were drawn through the experimental data. At four values of reaction time, concentrations of the two compounds and the rate of formation of bicyclohexyl were estimated from the smooth curves. The rate parameter k_6 is given by equation (A) below:

$$(C_{cat}) \cdot \left(\frac{dc}{dt}\right)_{bicyclohexyl} = k_6 \cdot (C)_{cyclohexylbenzene} \qquad (A)$$

The average value of k_6 was estimated to be 0.056 ± 0.002 g oil/ g cat-min.

Summary

The reaction networks have been determined for quinoline and indole hydrodenitrogenation, naphthalene hydrogenation and dibenzothiophene hydrodesulfurization. The hydrodenitrogenation of quinoline

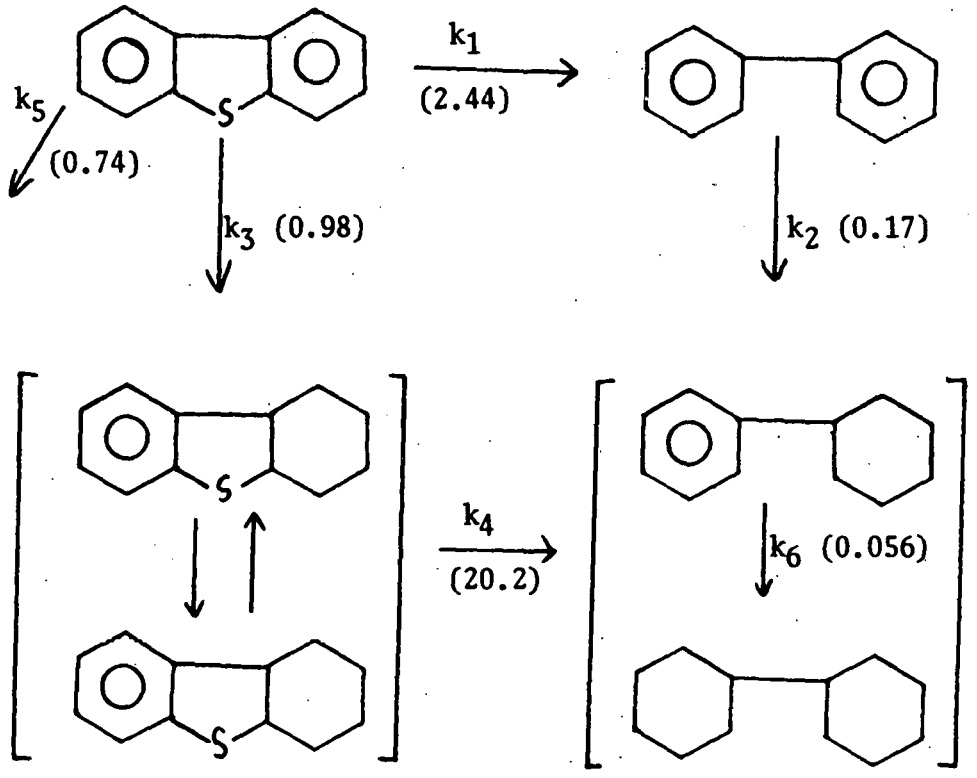

Figure 23. Reaction network for HDS of DBT

Kinetic analysis was carried out using the reaction network in Fig. 13. The rate constants are shown in Fig. 13. Solid lines in Fig. 14 represent predictions from the model and it can be seen that the predictions are in good agreement with experimental data.

and indole requires saturation of the nitrogen-containing ring prior to carbon-nitrogen bond scission; the reactions are bifunctional involving two kinds of catalytic sites. The hydrodesulfurization of dibenzothiophene occurs by two reaction routes, one involving and the other not involving prior hydrogenation. In single component studies, the overall reactivity decreases in the order:

naphthalene > dibenzothiophene > indole > quinoline.

b) Binary Interactions

Hydrogenation of naphthalene in the presence of quinoline

Three experiments were carried out determine the naphthalene-quinoline interaction under standard conditions. The initial naphthalene concentration was ~35 x 10^{-5} gmole/g oil (5 wt %) in all of the experiments. The initial quinoline concentration was 0.2, 0.5 and 2 wt % in the three experiments.

All hydrogenation steps in the naphthalene reaction network were strongly inhibited by quinoline. An interesting behavior was observed for rate of naphthalene hydrogenation. This is represented in Figs. 27-29 where log (concentration of naphthalene x 10^{6}, gmole/g oil) is plotted as a function of time (min). The rate of naphthalene hydrogenation followed first-order kinetic behavior to a given time (Region I) and then in a second region again followed first-order behavior but with a higher rate of reaction. This is contrary to the behavior expected for a reversible first-order reaction system in which the pseudo first-order rate should decrease as conversion increases at higher conversions.

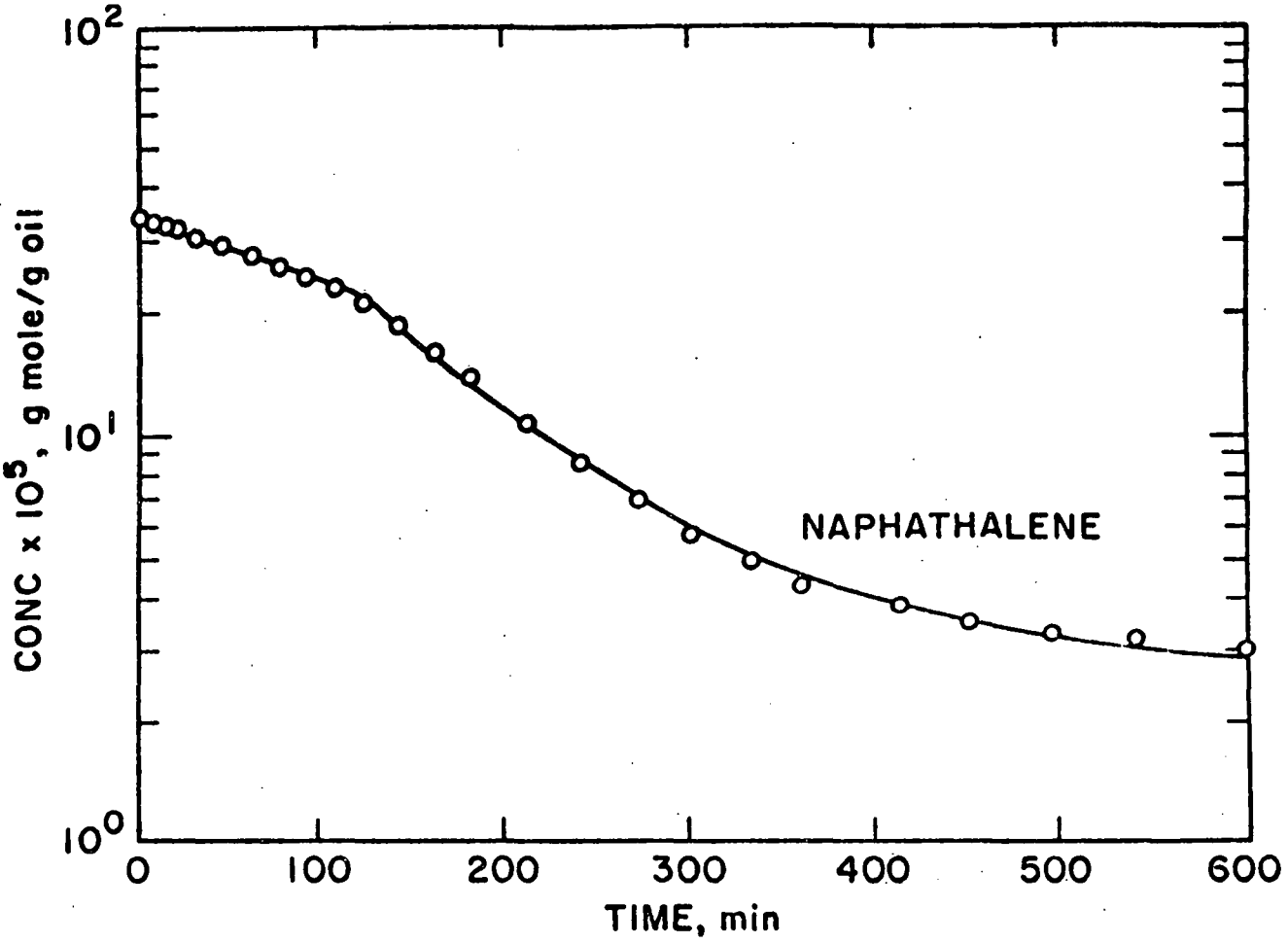

FIGURE 24. NAPHTHALENE HYDROGENATION (WITH 0.2 WT % QUINOLINE).

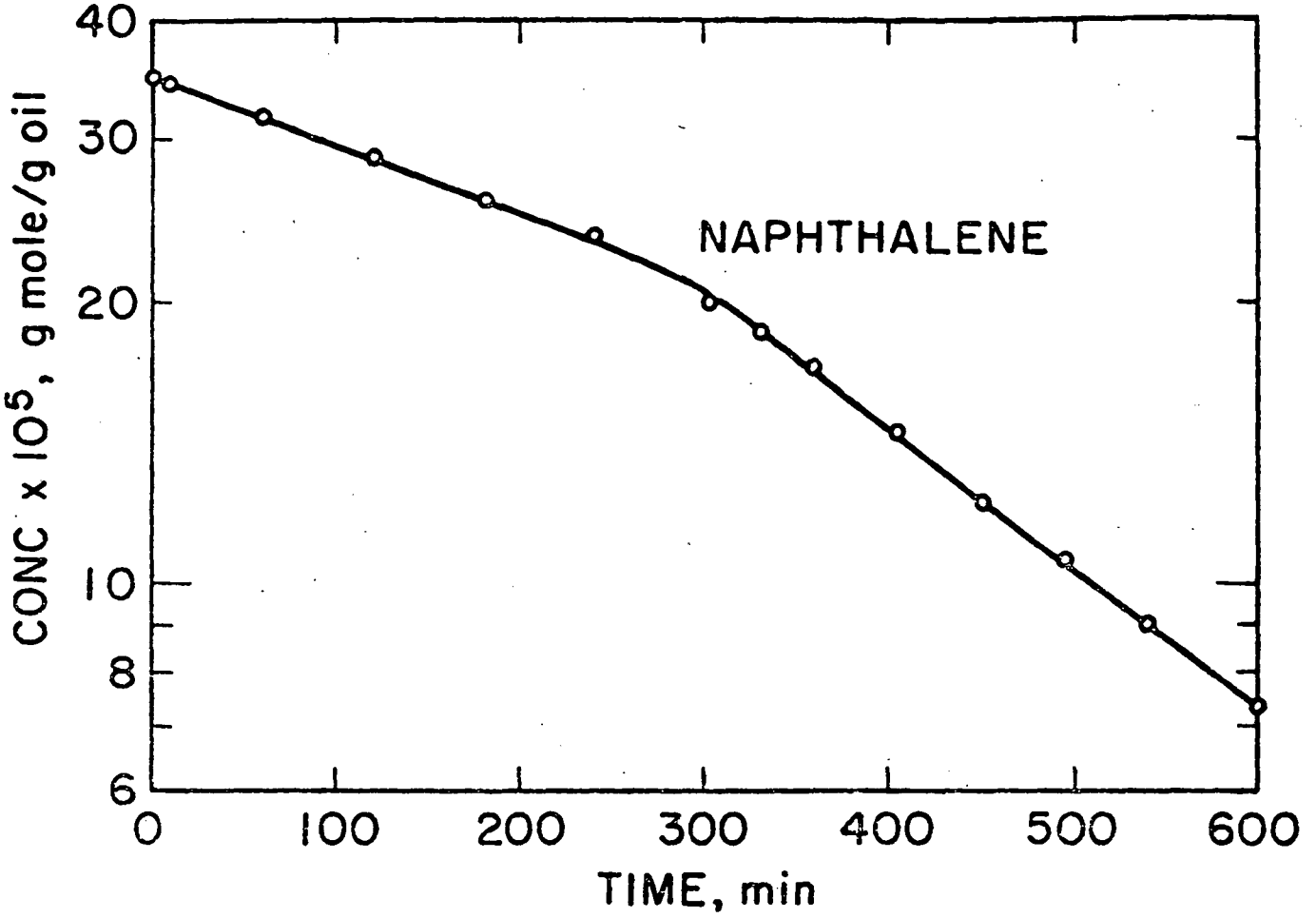

FIGURE 25. HYDROGENATION OF NAPHTHALENE (WITH 0.5 wt % QUINOLINE)

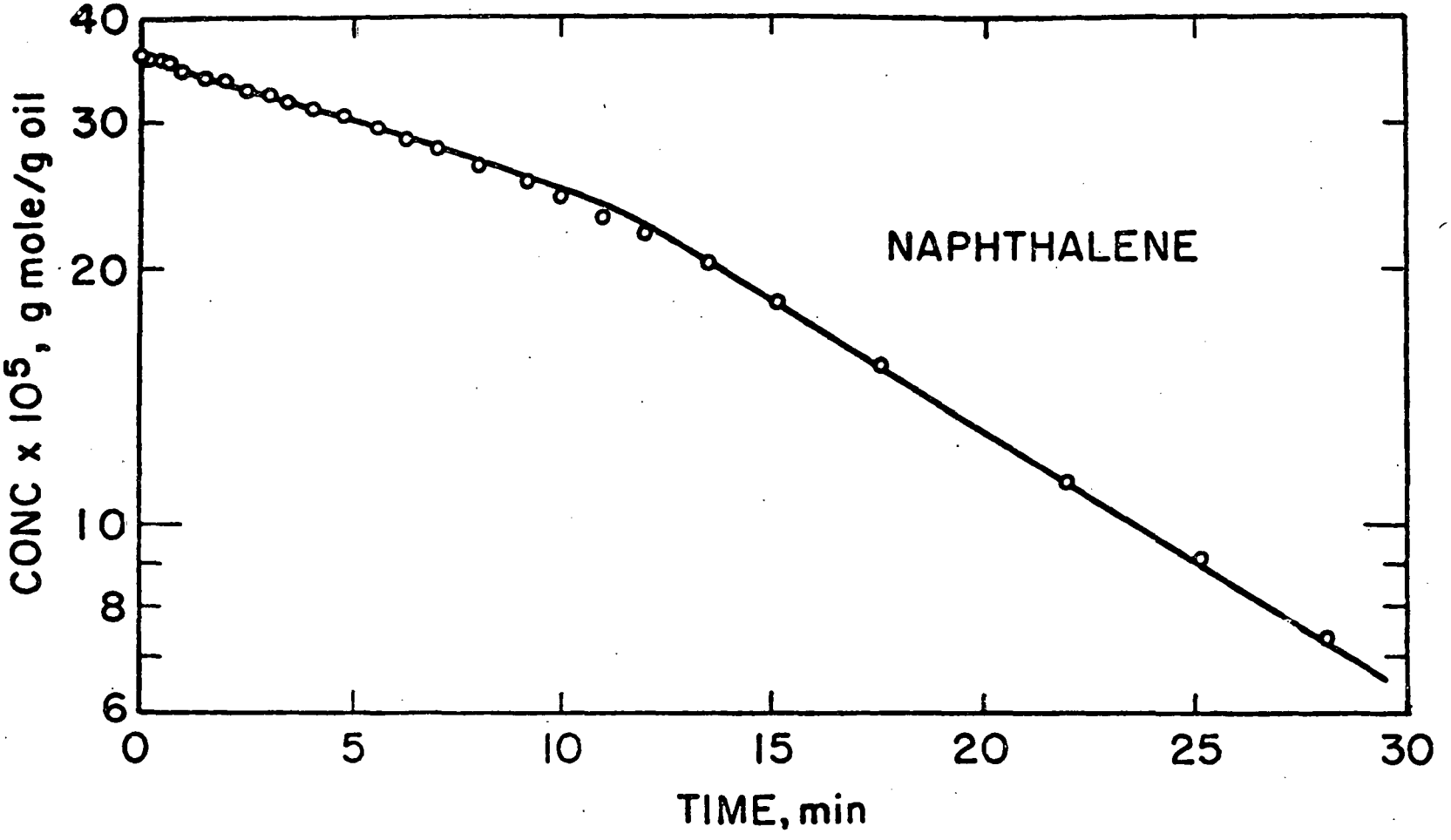

FIGURE 26. HYDROGENATION OF NAPHTHALENE (WITH 2.0 wt % QUINOLINE).

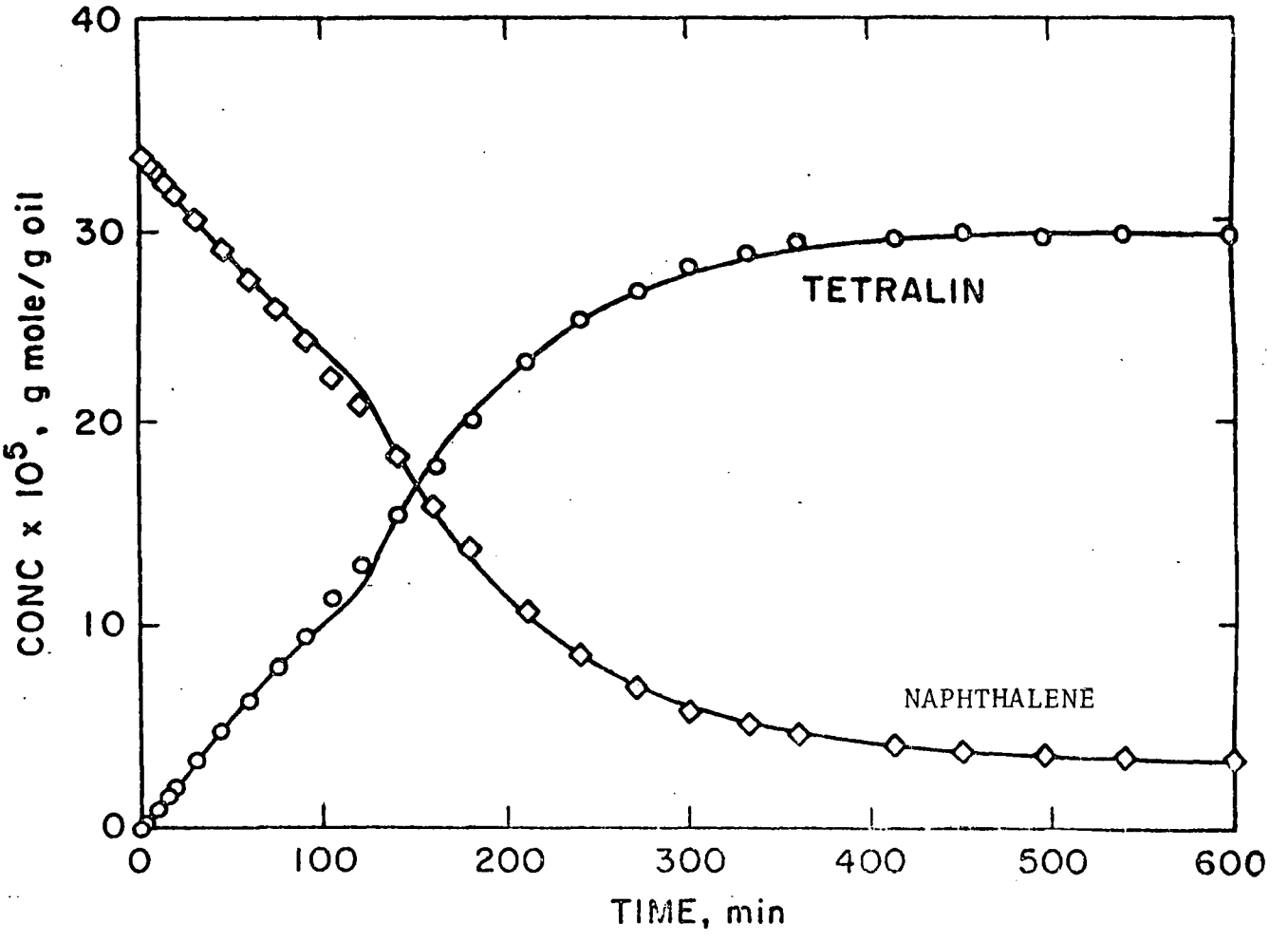

FIGURE 27. NAPHTHALENE HYDROGENATION (WITH 0.2 WT % QUINOLINE).

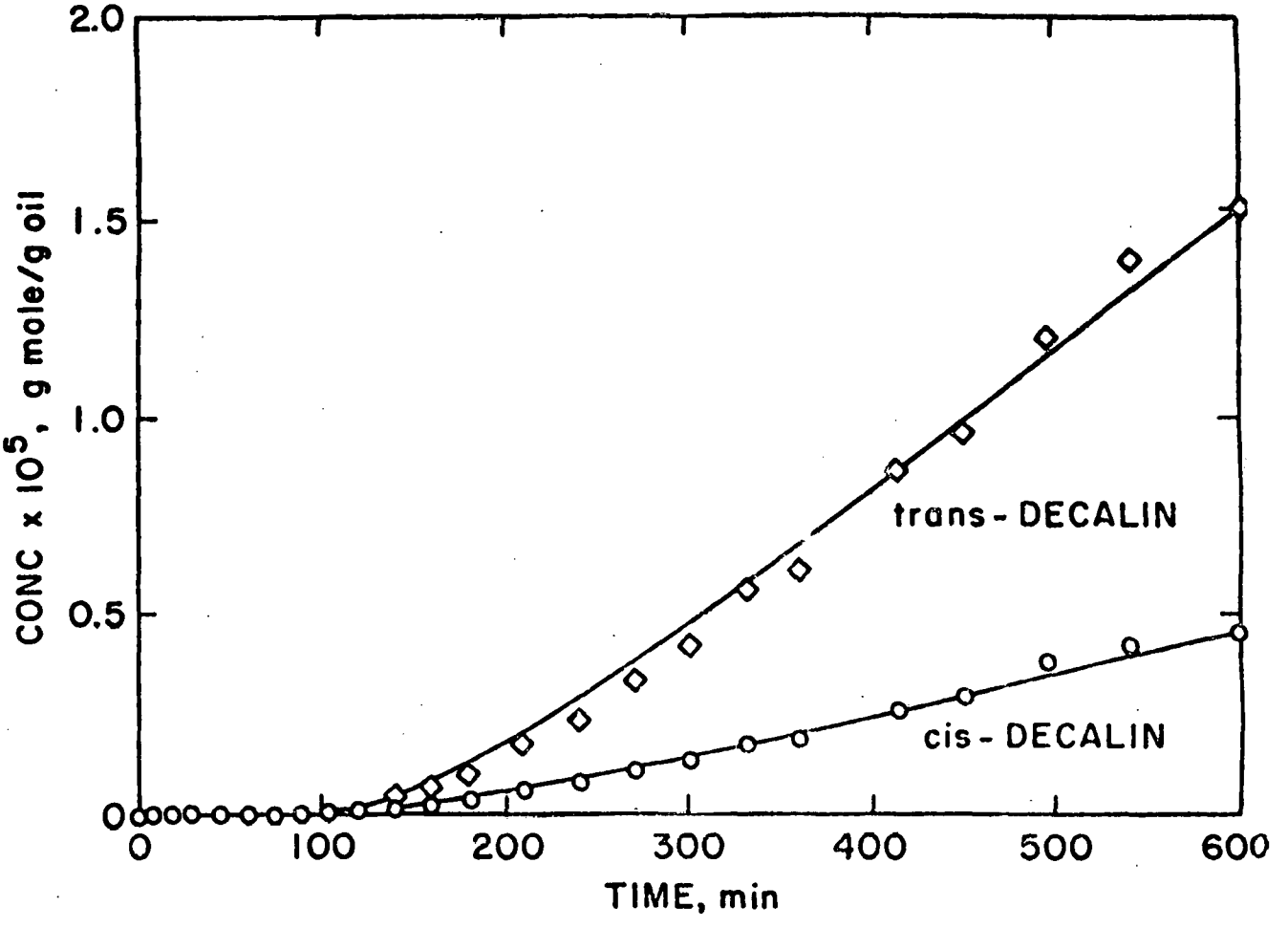

FIGURE 28. NAPHTHALENE HYDROGENATION (WITH 0.2 wt % QUINOLINE)

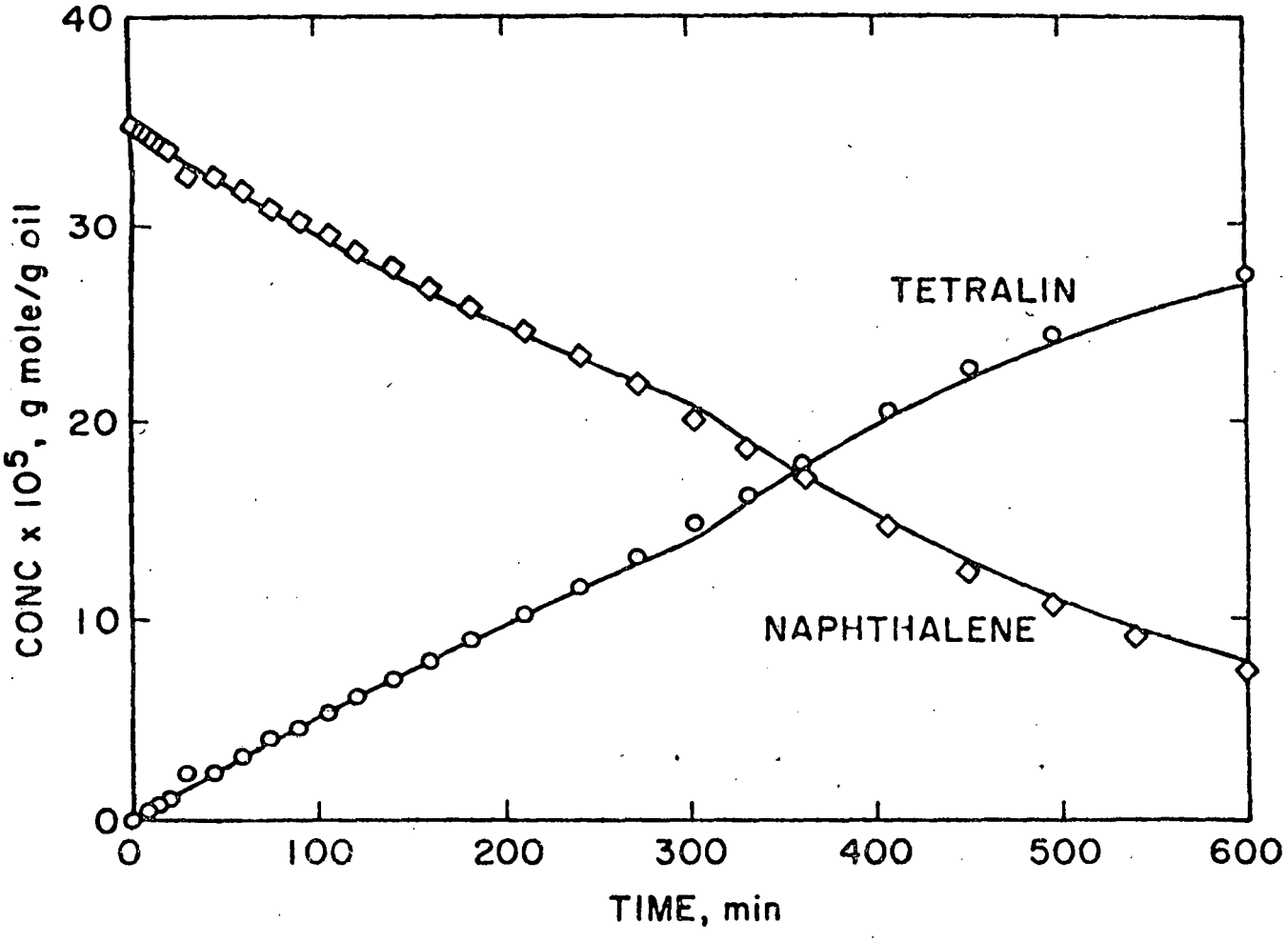

FIGURE 29. NAPHTHALENE HYDROGENATION (WITH 0.5 wt % QUINOLINE).

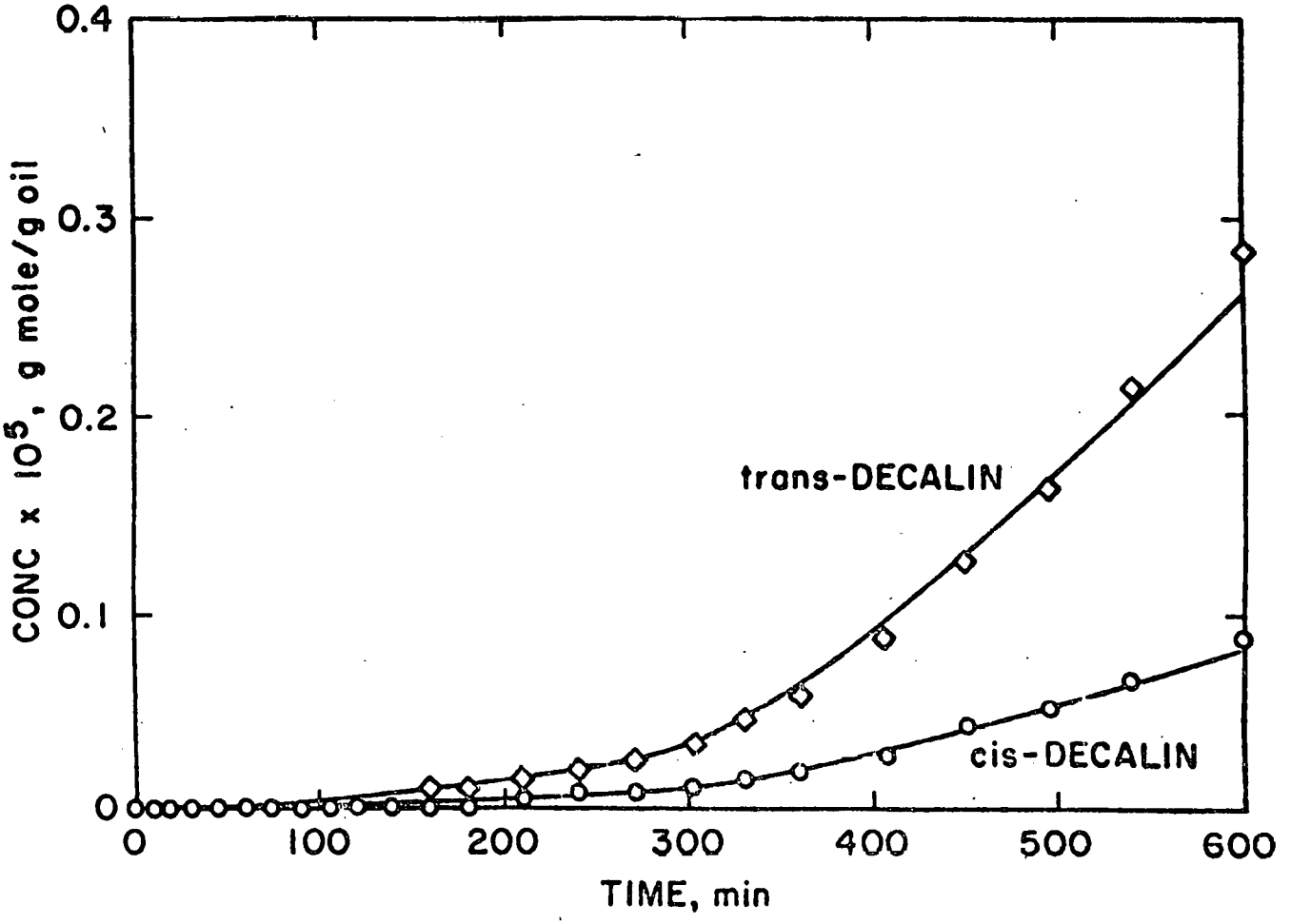

FIGURE 30. NAPHTHALENE HYDROGENATION WITH 0.5 WT % QUINOLINE

Product concentrations vs time for naphthalene hydrogenation in the presence of 0.2 and 0.5 wt % quinoline are presented in Figs. 30-33. All of the reaction rates increased at large conversions; this is particularly evident in the case of experiment with 0.2 wt % quinoline in which the rate of hydrogenation was the least inhibited; also, in this case, at very high conversions the rate of naphthalene hydrogenation decreased after an initial increase suggesting that reverse reaction from tetralin to naphthalene became kinetically important at high conversions.

Product distribution for naphthalene hydrogenation in the presence of 2 wt % quinoline was similar to those in Figs. 44-47.

A comparison of product concentration vs time data for naphthalene hydrogenation and for quinoline HDN indicated that quinoline and all of its nitrogen-containing reaction intermediates were present in region I, whereas o-propylaniline and ammonia were important nitrogen-containing compounds in region II. Since hydrogenation reactions were less inhibited in region II, it can be concluded that o-propylaniline is relatively less effective in inhibiting hydrogenation reactions.

The relative strength of different nitrogen-containing compounds in inhibiting hydrogenation reactions will be further discussed in the next report. For the time being, it should be sufficient to say that the rate parameters in naphthalene reaction network were estimated separately for regions I and II.

The hydrogenation of naphthalene to tetralin was assumed irreversible for all cases except for region II in the experiment with the smallest quinoline concentration where the reverse reaction was kinetically important.

For naphthalene hydrogenation experiment in the absence of quinoline, naphthalene $\underset{k_2}{\overset{k_1}{\rightleftharpoons}}$ tetralin equillibrium was established where k_1/k_2 was equal to 15. To verify the assumption that the dehydrogenation reaction of tetralin to naphthalene in the presence of quinoline was indeed negligible, the rate parameters were reestimated by assuming $k_2 = k_1/15$. The new estimates of the rate parameters were within 3% of the previously estimated values, where the reverse reaction was not included.

Figures 34-39 demonstrate the strong inhibition of hydrogenation reactions by quinoline and its reaction products. Solid lines in these figures are predictions from Langmuir-Hinshelwood type model which will be discussed in Chapter VI.

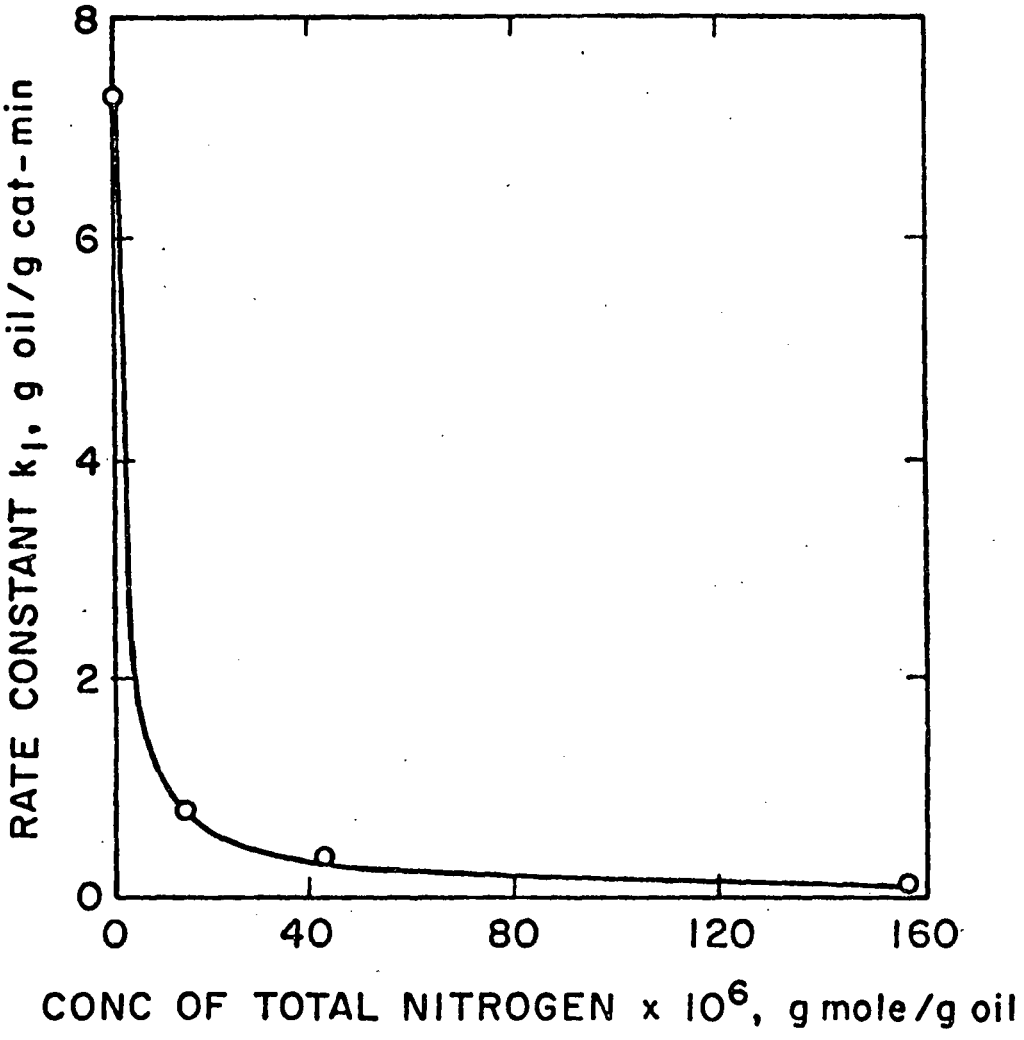

FIGURE 31. INHIBITION OF NAPHTHALENE HYDROGENATION BY QUINOLINE, REGION I.
NAPHTHALENE CONCENTRATION - 5 WT %

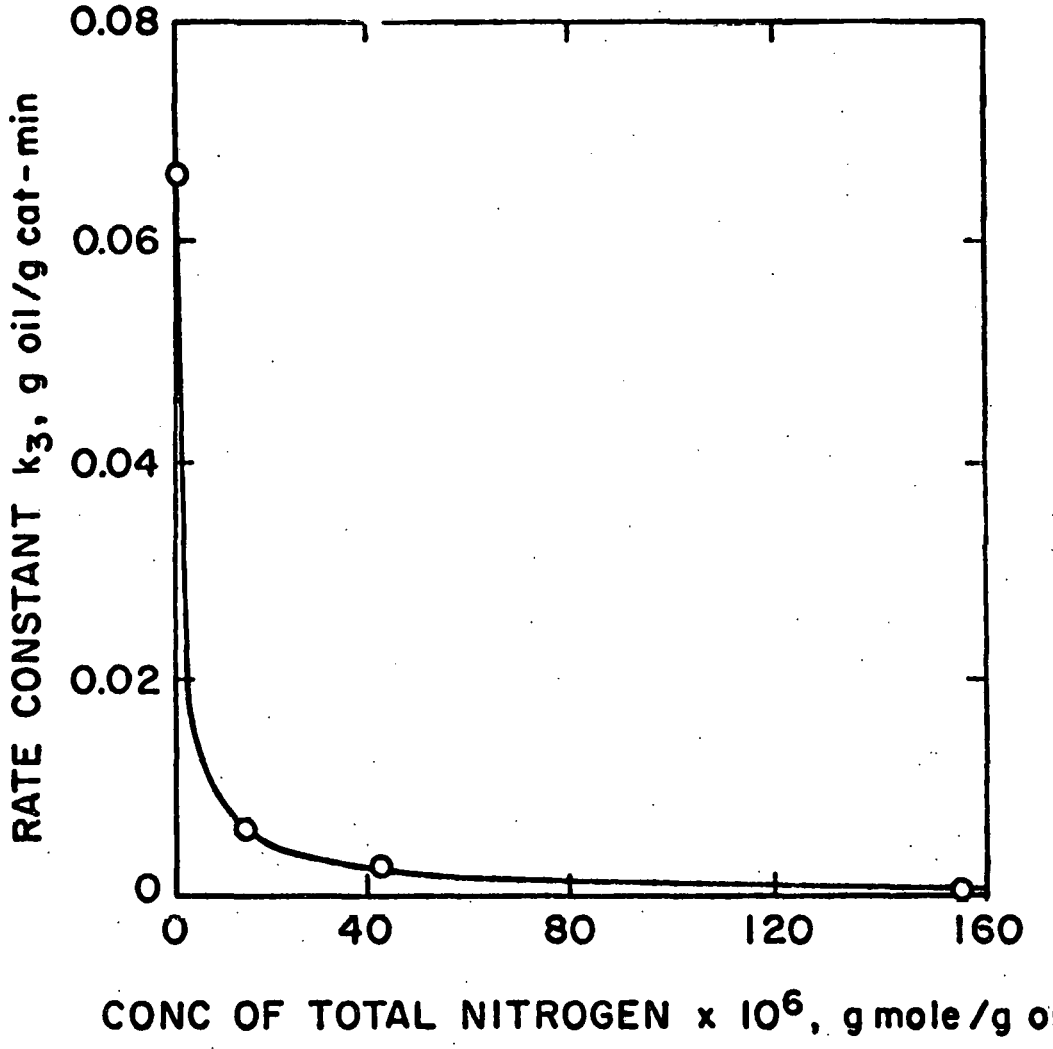

FIGURE 32. INHIBITION OF NAPHTHALENE HYDROGENATION BY QUINOLINE, REGION I.

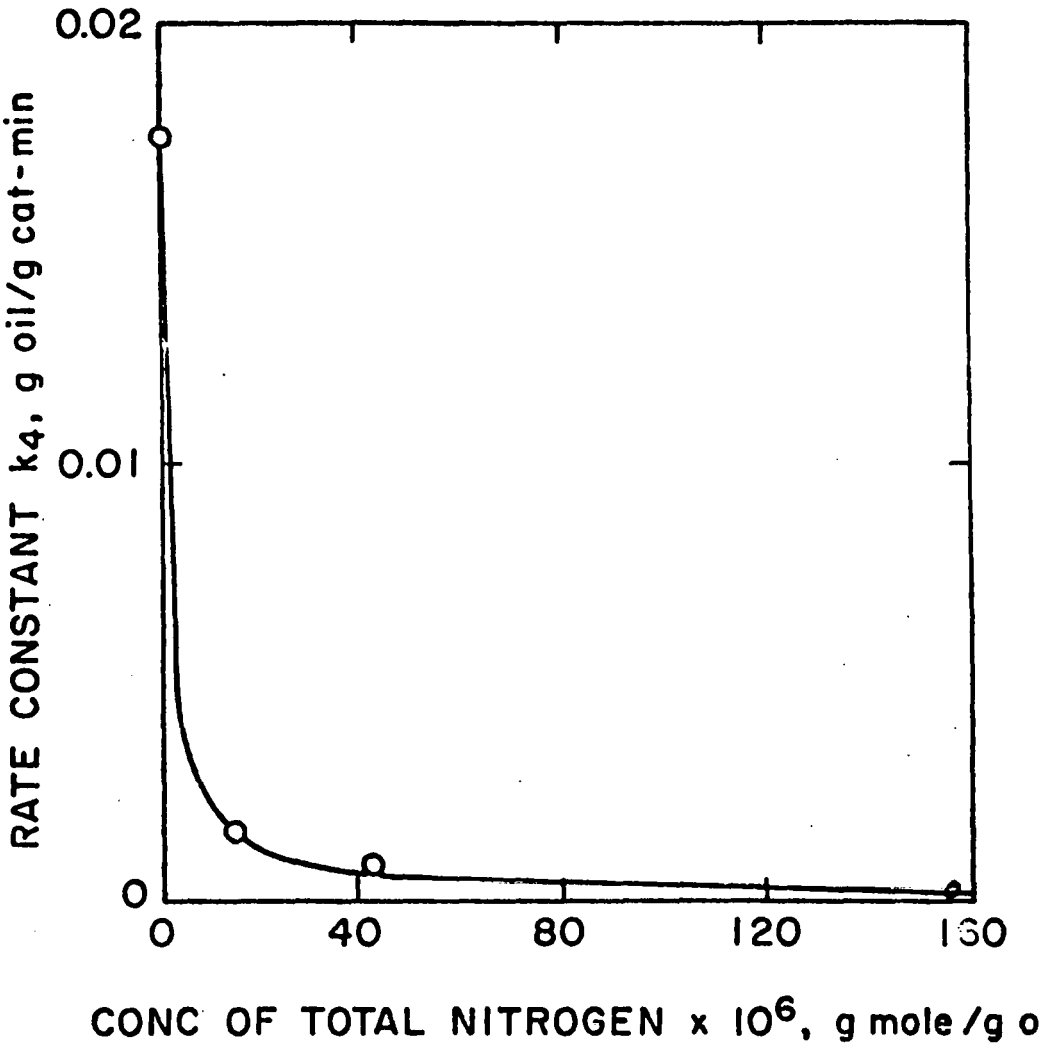

FIGURE 33. INHIBITION OF NAPHTHALENE HYDROGENATION BY QUINOLINE, REGION I. 5 WT % NAPHTHALENE

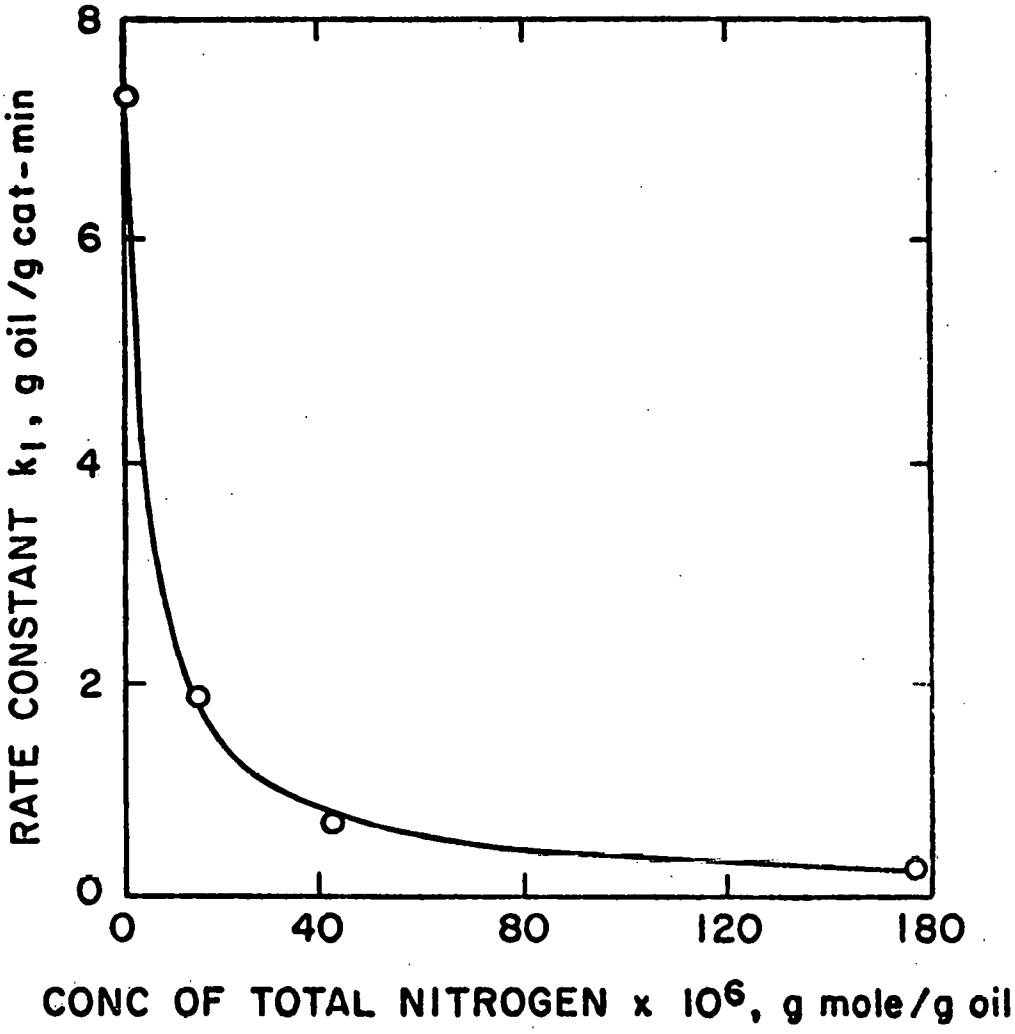

FIGURE 34. INHIBITION OF NAPHTHALENE HYDROGENATION BY QUINOLINE, REGION II.
5 WT % NAPHTHALENE

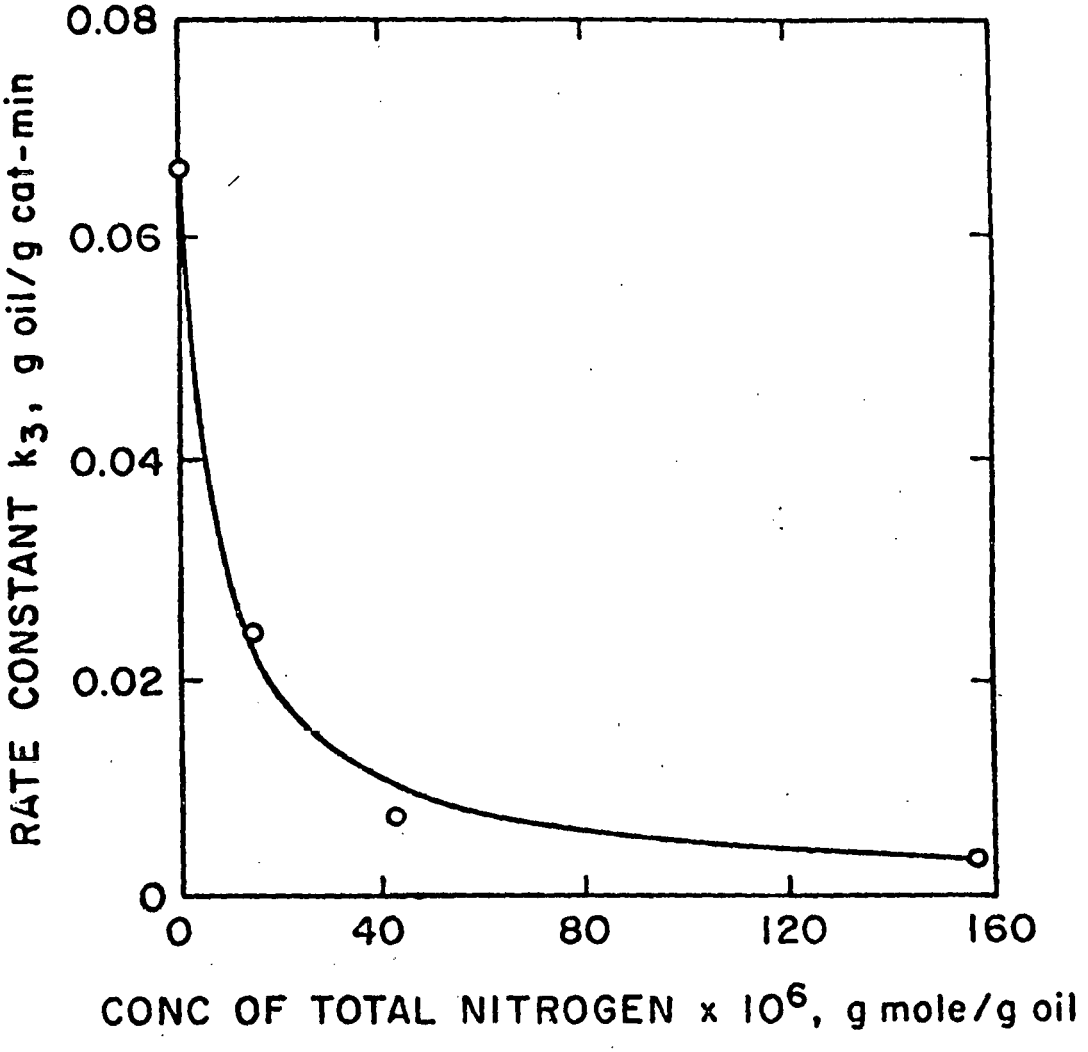

FIGURE 35. INHIBITION OF NAPHTHALENE HYDROGENATION BY QUINOLINE, REGION II.
5 WT % NAPHTHALENE

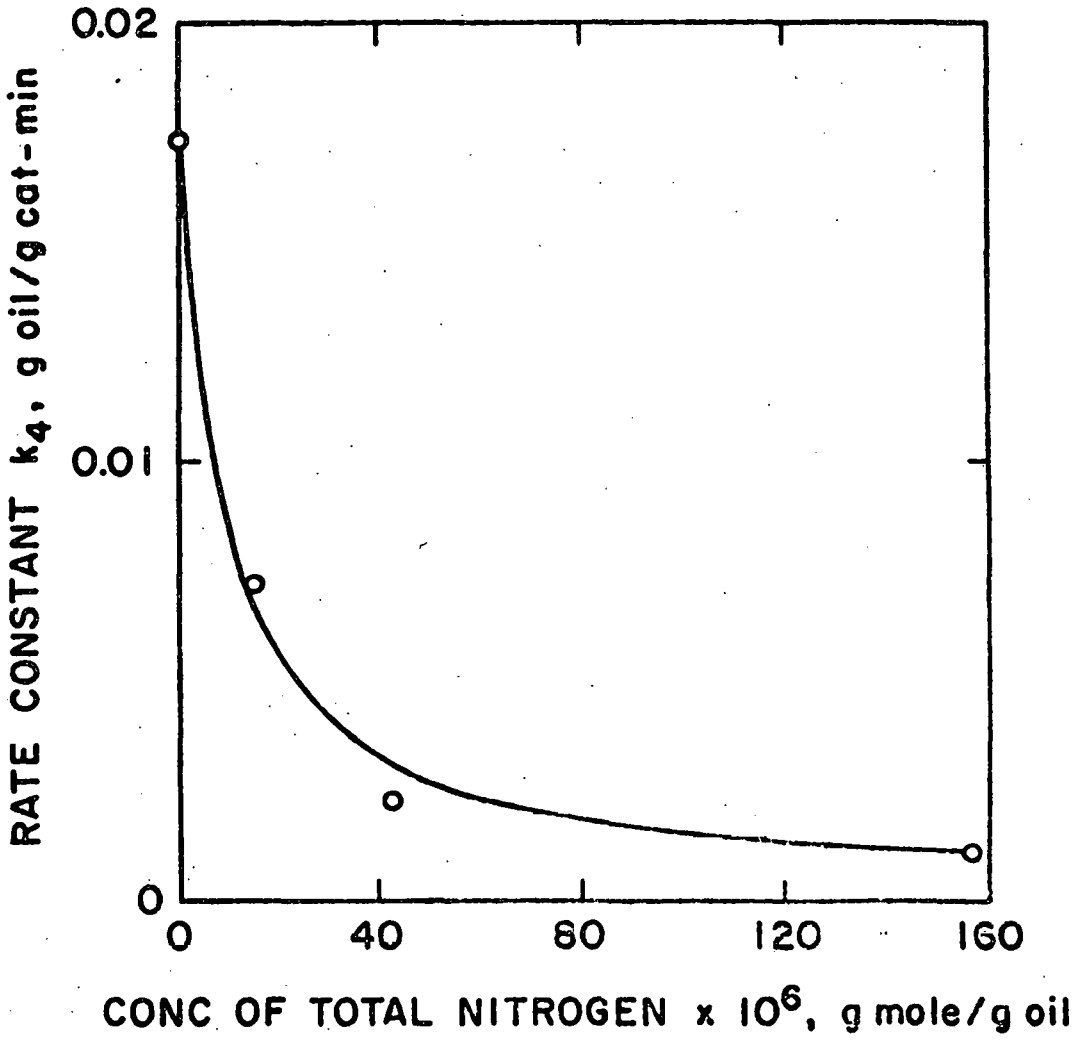

FIGURE 36. INHIBITION OF NAPHTHALENE HYDROGENATION BY QUINOLINE, REGION II.
5 WT % NAPHTHALENE

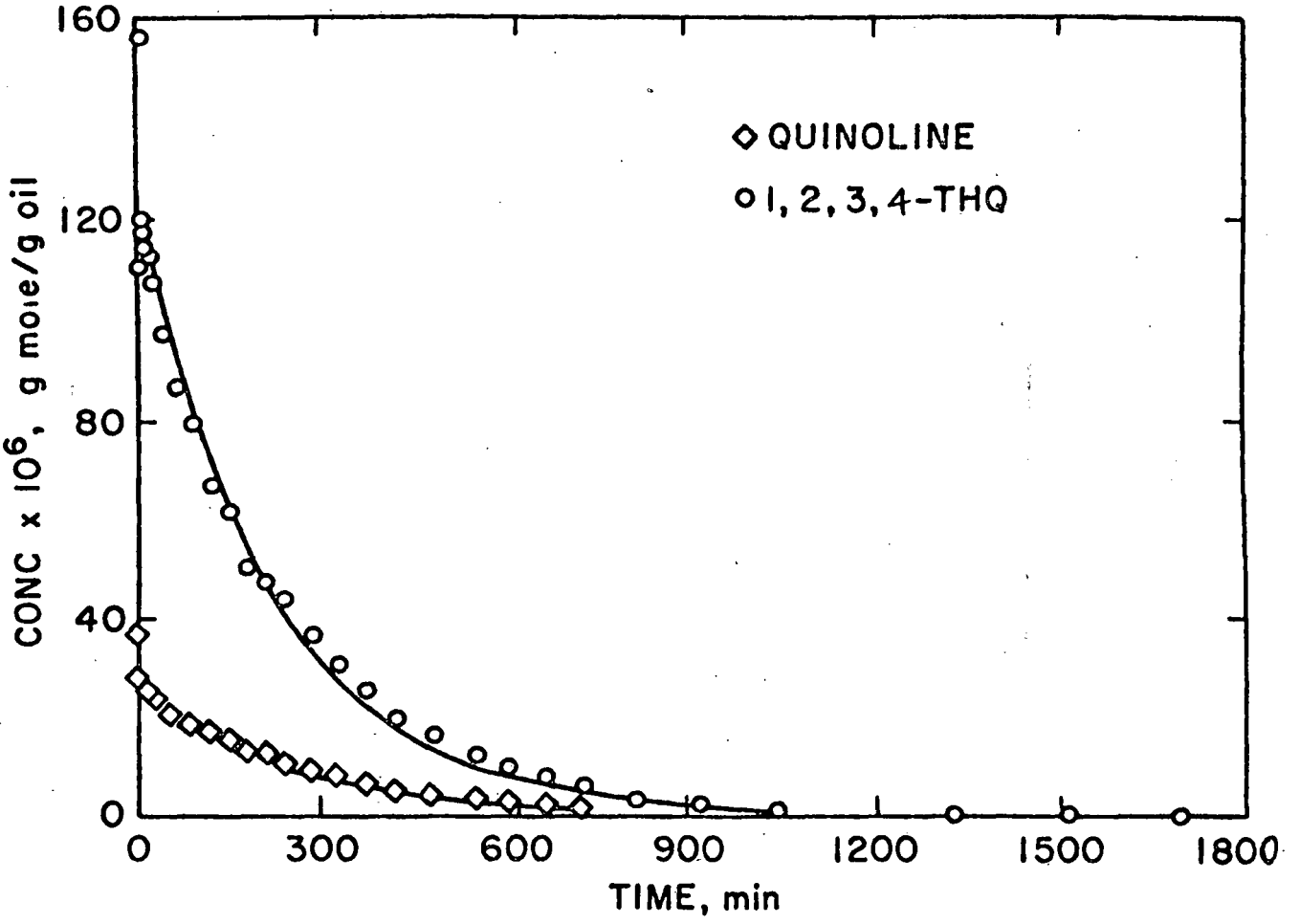

FIGURE 37. QUINOLINE HDN AT STANDARD CONDITIONS:
CONCENTRATION OF QUINOLINE 2 WT %

CONCENTRATION OF NAPHTHALENE 5 WT %

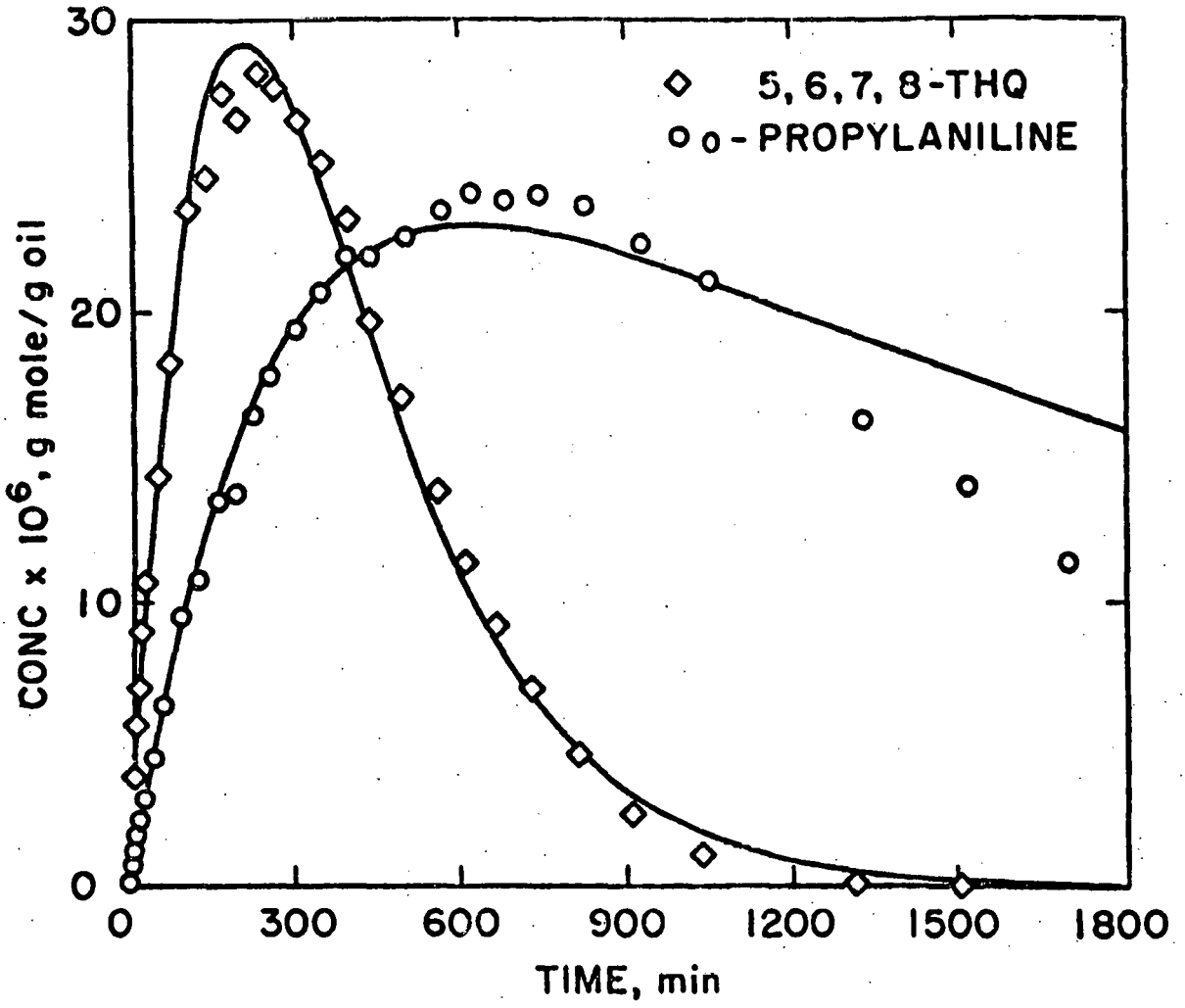

FIGURE 38. QUINOLINE HDN AT STANDARD CONDITIONS.
2 WT % QUINOLINE

5 WT % NAPHTHALENE

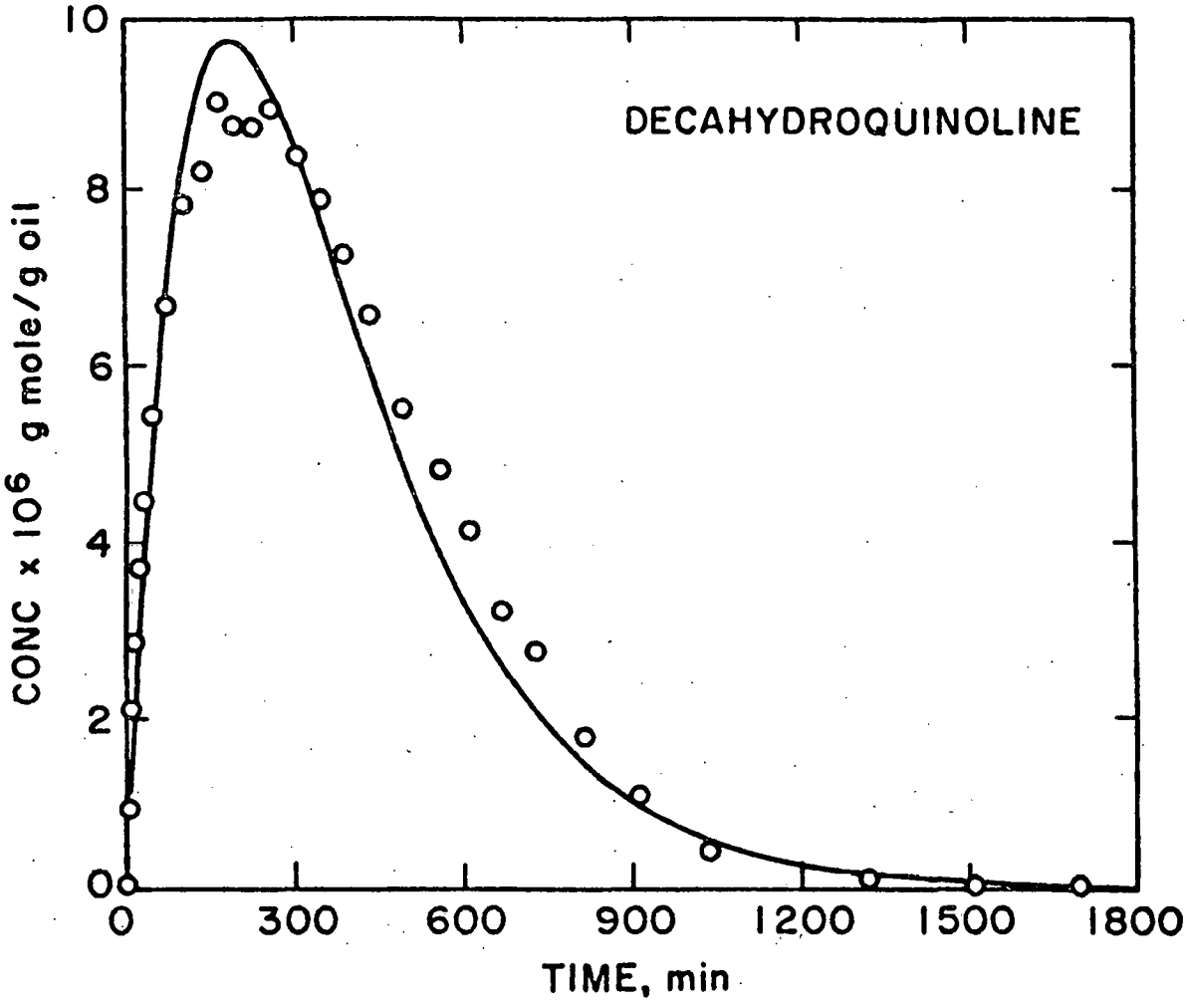

FIGURE 39. QUINOLINE HDN AT STANDARD CONDITIONS.

2 WT % QUINOLINE
5 WT % NAPHTHALENE

Hydrodenitrogenation of Quinoline in the Presence of Naphthalene

HDN of quinoline in the presence of naphthalene was studied in three experiments, under standard conditions (Table 1). Initial concentration of naphthalene was 5 wt % in all three experiments while the quinoline concentration was 0.2, 0.5 and 2.0 wt %, respectively.

A typical concentration-time data for HDN of quinoline (2 wt %) is presented in Figs. 40-42. Total nitrogen removal and the rate of disappearance of lumped group of quinoline and 1,2,3,4-tetrahydroquinoline followed pseudo first-order kinetics in all experiments.

Solid lines in Figs. 40-42 are predictions from the HDN reaction network model using the best-fit set of pseudo first-order rate constants the predictions are in good agreement with the experimental data.

It can be seen from Figs. 43-47 that all reactions in the quinoline HDN reaction network are inhibited by nitrogen-containing compounds. The behavior of apparent rate constant as a function of total nitrogen concentration in Figs. 43-48 is typical of Langmuir-type adsorption. The solid lines in Figs. 43-48 are predictions from Langmuir-Hinshelwood type models which will be discussed in the next report.

HDN of indole in the presence of quinoline

To study the interaction between non-basic and basic nitrogen-containing compounds, HDN of indole was carried out in the presence of quinoline under standard conditions (Table I). The initial concentrations of each of the reactants was 35×10^{-6} gmole/g oil (0.5 wt %). Product distribution for indole-compounds was similar to that obtained

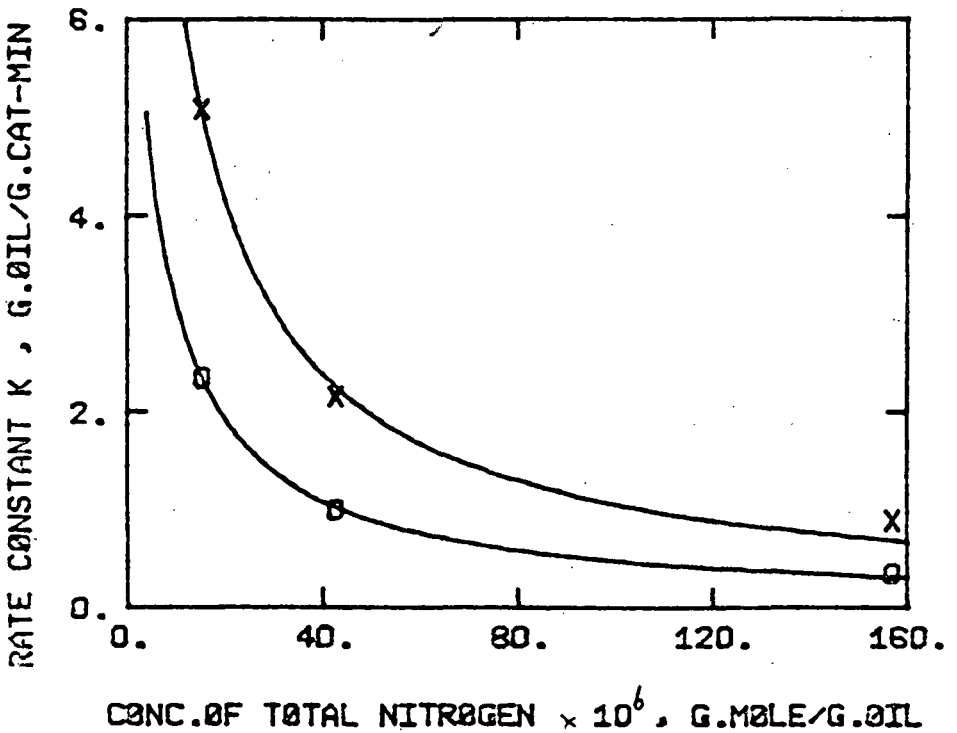

Figure 40. Effect of quinoline concentration on HDN of quinoline
x = $k_{(quinoline + 1,2,3,4\text{-THQ})}$
□ = $k_{total\ nitrogen}$

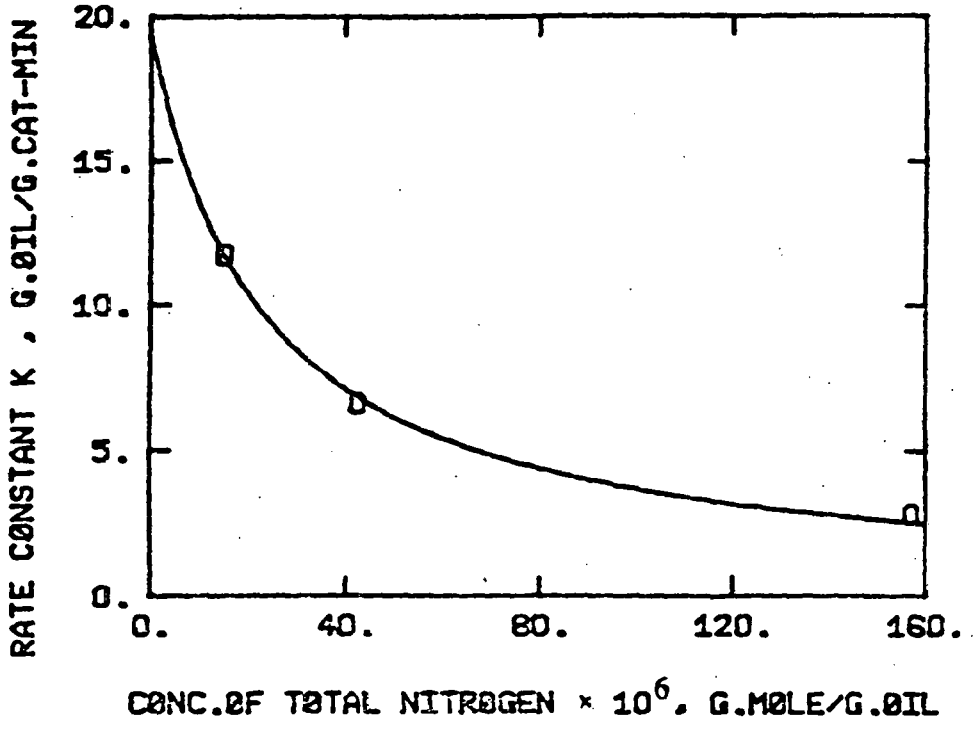

Figure 41. Effect of quinoline concentration on HDN of quinoline.
k_Q → 5,6,7,8-THQ

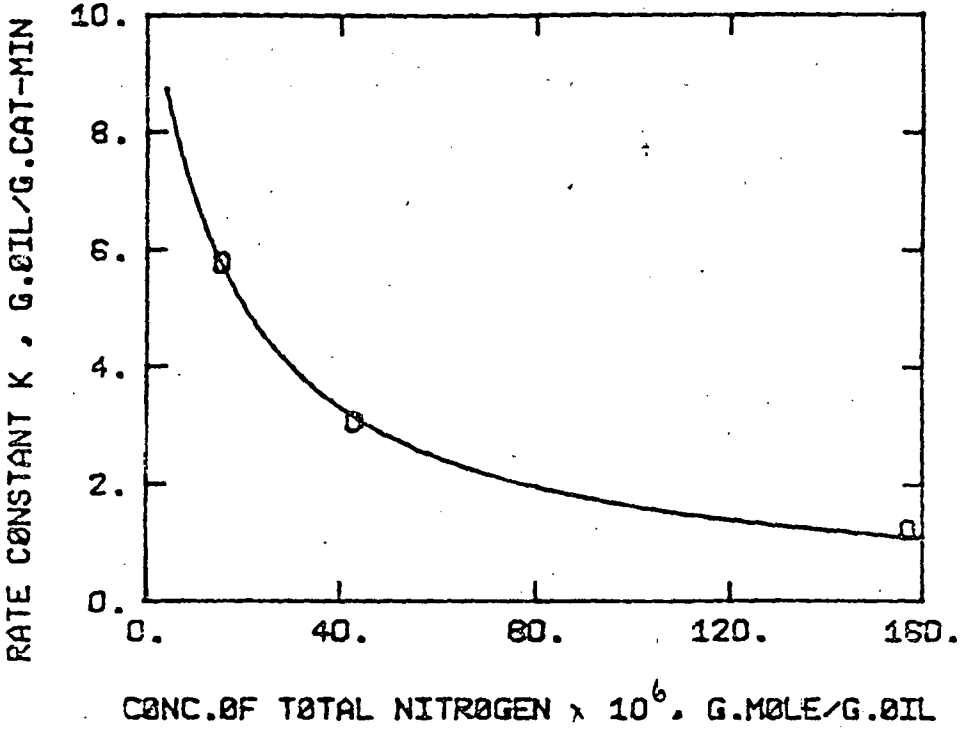

Figure 42. Effect of quinoline concentration on HDN of quinoline.
$k_{5,6,7,8\text{-THQ} \rightarrow \text{DHQ}}$

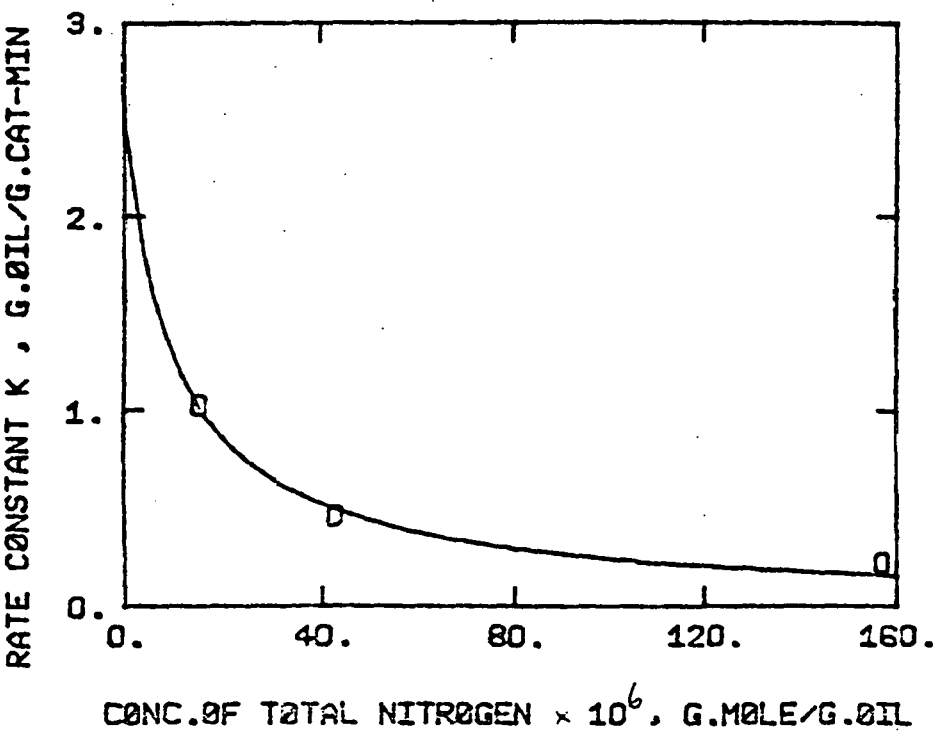

Figure 43. Effect of quinoline concentration on HDN of quinoline.
$k_{1,2,3,4\text{-THQ} \rightarrow \text{OPA}}$

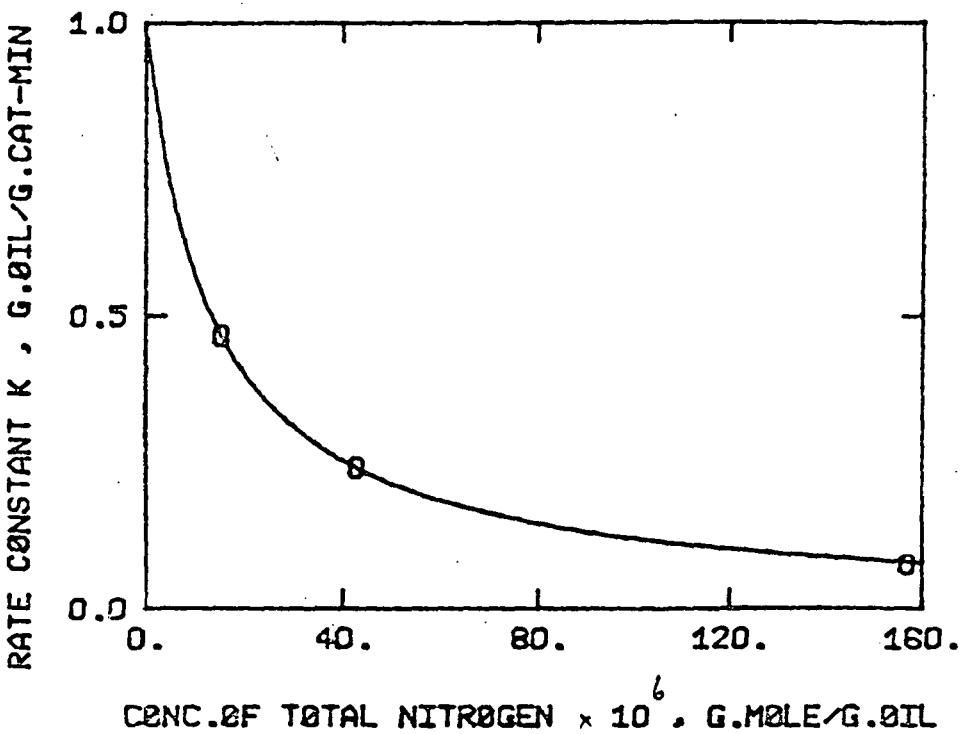

Figure 44. Effect of quinoline concentration on HDN of quinoline. k_{OPA} → H.C.

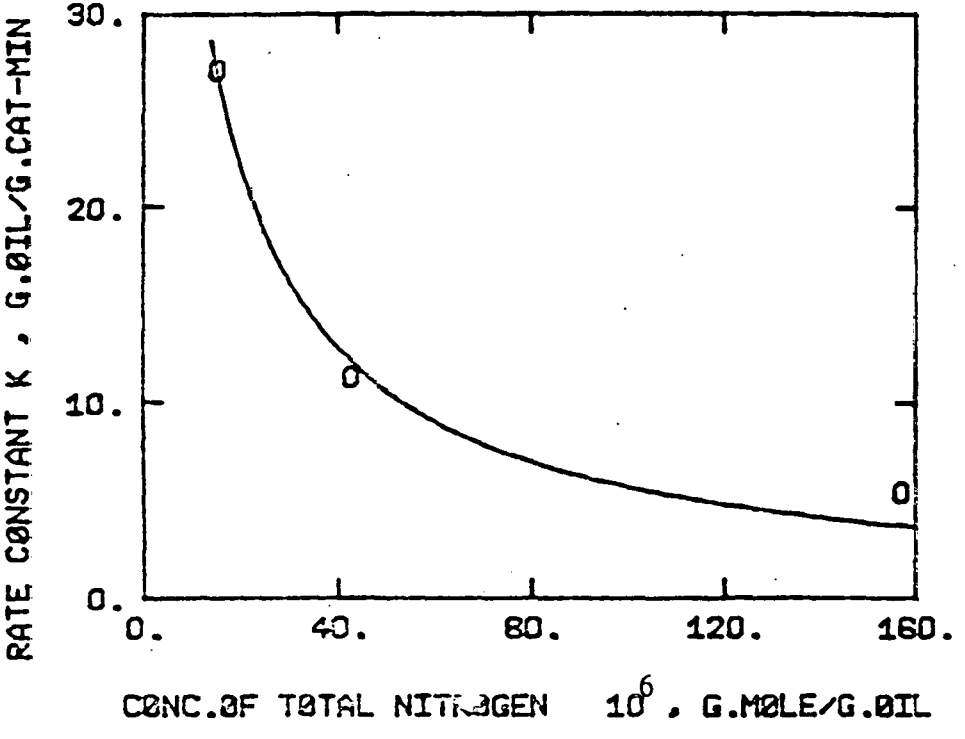

Figure 45. Effect of quinoline concentration on HDN of quinoline.
$k_{(DHQ \rightarrow H.C. + NH_3)}$

in single compound studies; however, all reactions progressed at slower rates, again showing that basic compounds adsorb strongly on catalyst surface inhibiting the rate of reaction. All reactions in the indole reaction network were markedly inhibited in the presence of quinoline.

HDN of quinoline in the presence of indole

Product distribution for quinoline HDN reaction in the presence of indole was similar to that observed in single component studies. The effect of indole on the HDN of quinoline was not important.

HDS of DBT in the presence of quinoline

Three experiments were carried out under standard conditions (Table I) to study HDS of DBT in the presence of quinoline. The initial concentration of DBT was ~0.7 wt % and the initial quinoline concentration was ~0.2, ~0.5 and ~2 wt % in the three experiments.

All reactions in the HDS reaction network were retarded in the presence of quinoline. In the experiment with 0.5 wt % initial quinoline concentration, some tetrahydroDBT was observed, but no hexahydroDBT could be detected. In the experiment with 2 wt % quinoline, none of the sulfur-containing reaction intermediates were detected in the reactor samples. Bicyclohexyl was not detected in any of the experiments with quinoline present.

Product distributions for HDS reaction in the presence of 0.5 and 2 wt % quinoline are shown in Figs. 49-51. No significant loss in mass balance was observed in any of the inhibition runs suggesting that active sites responsible for polymerization reactions were poisoned by

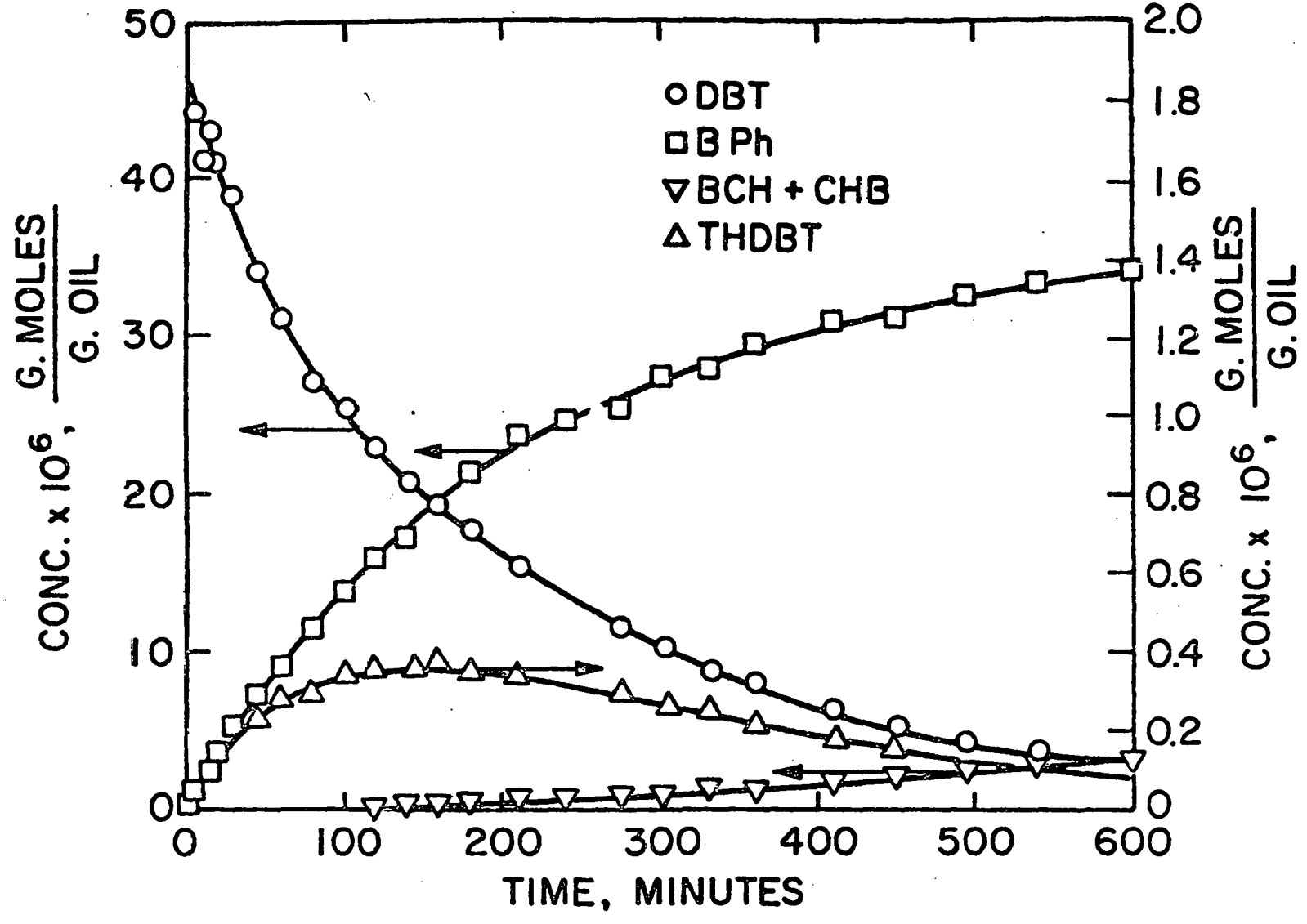

Figure 46. HDS of 0.7 wt % dibenzothiophene (with 0.5 wt % quinoline).

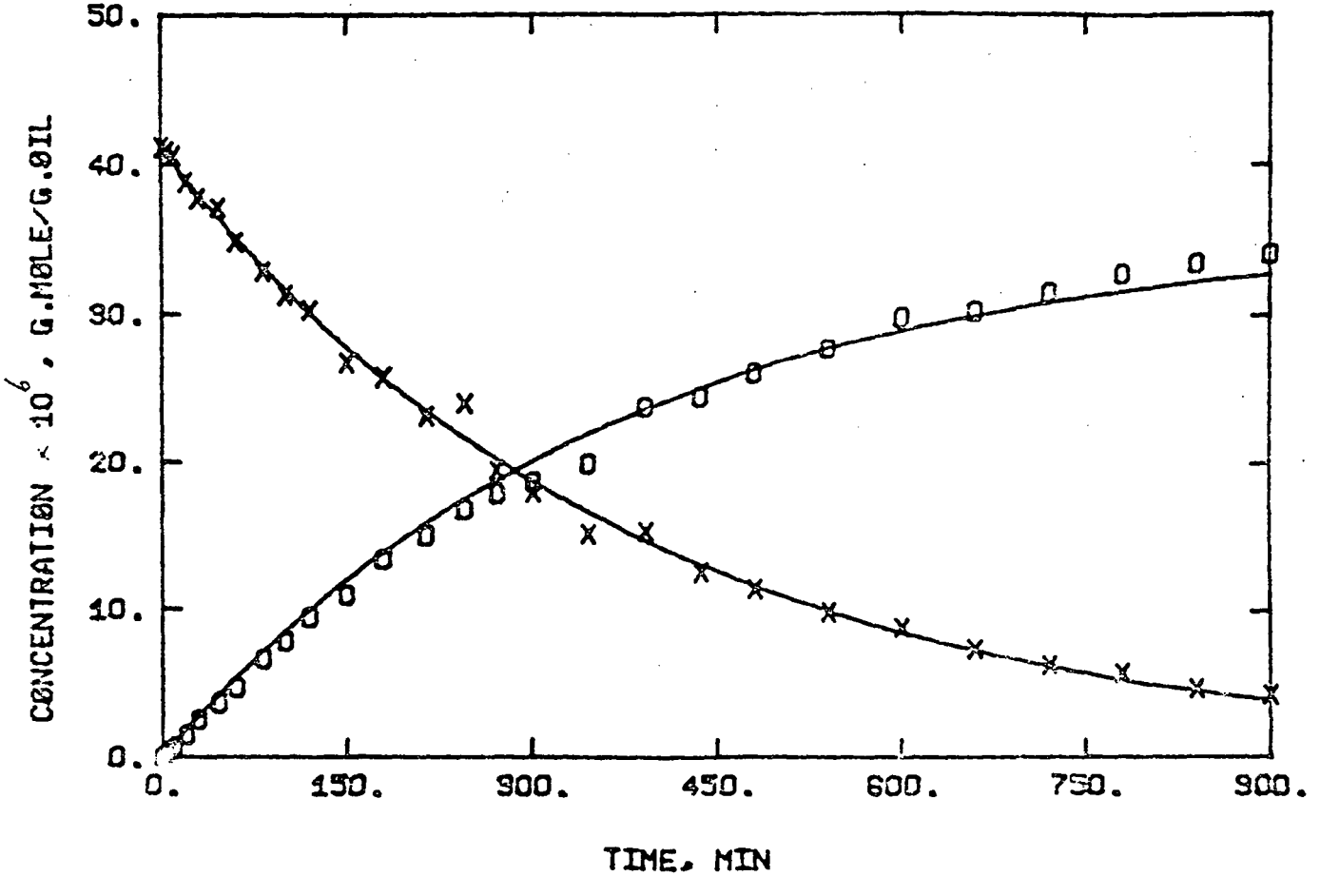

Figure 47. HDS of 0.7 wt % DBT (with 2 wt % quinoline).
x = dibenzothiophene
□ = biphenyl

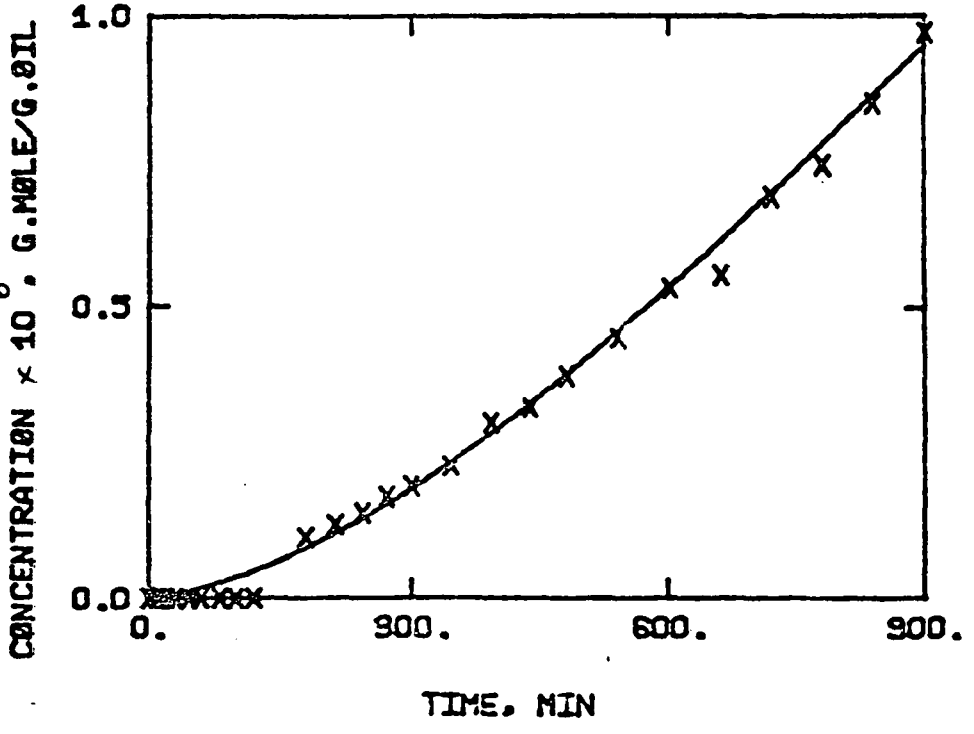

Figure 48. HDS of 0.7 wt % DBT (with 2 wt % quinoline); x = cyclohexylbenzene.

quinoline. The reaction step k_5 (Fig. 26) was, however, included in the parameter estimation routine. In the experiment with 2.0 wt % quinoline, no hydrogenated dibenzothiophenes were detected hence k_3 and k_4 could not be estimated for these runs. However, a reaction step k_3 was included to represent direct reaction of DBT to cyclohexylbenzene. This procedure was justified on the basis that $k_4 >> k_3$, i.e., hydrogenated dibenzothiophenes are reacted as soon as they are formed. The value of k_3 obtained by this procedure can be a good estimate of the rate of hydrogenation of dibenzothiophene; this procedure also allows a more correct estimation of k_2, the rate of hydrogenation of biphenyl to cyclohexylbenzene.

Solid lines in Figs. 49-51 are model predictions which are in good agreement with experimental data.

Figs. 52-56 show the inhibition effect on the HDS reactions of initial quinoline concentration. The solid lines in these figures are predictions from a Langmuir-Hinshelwood type model which will be discussed in the next report.

In inhibition studies of naphthalene

$$\frac{M_o}{M_c}\frac{dCl}{dt} = k_{ij}C_i$$

hydrogenation by quinoline, two distinct regions of inhibition were observed. These two regions were not clearly visible during inhibited hydrodesulfurization studies. Analysis of data revealed that: (1) the rate of biphenyl hydrogenation increased at higher conversions in experiments with 0.2 and 0.5 wt % quinoline.

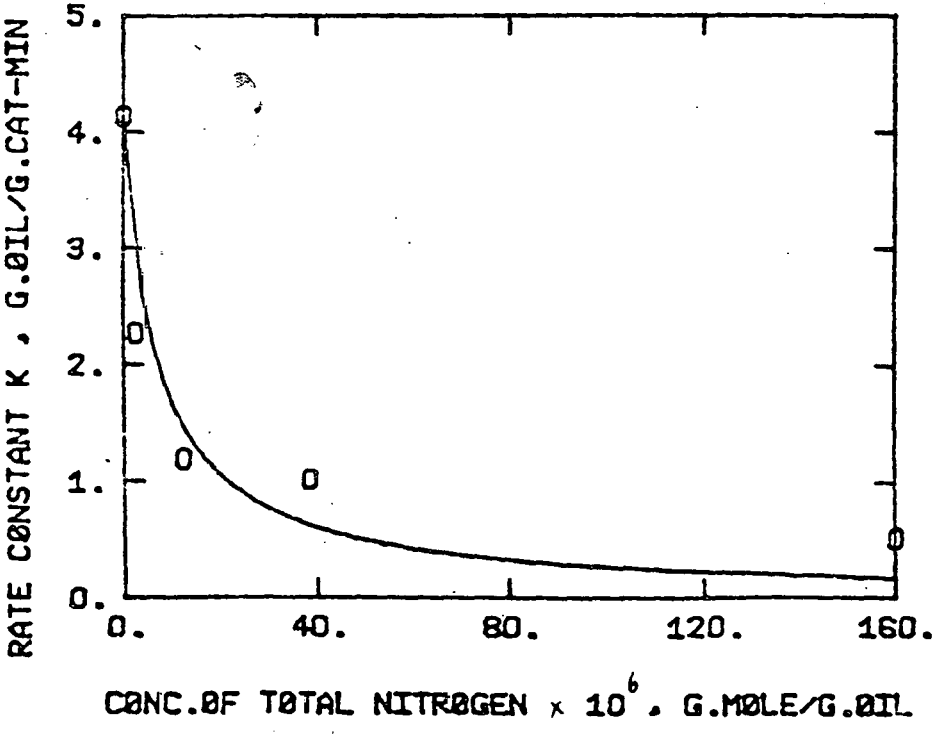

Figure 49. Effect of quinoline on HDS of DBT (0.7 wt %) first order k for disappearance of dibenzothiophene.

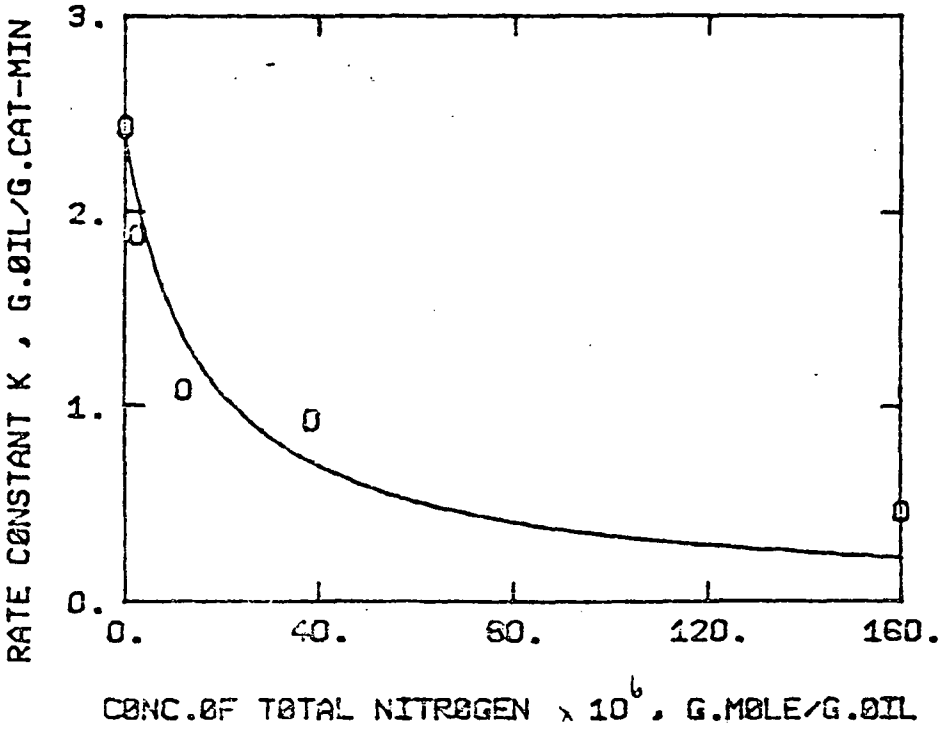

Figure 50. Effect of quinoline on HDS of DBT (0.7 wt %) first order k for disappearance of dibenzothiophene. $k_{(DBT \rightarrow Biphenyl)}$

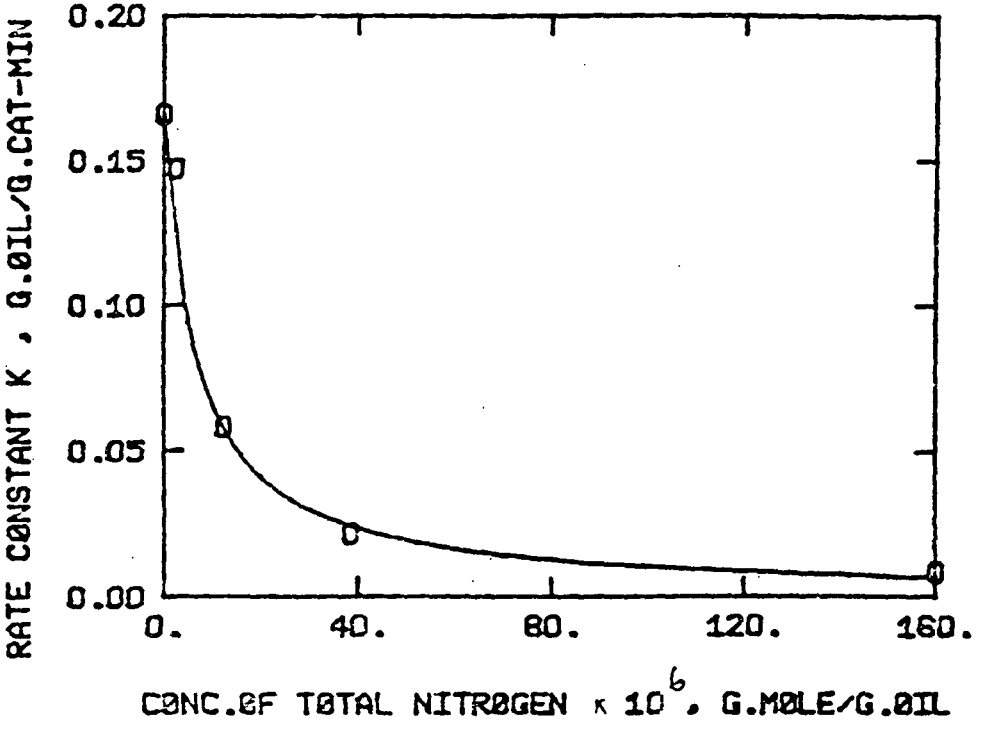

Figure 51. Effect of quinoline on HDS of DBT (0.7 wt %) first order k for disappearance of dibenzothiophene. $k_{(\text{biphenyl} \rightarrow \text{cyclohexylbenzene})}$

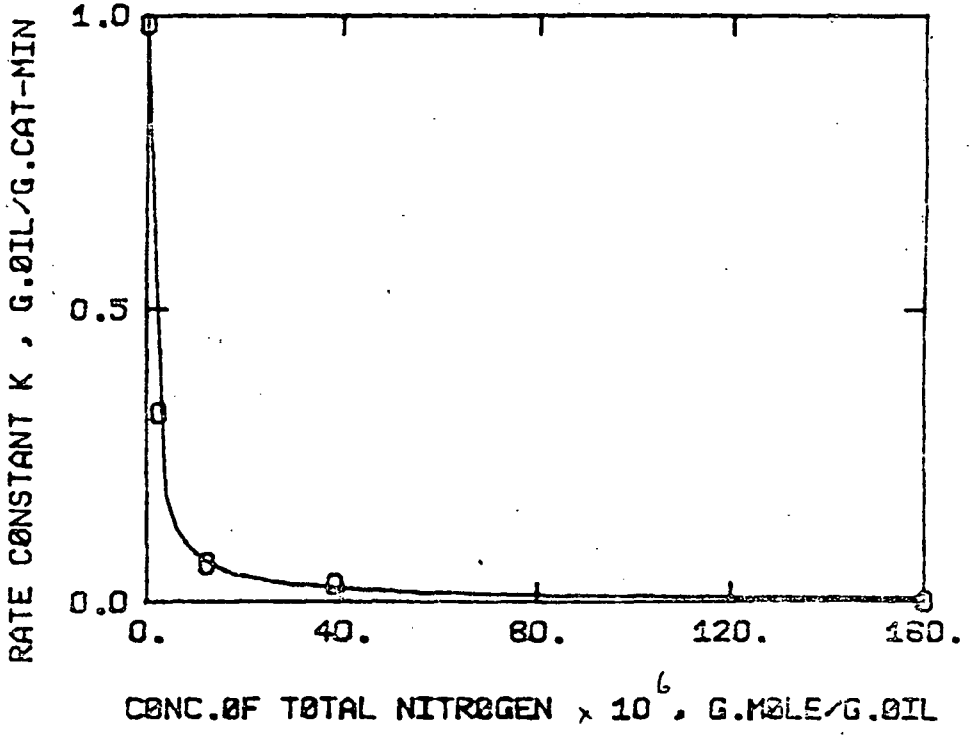

Figure 52. Effect of quinoline on HDS of DBT (0.7 wt %) first order k for disappearance of dibenzothiophene. $k_{(DBT \rightarrow tetrahydroDBT)}$

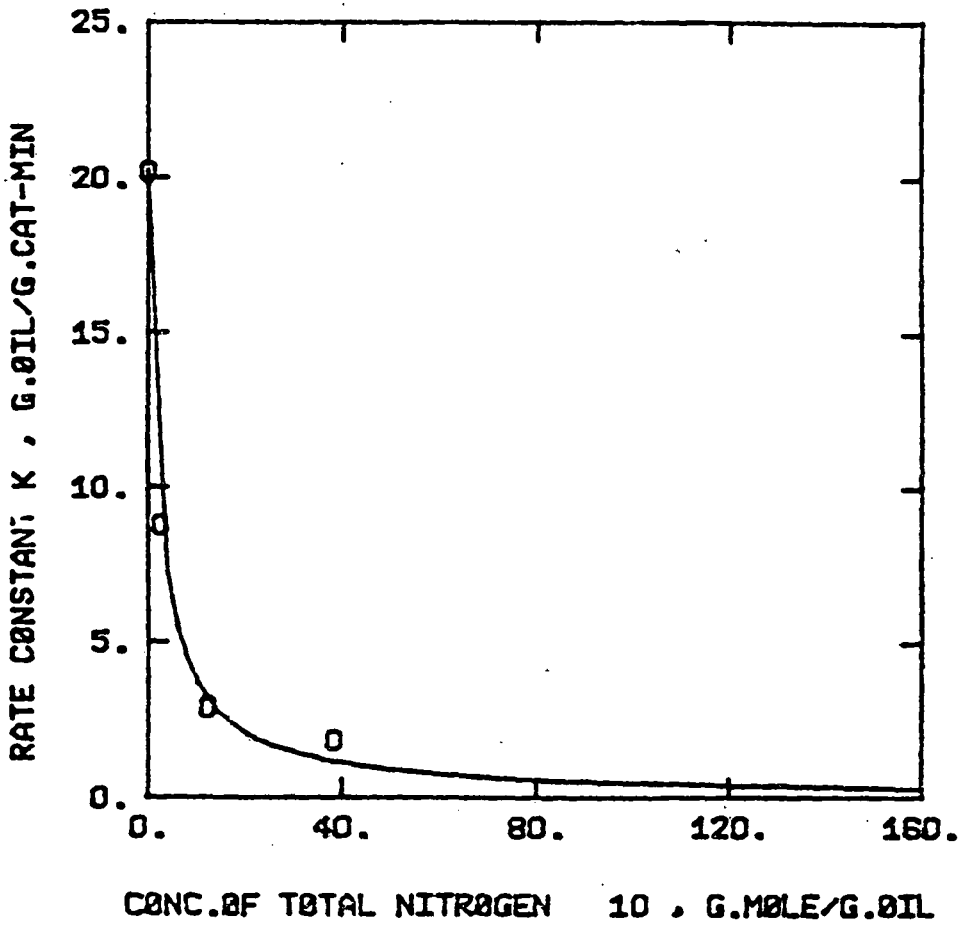

Figure 53. Effect of quinoline on HDS of DBT (0.7 wt %) first order k for disappearance of dibenzothiophene. $k_{(\text{tetrahydrodibenzothiophene} \rightarrow \text{cyclohexylbenzene})}$

(2) Most of the HDS reactions were complete before o-propylaniline became the predominant nitrogen-containing compound in the reaction mixture, i.e., the reactions took place in kinetic region I. Biphenyl hydrogenation continued into region II only in experiments with 0.2 and 0.5 wt % quinoline.

Fig 57 shows the inhibition of the rate parameters by quinoline. Solid lines in Fig. 57 are predictions from a Langmuir-Hinshelwood type model and will be discussed in the next report.

Summary

Catalytic hydroprocessing reactions were carried out in the liquid phase in a batch autoclave reactor for the following binary systems: quinoline and naphthalene, quinoline and indole, quinoline and dibenzothiophene. The results show that quinoline and its reaction intermediates inhibit carbon-nitrogen and carbon-sulfur scission and especially, hydrogenation reactions. The overall inhibition by quinoline and its reaction products decreases in the order: naphthalene > dibenzothiophene > indole. The pattern of inhibition indicates that the hydrogenation of aromatics and of the aromatic ring structure of nitrogen and sulfur-containing compounds occur on the same type of site, whereas hydrodesulfurization occurs on a different type of site. Carbon-nitrogen bond scission occurs on still another site, possibly associated with the support.

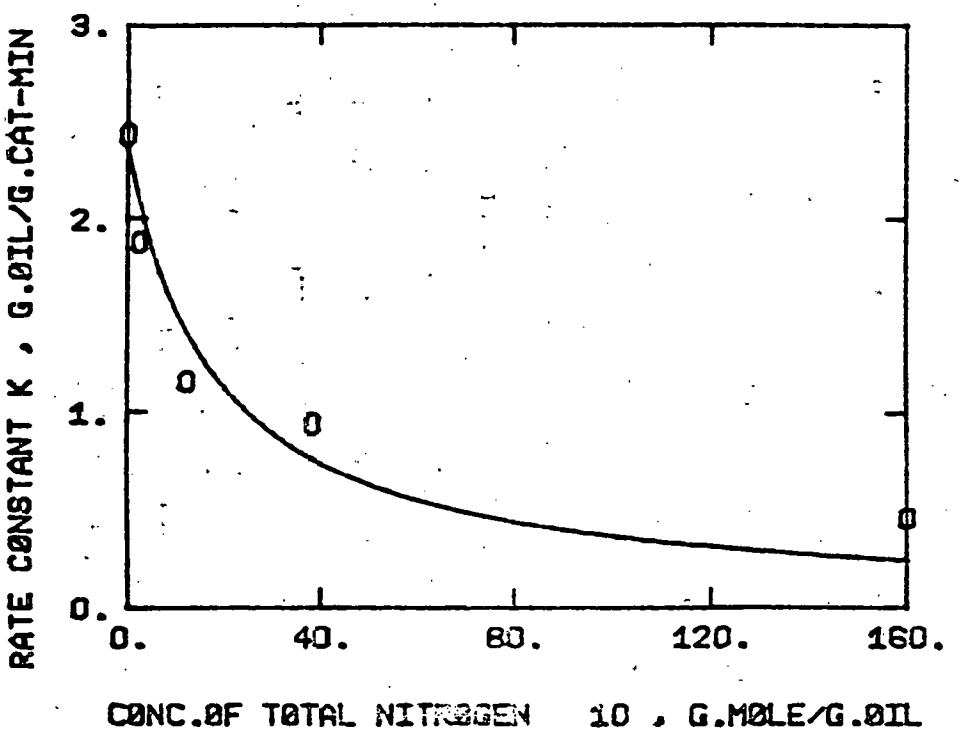

Figure 54. Effect of quinoline on HDS of DBT (0.7 wt %) $k_{(DBT \rightarrow biphenyl)}$ estimated from data points in region I.

D) Adsorption of Quinoline on Catalyst Under Reaction Conditions

To determine the amount of quinoline adsorbed on the catalyst at standard reaction conditions and thereby to estimate an approximate number of active sites on the catalyst, an experiment was carried out at a very low quinoline concentration. The experiment was carried out as described below.

Procedure

Reaction conditions were standard (Table I). The catalyst concentration was 1.25 wt %. The quinoline was not added with the catalyst in the injection loader as was usually done, but the reactor was loaded with ~0.05 wt % quinoline in n-hexadecane, instead of pure n-hexadecane. Catalyst, dibenzothiophene, and carbon disulfide in 30 cm^3 of 0.05 wt % quinoline solution were placed in the catalyst loader. The autoclave was heated to the desired temperature. Five samples were taken during the heating period. After catalyst injection, samples were collected in the normal fashion.

The concentration of total nitrogen in samples before and after catalyst injection is shown in Fig. 58. The concentration of total nitrogen remained unchanged in the absence of catalyst at a value of $3.47 \pm 0.04 \times 10^{-6}$ gmole/g oil (average of 5 samples); however, a significant amount of quinoline was converted to 1,2,3,4-tetrahydroquinoline. Removal of nitrogen after injecting catalyst into the reactor proceeded at a rapid rate as shown in Fig. 59. The vertical line in Fig. 58 represents the time of catalyst injection. The initial concentration of quinoline in the reaction mixture immediately after the

Figure 55 HDN of quinoline (.05 wt %) Total nitrogen before and after catalyst injection. Concentration x 10^6 (g.mole/g.oil)

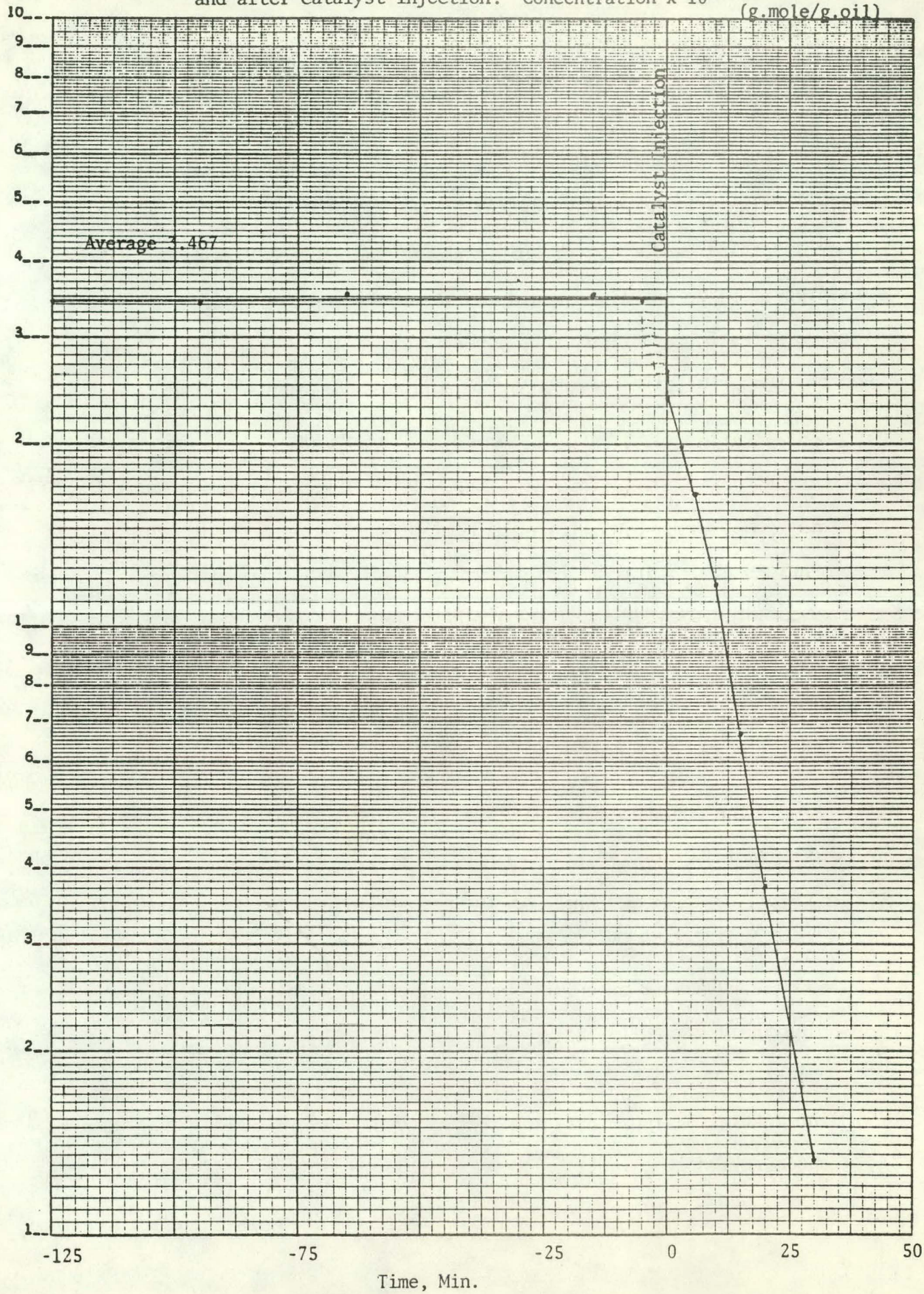

catalyst injection was estimated to be $2.47 \pm 0.14 \times 10^{-4}$ gmole/g oil by extrapolation.

From values of quinoline concentration before and immediately after contacting the catalyst with the reaction mixture, it was estimated that 4.7×10^{19} molecules of quinoline were adsorbed per gram of catalyst. Since quinoline would adsorb on the support as well as on the active sites for reaction, this number represents only an upper limit on the number of sites covered by quinoline under reaction conditions.

REACTION NETWORK MODELING

The reaction network modeling has involved developing a program to do each of the following tasks:

- convert conc-time data to kinetic parameters
- predict conc-time curve by solving system of ODE using values of kinetic parameters solved
- handle n-th order (including 1st order (pseudo)) system
- handle system with any inhibition form (Appendix pg. 1-2)
- compare original with predicted data on-screen.

QUINOLINE NETWORK

- lumping of different components in the network was simulated with the program

- successful schemes (3) are: (Appendix pg. 3-6)

(i) 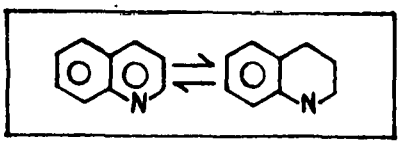 (thermodynamic equil.)

(ii) (i) and 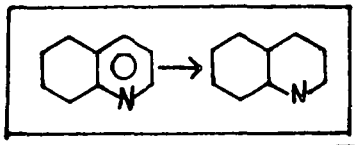

(iii) 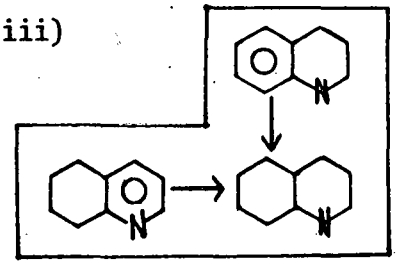 and 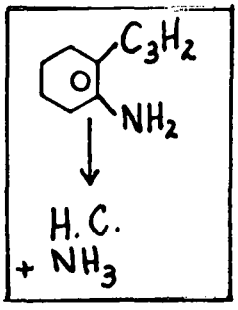

(hydrogenation products)

(hydrogenolysis products)

- Criteria for 'success':
  - (i) matching of predicted conc-time curve with that of the original
  - (ii) kinetic parameters' magnitude changing in the expected direction

- reasons for 'success':
  - (i) indirectly independent on chemical natures of components involved
  - (ii) directly--mathematically--dependent on components' positions in the network and their associated kinetic parameter magnitude

e.g., success of scheme II; (Appendix pg. 5)

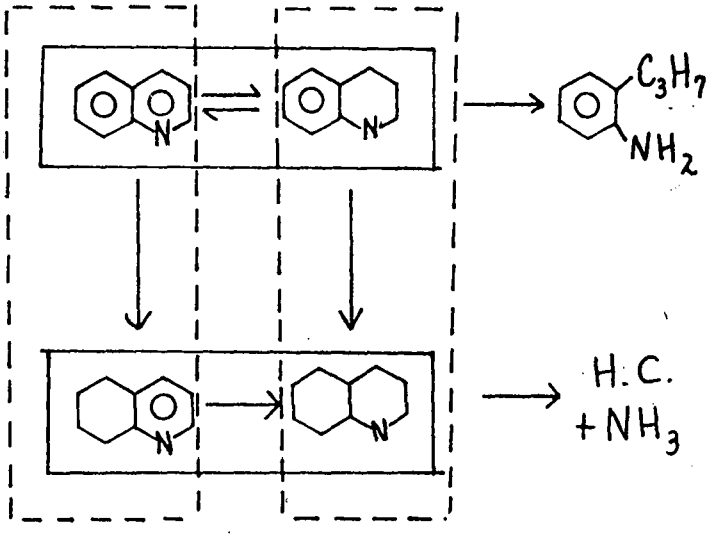

--lumping was along main rxn pathway--

This also accounts for failure of scheme because the lumpting was across the pathway and not along it (Appendix pg. 7).

- Comments:

  (i) a priori info of the rxn network is required so successful lumping along the major rxn pathway can be achieved

  (ii) more than 1 major pathway crisscrossing, what then? lump along all major pathways independent of others?

  (iii) introducing inhibition into the network as suggested by Froment? Question: fairly constant basic N conc!

  (iv) this lumping exercise provides guidelines for lumping within the same network! For lumping involving different networks, the following analysis on the quinoline-indole system may provide some insights.

QUINOLINE-INDOLE NETWORK

- The indole network is modelled as follows:

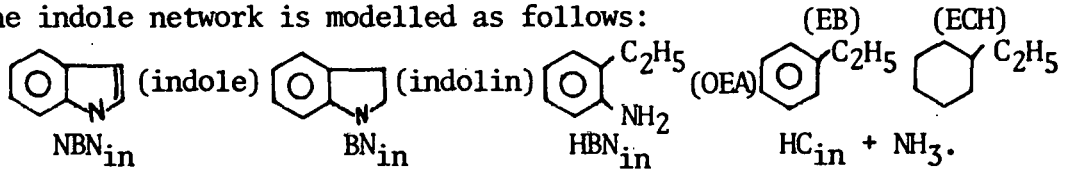

- The quinoline network:

$$BN_q \longrightarrow HBN_q \longrightarrow HC_q + NH_3$$

- with $C_{NBN_{in_0}} = 300$ and $C_{BN_{q_0}} = 100$, ballpark values for $\frac{k_i}{1+K_iC_I}$ were used to generate conc-time data for both networks separately. The 2 networks were then 'combined' as follows:

$$HBN_{in} \longrightarrow {}^{BN_{in}}_{+\ BN_q} \longrightarrow {}^{HBN_{in}}_{+\ HBN_q} \longrightarrow {}^{HC_{in}}_{+\ HC_q} + NH_3$$

The generated conc-time profiles were then combined as shown above. These combined profiles would then yield a set of kinetic parameters.

Predicted conc-time profiles would be obtained by solving system of ODE using the calculated values of the kinetic parameters.

- Criteria for a 'successful' scheme are the same as those for the quinoline network analysis.

- This scheme, using fixed and matching K_i, was successful. (Appendix pg. 8-16).

- To handle non-matching K_i and to solve k_i and K_i simultaneously, the original HBJ method was modified. (Appendix pg. 1-2).

- Conc-time profiles generated for the 2 systems (using ballpark values for k_i and K_i) were solved for a set of k_i and K_i for the 2 systems independently.

- Conc-time profiles matched well but some K_i turned negative. (Appendix 17-24)

- 4 parameters had to be solved in the quinoline system and 6 in the indole system. Combining the 2 systems would mean 10 parameters would have to be solved simultaneously!

- Reasons for 'failure':
  - (i) too many parameters
  - (ii) parameters in the denominator of kinetic expression K_i hard to solve because conc. will be integrated w.r.t. conc.
  - (iii) 'broad' solution base of system mathematically.

- Future directions:
  - (i) Perturb conc-time data to test sensitivity
  - (ii) Set one K_i to real values and solve for other k_i, K_i
  - (iii) Assume ratios between different K_i to minimize no. of parameters, e.g., K_i for hydrogenation for both networks may be assumed the same.
  - (iv) Try a different kinetic expression, e.g., $\frac{k_i}{(1+K_iC_I)^2}$
- Comments:
  - (i) A priori info on the kinetics and rxn network for the systems is essential for taking a good future direction.
  - (ii) The HBJ method has its limits.
  - (iii) This type of analysis will include also: Dibenzothiophene and Naphthalene.

TYPES OF LUMPS IN LITERATURE

3 types of analytical (functional group) lumps:

(i) Mobil - Gradient Elution Chrom (GEC)
13 lumps

(ii) Mobil - Solvent Elution Sequential Chrom (SESC)
10 lumps

(iii) Silver-Wang - 5 nitrogen lumps

APPENDIX

As an example, we consider the system

$$A \xrightarrow{k_1} B$$

$$B + C \xrightarrow{k_2} \text{products}$$

in which it is assumed that A and B adsorb according to the Langmuir isotherm, that the second reaction proceeds *via* collision of gaseous C with adsorbed B, and that neither C nor the products are strongly adsorbed. Putting

$$k_1' = k_1 k_A; \quad k_2' = k_2 k_B$$

the rate equations can be written

$$\frac{-dP_A}{dt} = \frac{k_1' P_A}{1 + k_A P_A + k_B P_B} \tag{16}$$

$$\frac{dP_B}{dt} = \frac{k_1' P_A - k_2' P_B P_C}{1 + k_A P_A + k_B P_B} \tag{17}$$

$$\frac{-dP_C}{dt} = \frac{k_2' P_B P_C}{1 + k_A P_A + k_B P_B} \tag{18}$$

rearranging and integrating, one obtains

$$A_0 - A = k_1' \int_0^t A\,dt + k_A \frac{A^2 - A_0^2}{2} + k_B \int_{A_0}^{A} B\,dA \tag{19}$$

$$B - B_0 = k_1' \int_0^t A\,dt - k_2' \int_0^t BC\,dt - k_A \int_{B_0}^{B} A\,dB - k_B \frac{B^2 - B_0^2}{2} \tag{20}$$

$$C - C_0 = -k_2' \int_0^t BC\,dt - k_A \int_{C_0}^{C} A\,dC - k_B \int_{C_0}^{C} B\,dC \tag{21}$$

where for simplicity A, B, C have been written for P_A, P_B, P_C and A_0, B_0, C_0 for their initial values.

If one has measurements of A, B, C as functions of time, these also define A, B, C as functions of each other, and hence integrals such as $\int_{A_0}^{A} B\,dA$ may be numerically evaluated for all experimental points. Equations 19–21 thus comprise a system in which k_1', k_2', k_A, and k_B are unknown, and all other quantities are calculable at each point from experimental data. They are therefore a system which may be solved by linear least squares, again with some reservations about the effect of correlations on the results.

As a test, we have solved eq 16–18 by the proposed method, again using artificial data with randomly generated perturbations. In general, it was found that the method worked satisfactorily provided that the constants assumed were such that $k_A P_A$ and $k_B P_B$ were of the order of magnitude of unity during at least part of the reaction, and that P_A and P_B varied significantly during the reaction. If these conditions did not hold, the system became very ill-conditioned, as would be expected from the form of eq 16–18. When the above conditions did hold, it was found that the rate constants obtained were again correct, and that standard deviations from the linear regression were again too small.

It can be concluded, then, that the proposed method can be used to solve a certain class of heterogeneous systems, provided that the experimental data adequately define the constants involved. It should be noted that equations of the form of (19) to (21) arising from several experimental runs at different reactant pressures could be simultaneously least-square fitted, which would be preferable when k_A and k_B are not of the same order of magnitude.

JB $\frac{dC_i}{dt} = \sum_{l=1}^{N} k_l \cdot R_{i,l}(C_i, t) \qquad i = 1, \cdots M$

N = parameters
M = components

$$C_i(t_j) - C_i(t_0) = \sum_{l=1}^{N} k_l \int_{t_0}^{t_j} R_{i,l}(C_i, t)\, dt \qquad j = 1, \cdots, NP$$

NP = time points

Modified HJB

$$\frac{dC_i}{dt} = \frac{k_\alpha C_i \cdots C_M}{1 + K_{\alpha 1} C_1 + \cdots + K_{\alpha M} C_M} + \frac{k_\beta C_1 \cdots C_M}{1 + \cdots K_{\beta M} C_M} + \cdots$$

$$C_i(t_j) - C_i(t_0) = k_\alpha \int_{t_0}^{t_j} C_1 \cdots C_M\, dt - K_{\alpha 1} \int_{C_i(t_0)}^{C_i(t_j)} C_1\, dC_i - \cdots - K_{\alpha i} \frac{C_i(t_j)^2 - C_i(t_0)^2}{2} - \cdots - K_{\alpha M} \int_{C_i(t_0)}^{C_i(t_j)} C_M\, dC_i$$
$$+ k_\beta \int_{t_0}^{t_j} C_1 \cdots C_M\, dt - K_{\beta 1} \int_{C_i(t_0)}^{C_i(t_j)} C_1\, dC_i - \cdots$$
$$+ \cdots$$

Ref: Gay, J. Phy. Chem. 75, 10, 1613 (1971)

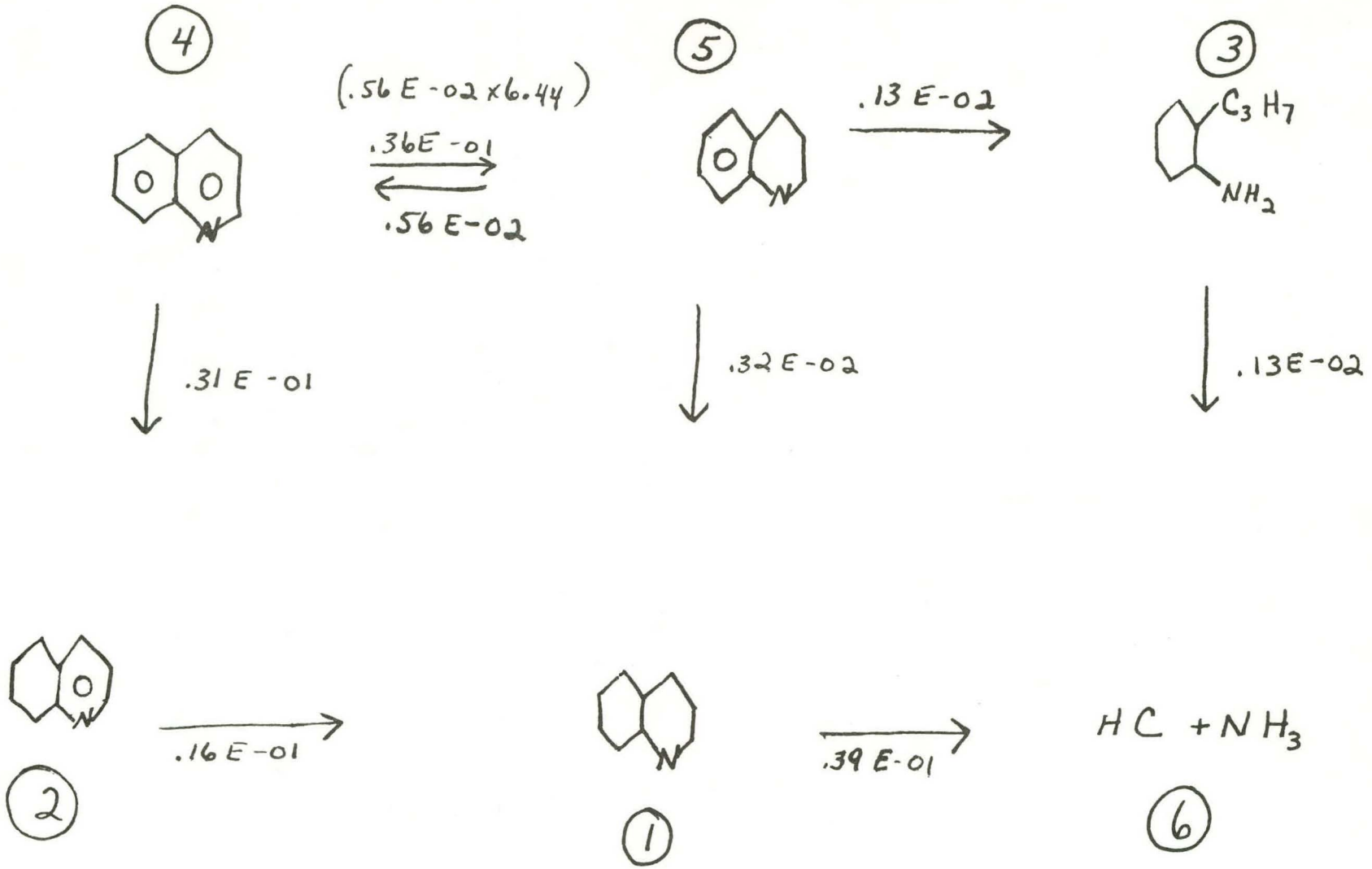
4
(.56 E-02 x 6.44)
.36E-01
.56 E-02
5
.13 E-02
3
C_3H_7
NH_2
.31 E-01
.32 E-02
.13E-02
2
.16 E-01
1
.39 E-01
HC + NH_3
6

k's : E

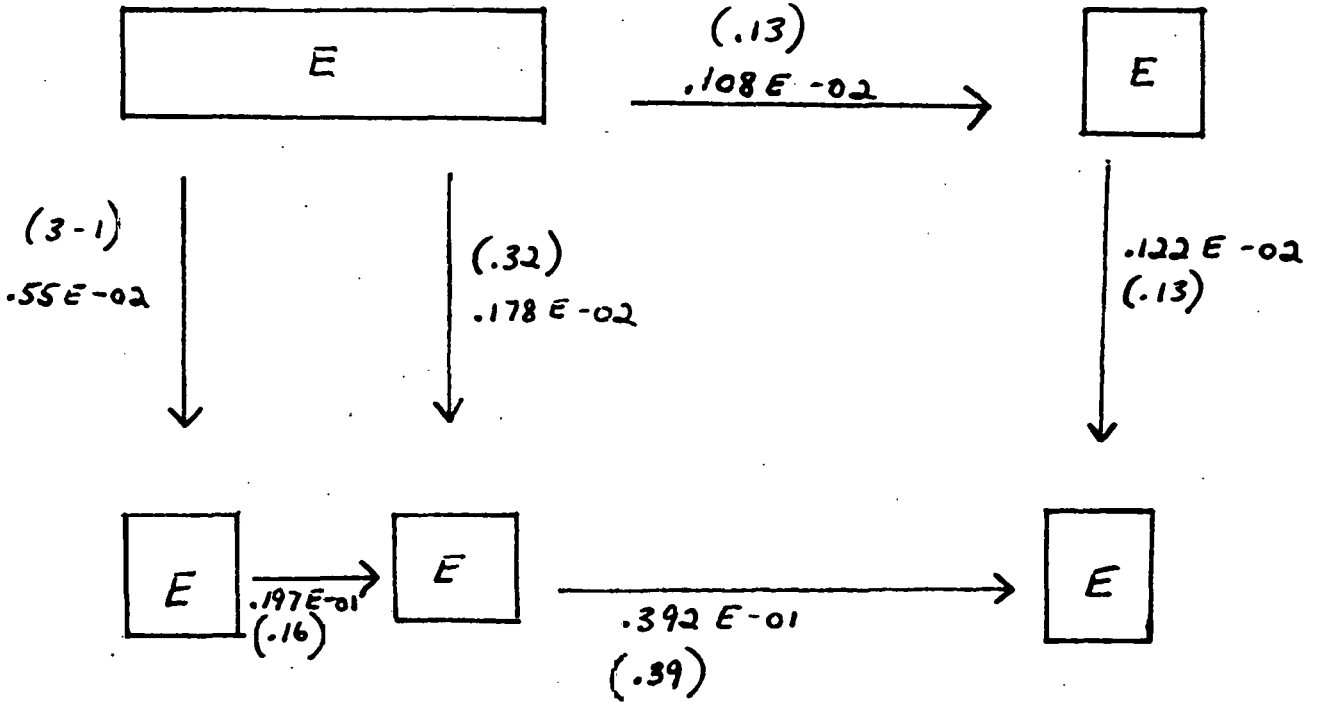
E
(.13)
.108 E -02
E
(3-1)
.55 E -02
(.32)
.178 E -02
.122 E -02
(.13)
E
.197 E-01
(.16)
E
.392 E -01
(.39)
E

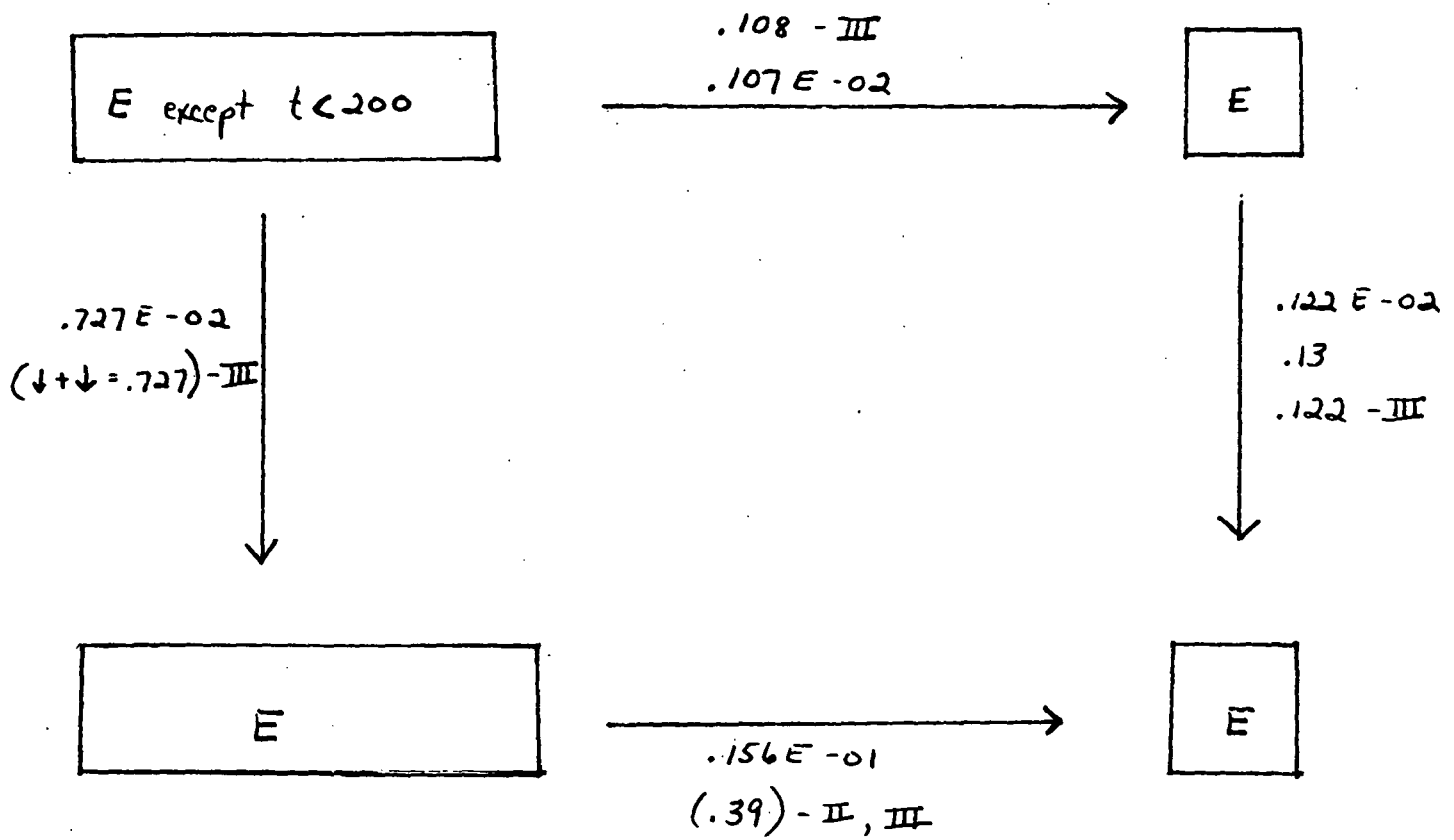
E except t<200
.108 - III
.107 E -02
E
.727 E -02
(↓+↓ = .727) - III
.122 E -02
.13
.122 - III
E
E
.156 E -01
(.39) - II, III

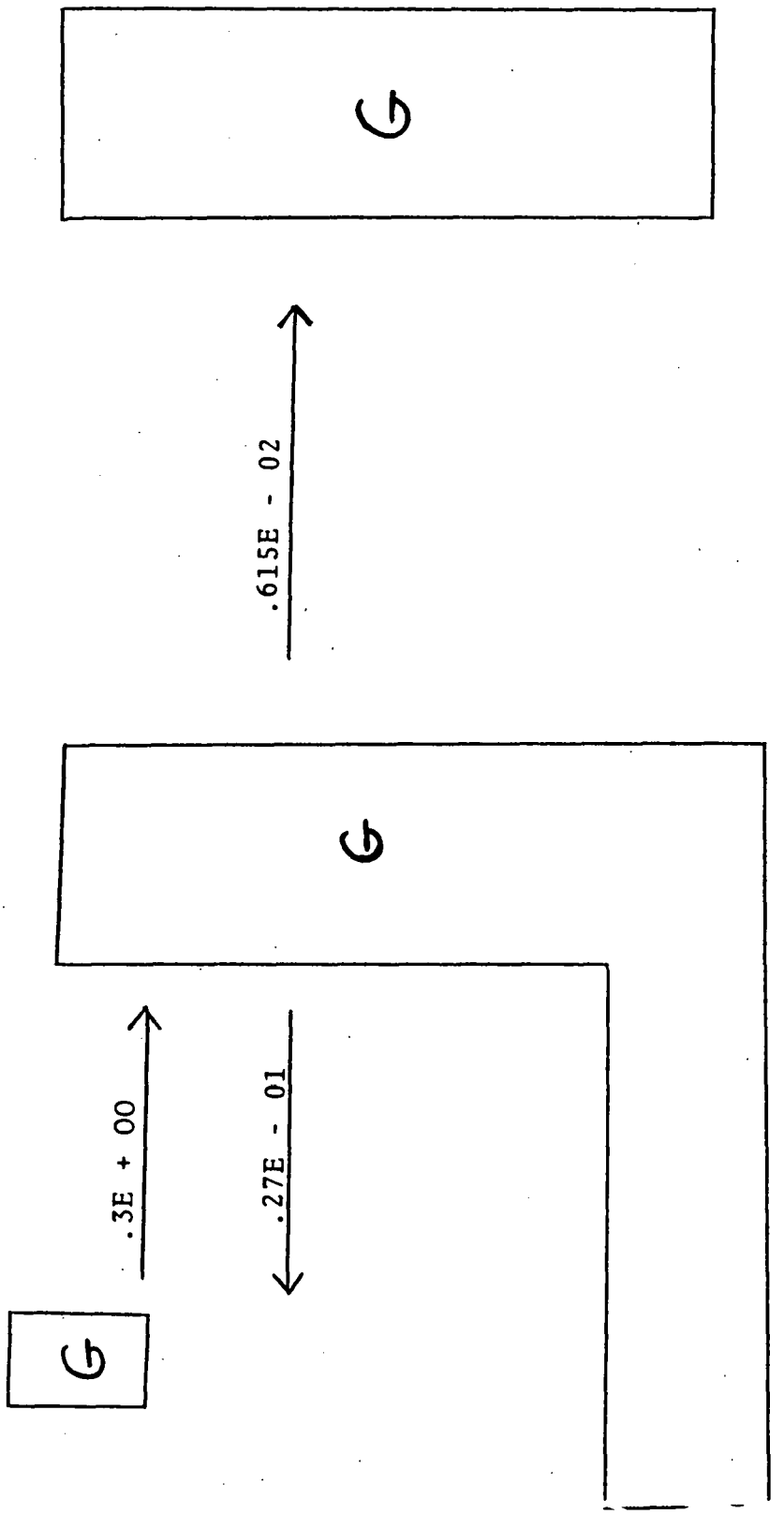
G
.615E - 02
G
.3E + 00
.27E - 01
G

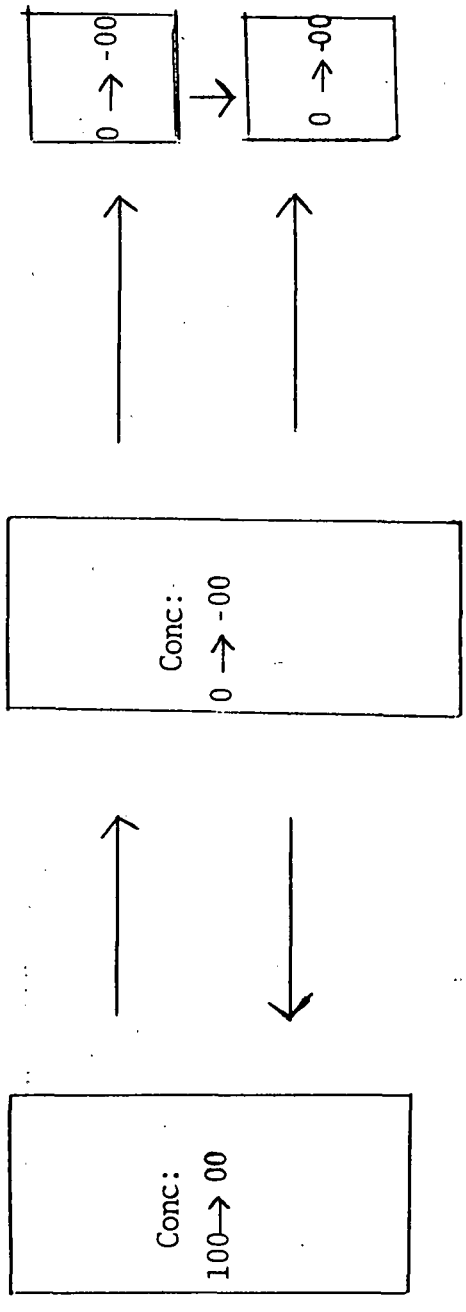
0 → -00
0 → 0
Conc:
0 → -00
Conc:
100 → 00

Indole:

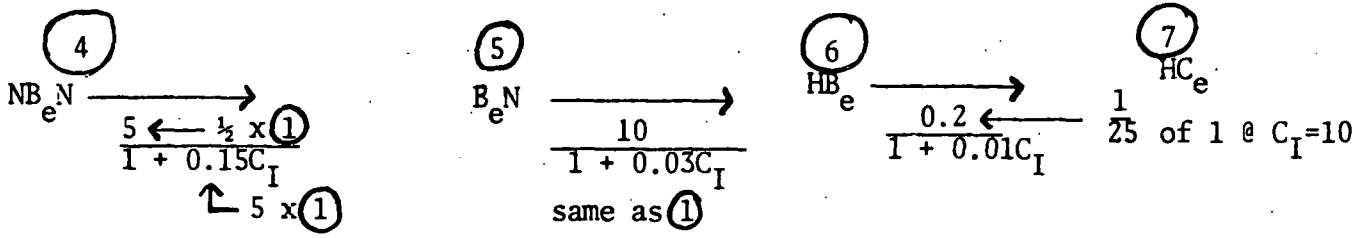

$C_{indole}=C_{Quinoline}=3:1$

Quinoline:

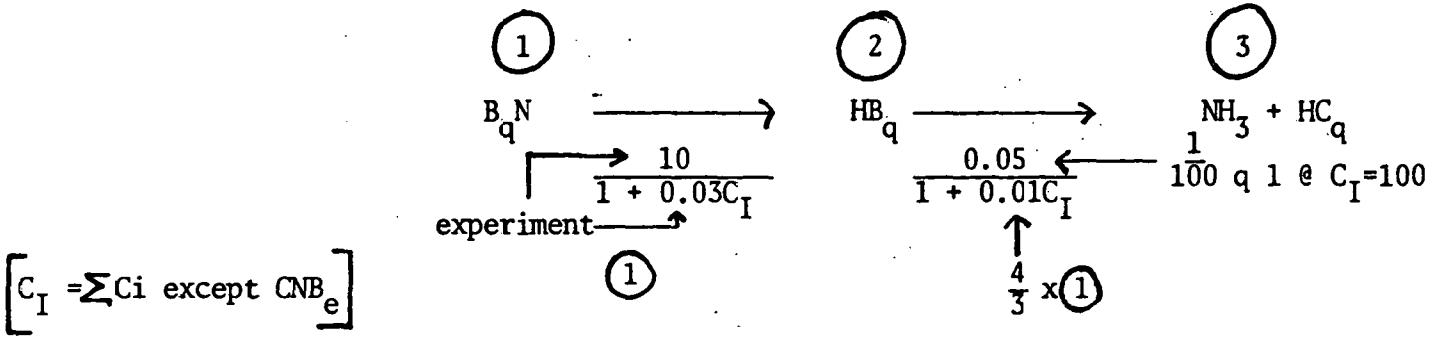

Indole + Quinoline:

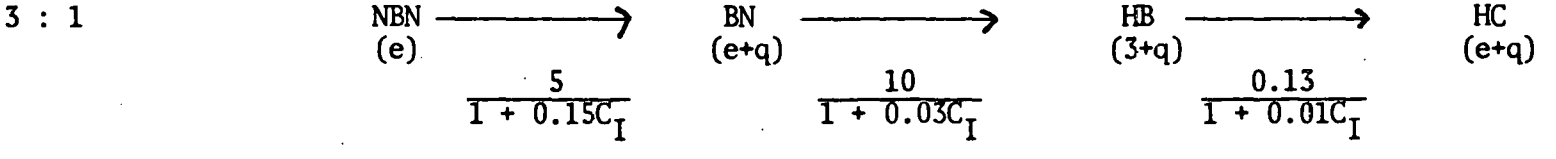

A-9

Computer data

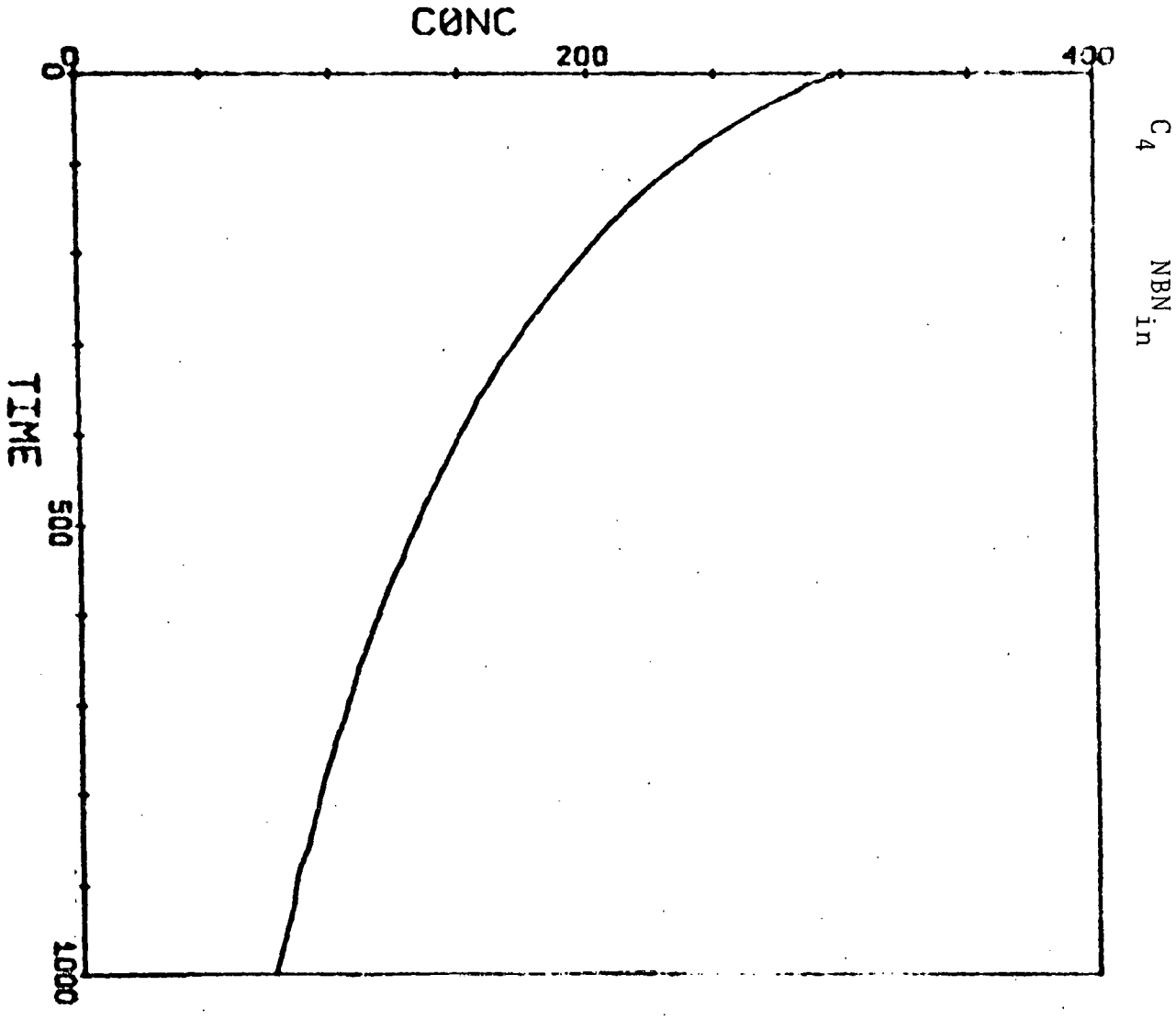

HJB fitting using generated k's but K fixed
(Fixed inhibition)
1
E
NBN in, predicted
400
200
0
CONC
0
500
1000
TIME

$(BN_{in}+BN_q)$

$C_2=(C_1+C_5)$ Q1 USE 2 → [1]

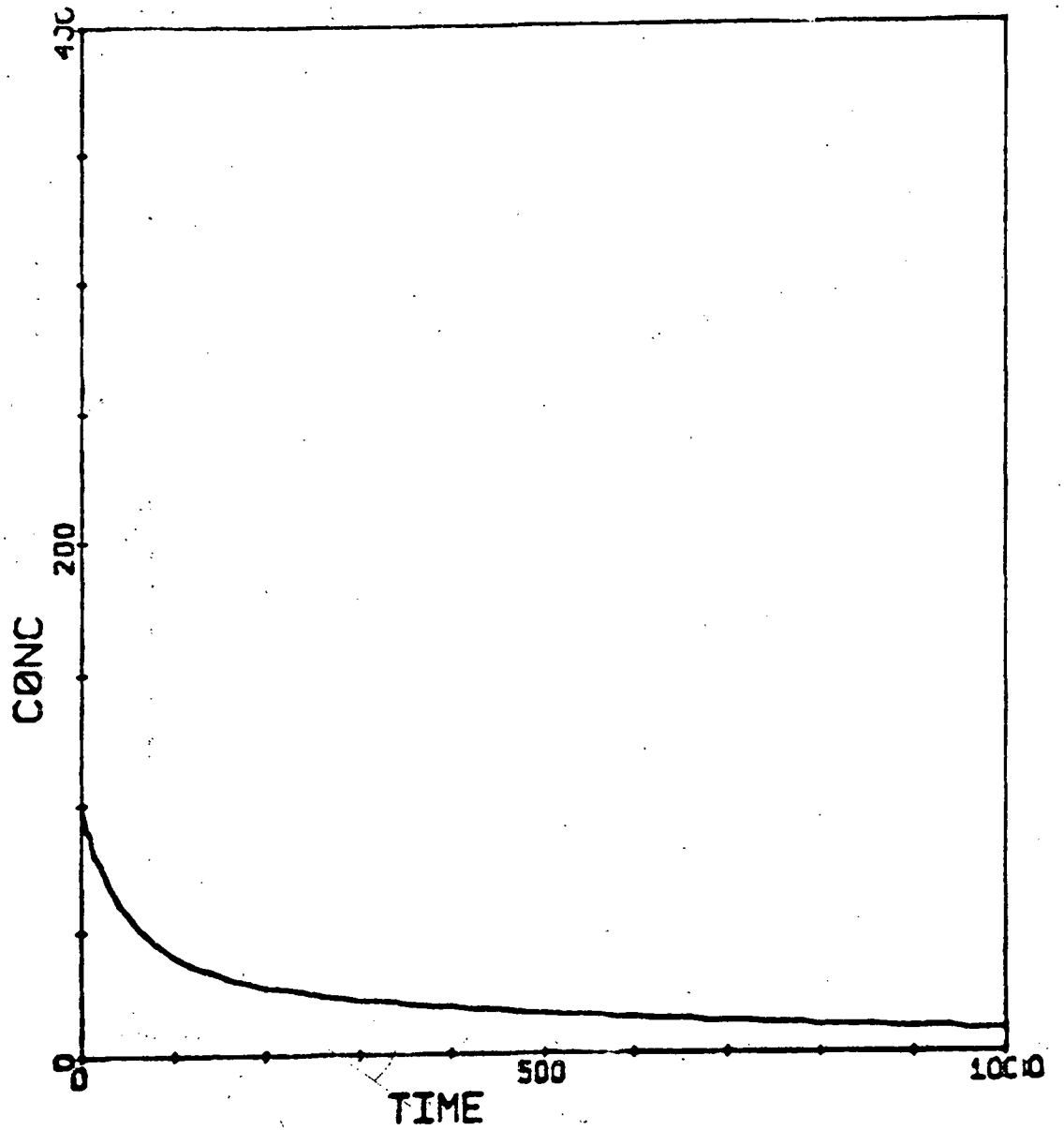

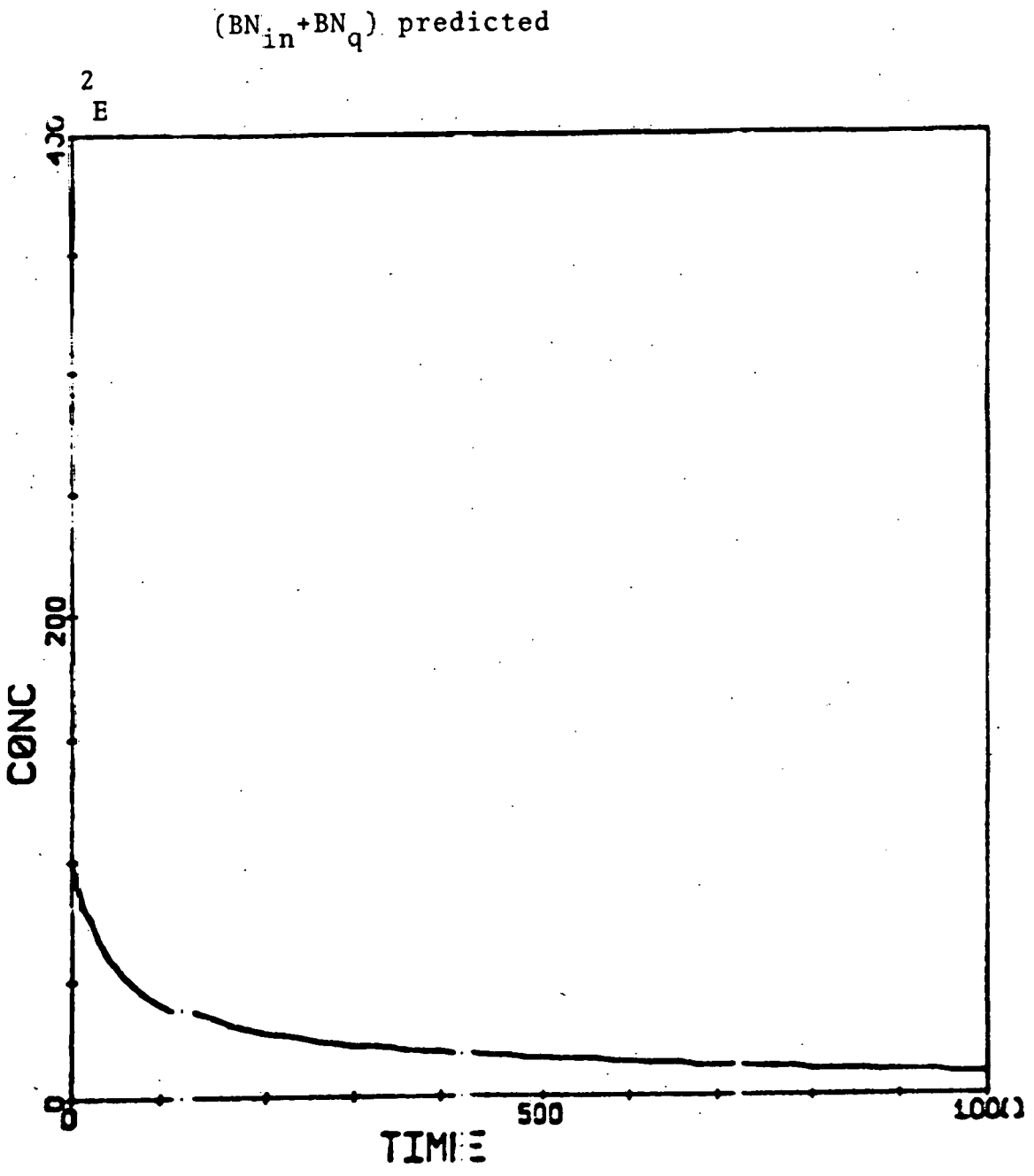
(BN$_{in}$+BN$_q$) predicted
2
E
CØNC
200
0
0
500
1000
TIME

$(HBN_{in}+HBN_{q})$

$C_3=(C_2+C_6)$

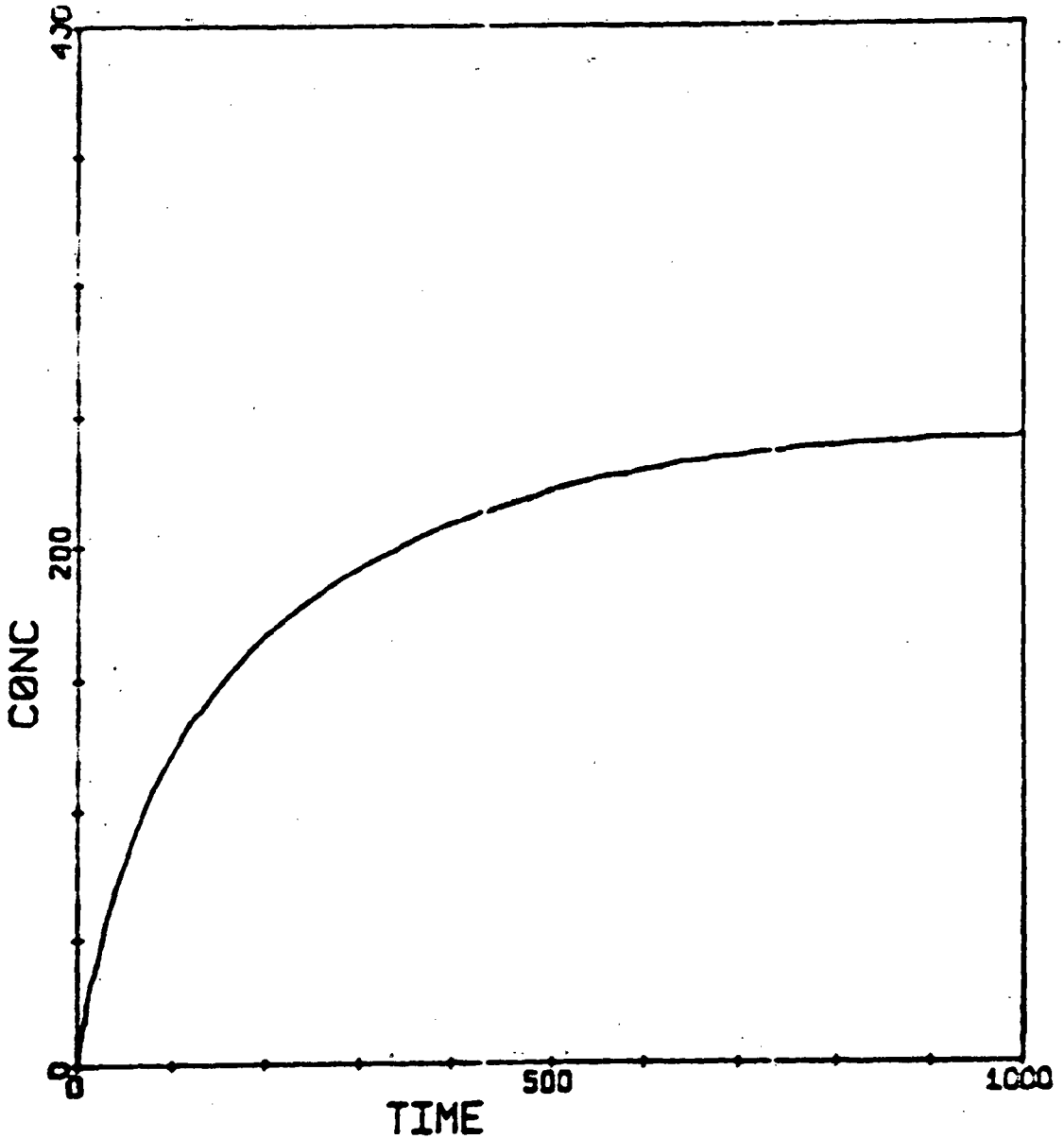

$(HBN_{in}+HBN_{q})$ predicted

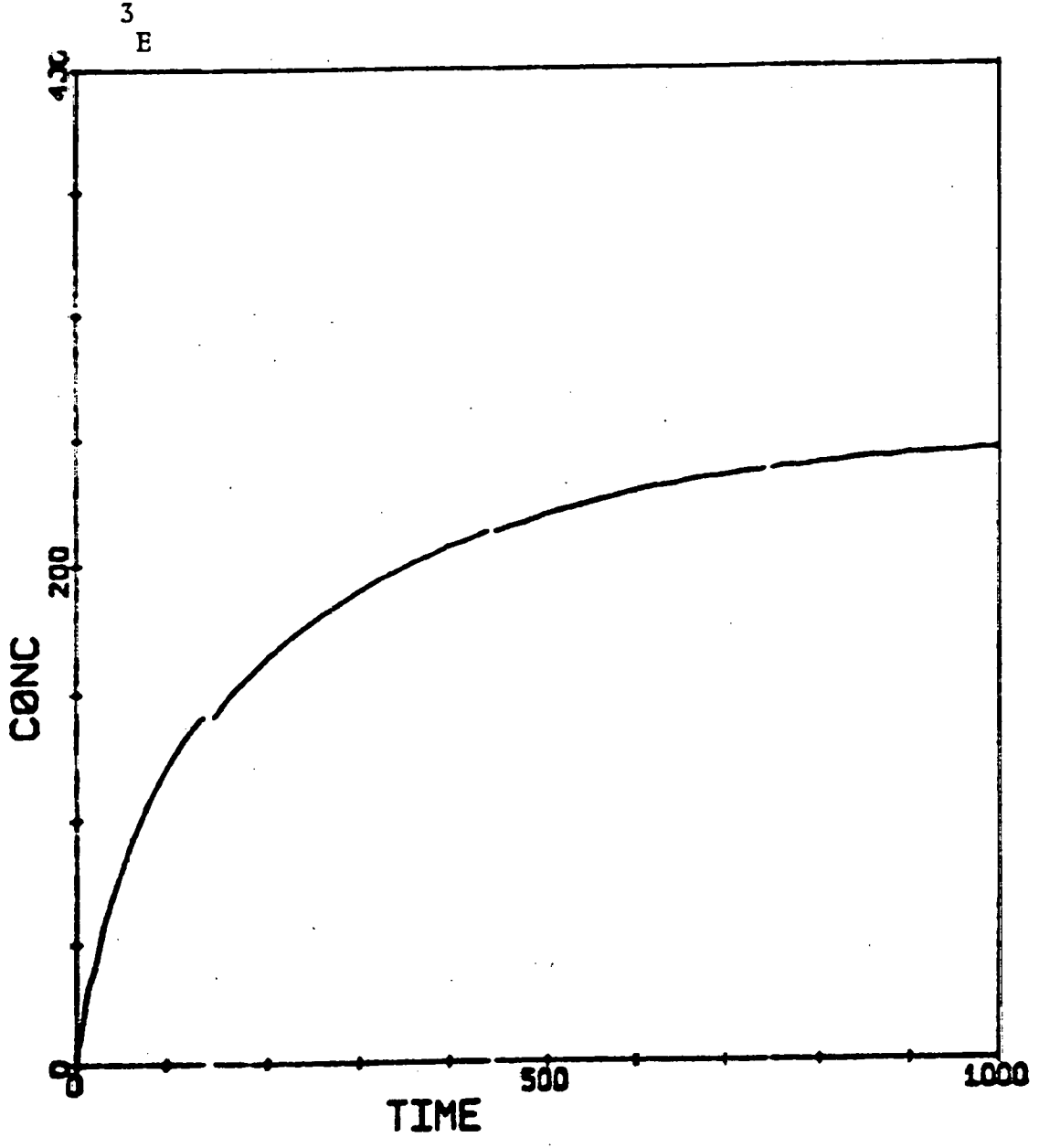

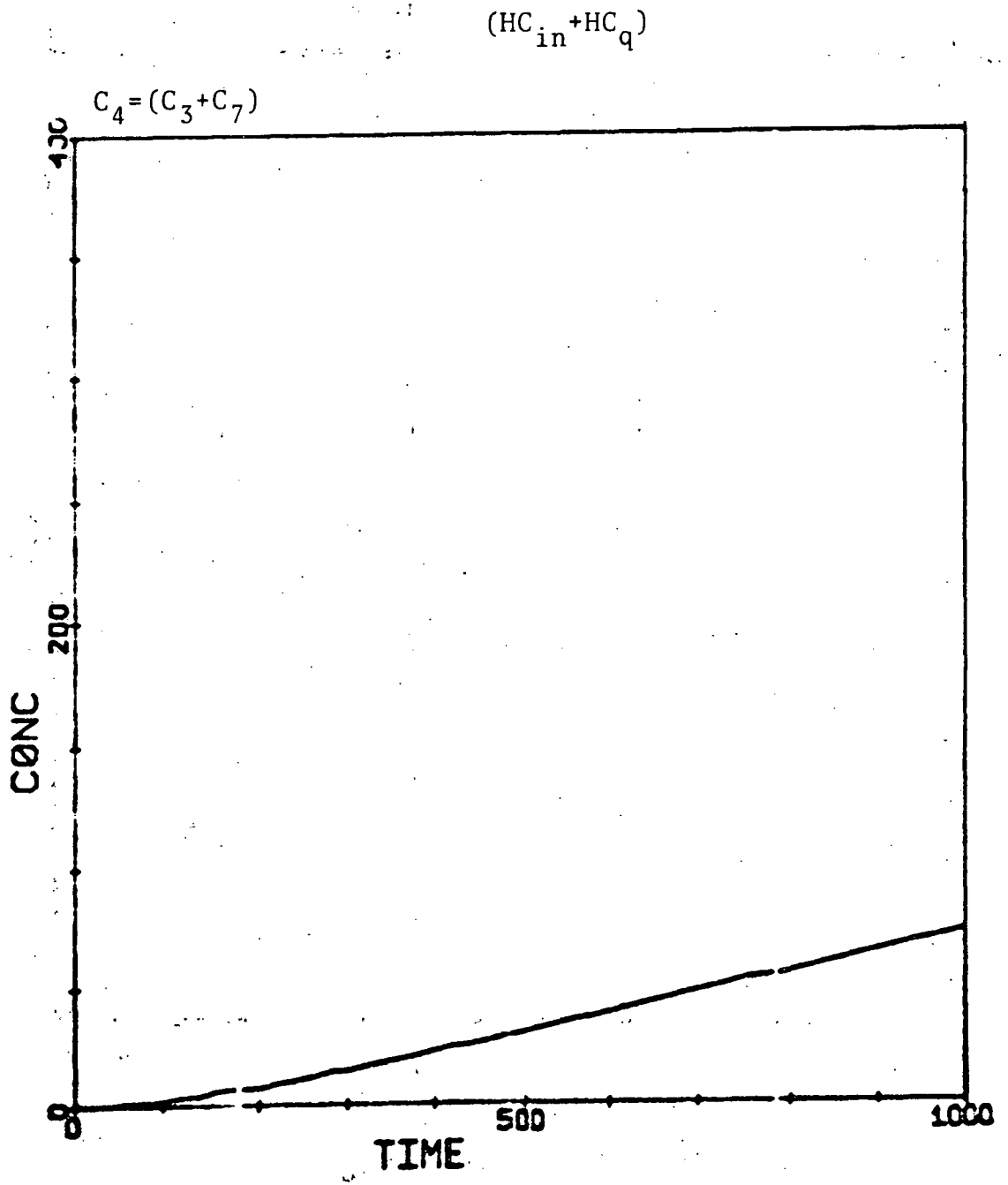
$(HC_{in}+HC_q)$
$C_4=(C_3+C_7)$
CØNC
200
0
500
1000
TIME

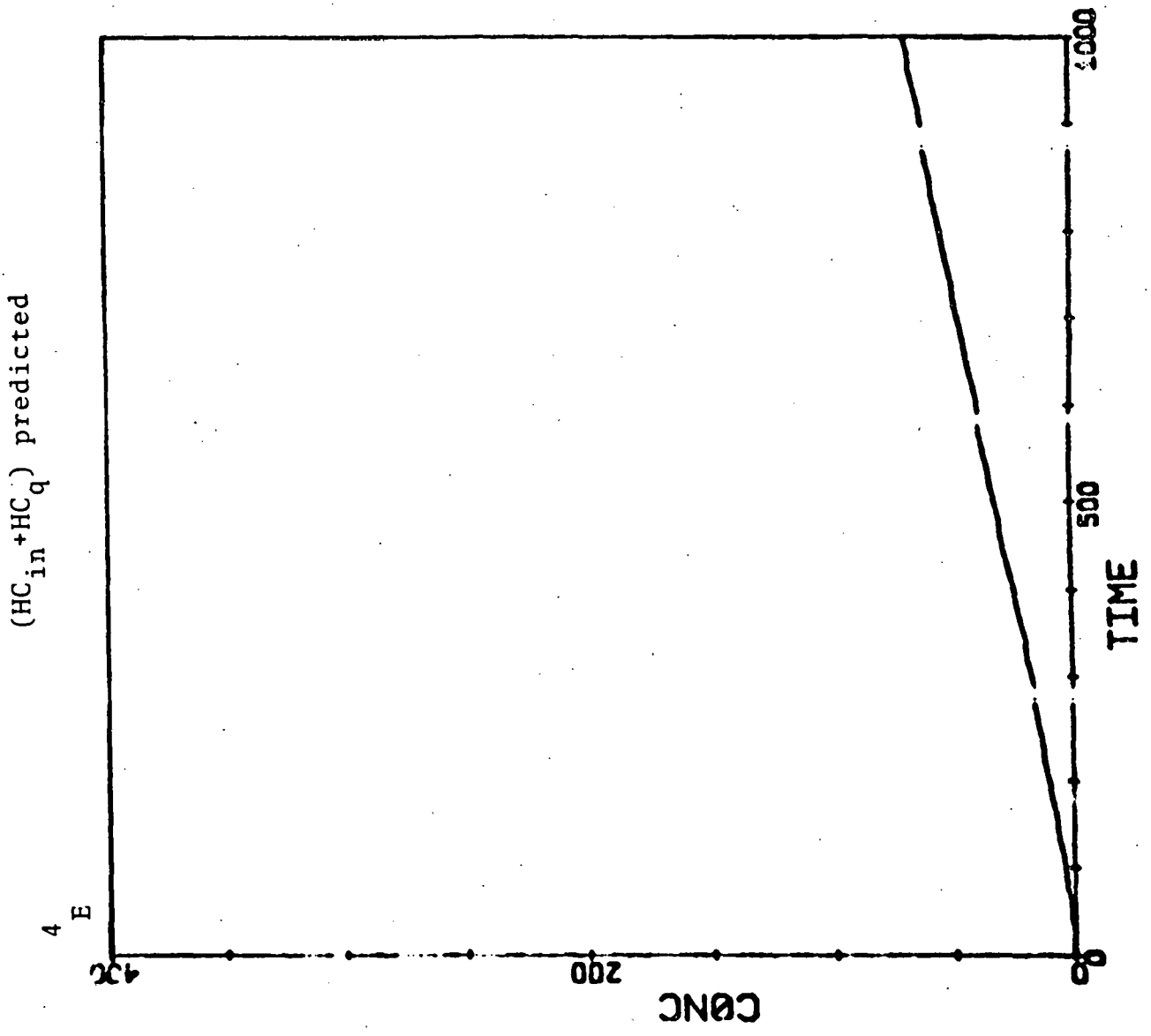
(HC_in+HC_q) predicted
4
E
0
200
400
CONC
0
500
1000
TIME

Graphs

$*$: generated data

——— : predicted data

$$NBN_{in} \xrightarrow[\frac{0.3(5)}{1+.009C_I}]{} BN_{in} \xrightarrow[\frac{27(10)}{1+(-.0027)C_I}]{} HBN_{in} \xrightarrow[\frac{0.14(0.2)}{1+.009C_I}]{} HC_{in}$$

$(.15)$ $(.03)$ $(.01)$

$(BN+HBN+HC)_{in} \neq const.$

values used for generating data

$$BN_g \xrightarrow[\frac{2(10)}{1+.001C_I}]{} HBN_g \xrightarrow[\frac{0.015(.05)}{1+(-.0002)C_I}]{} HC_g$$

$(.03)$ $(.01)$

$(BN+HBN+HC)_g = const.$

$$\frac{C_{NBN_{in},0}}{C_{BN,g}} = \frac{3}{1}$$

HBJ on separate indole, quin.

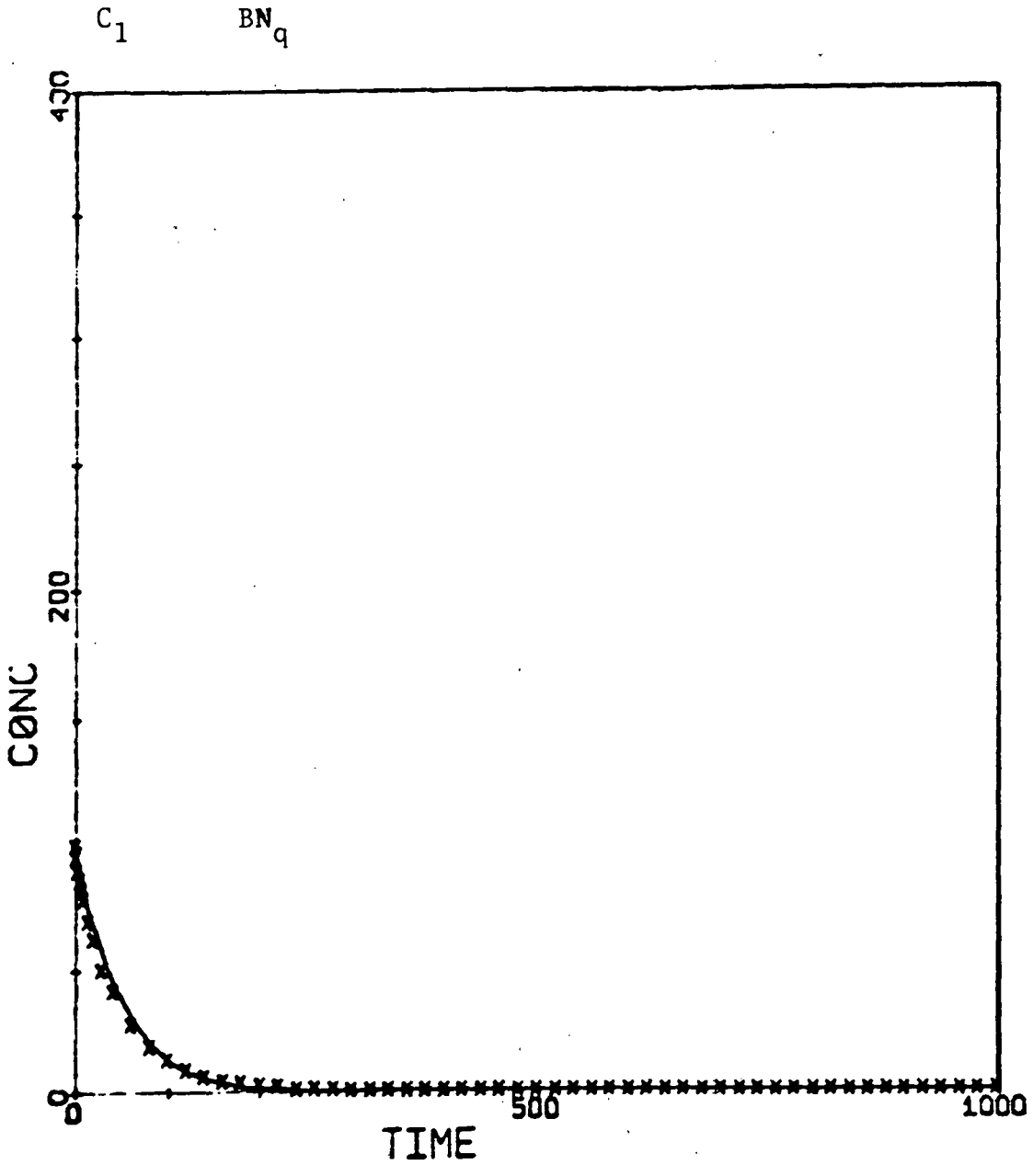

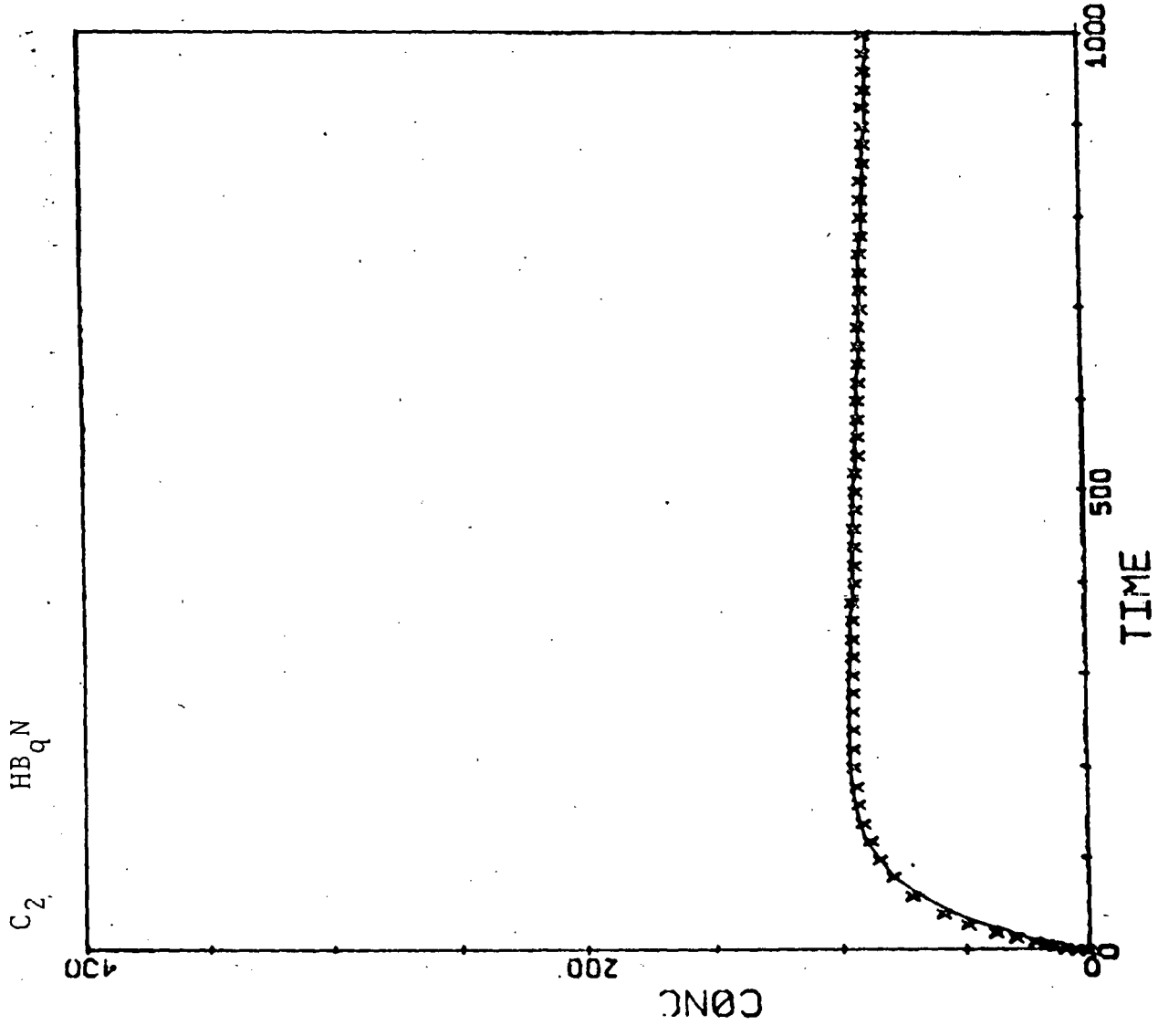
1000
500
0
TIME
400
200
0
CONC
C_2HB_qN

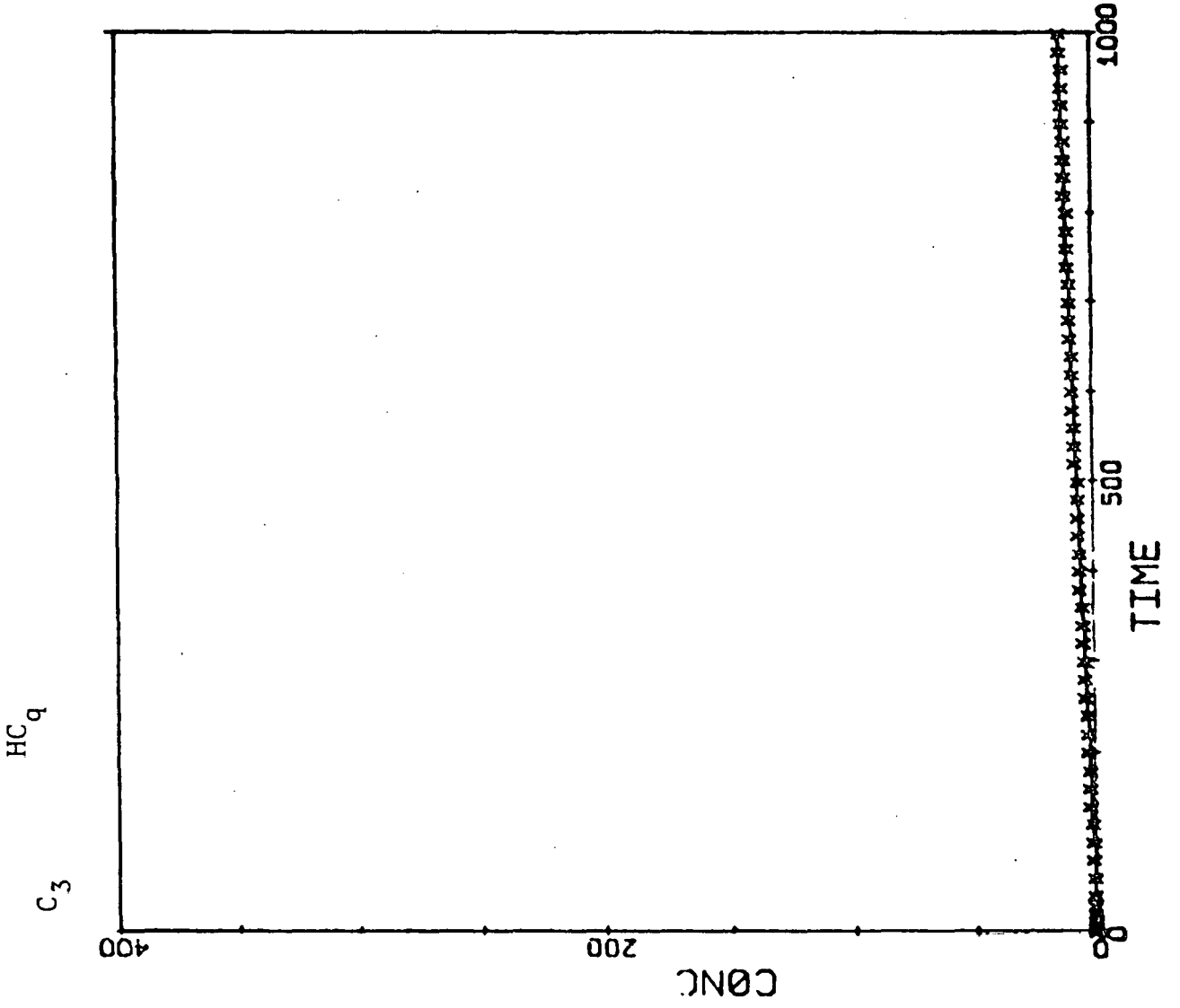
HC
q
C
3
CONC
0
200
400
TIME
0
500
1000

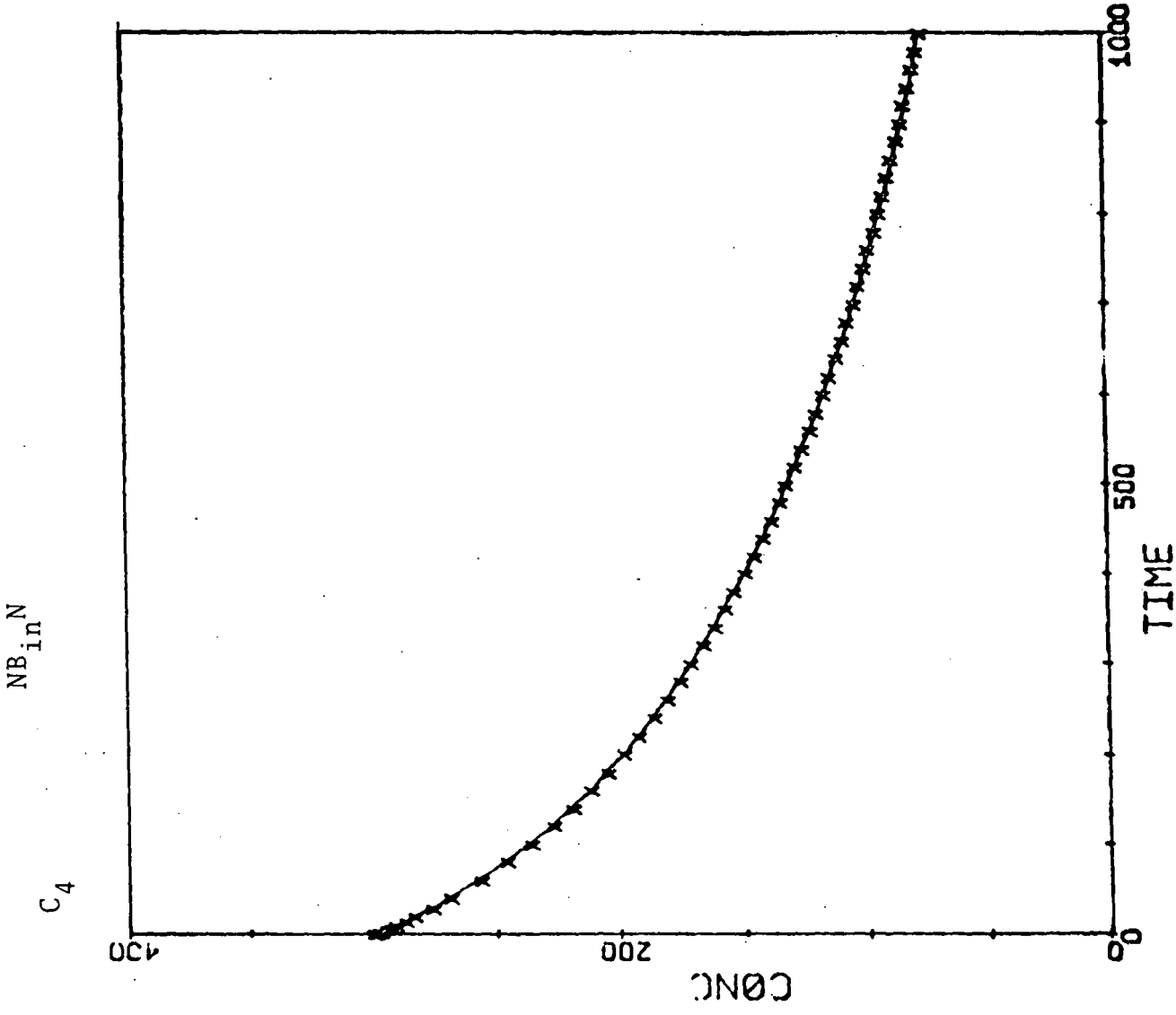
$NB_{in}N$
C_4
CONC
0
200
400
TIME
0
500
1000

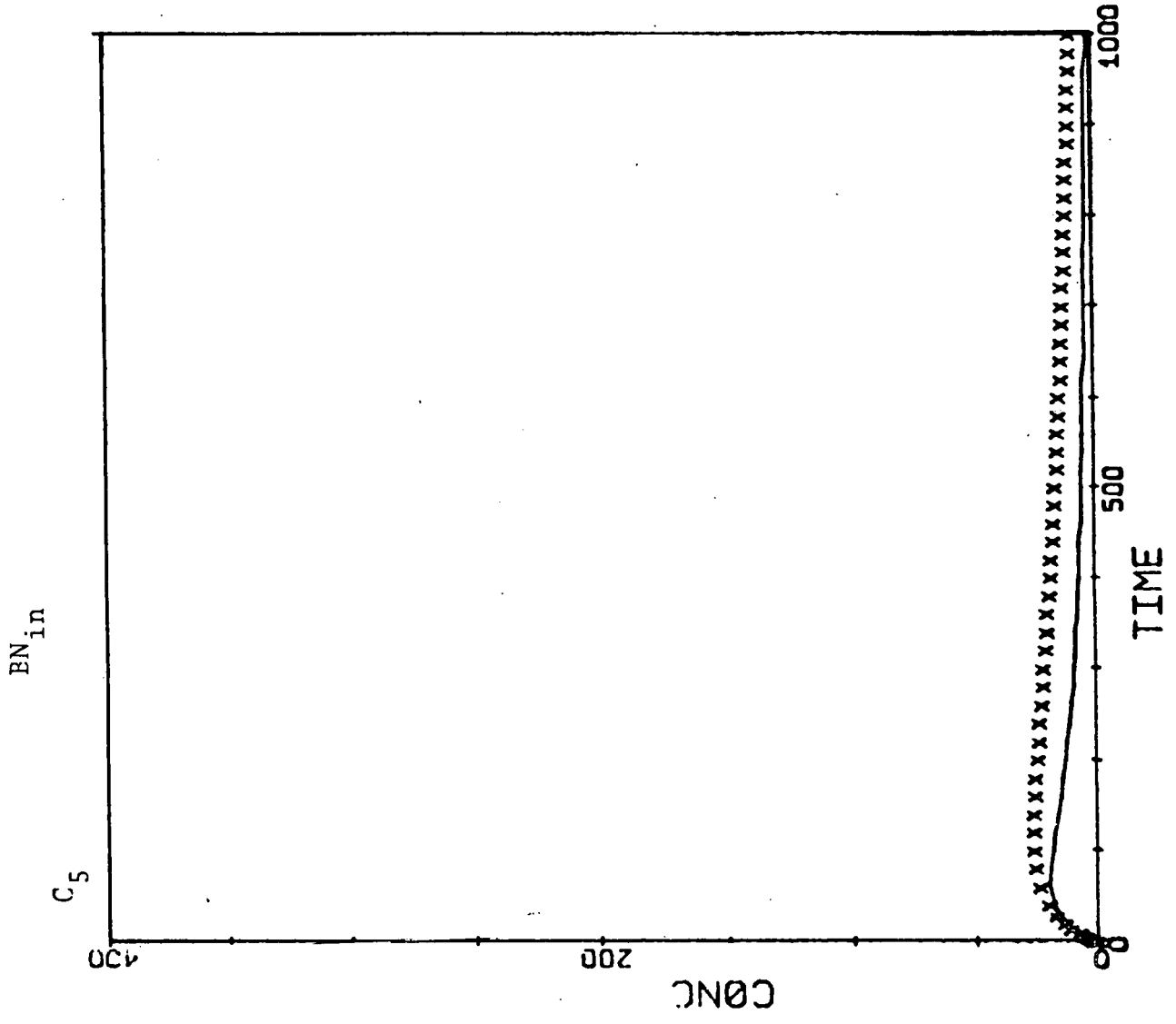
BN_{in}
C_5
CONC
400
200
0
0
500
1000
TIME

HBN_{in}

C_6

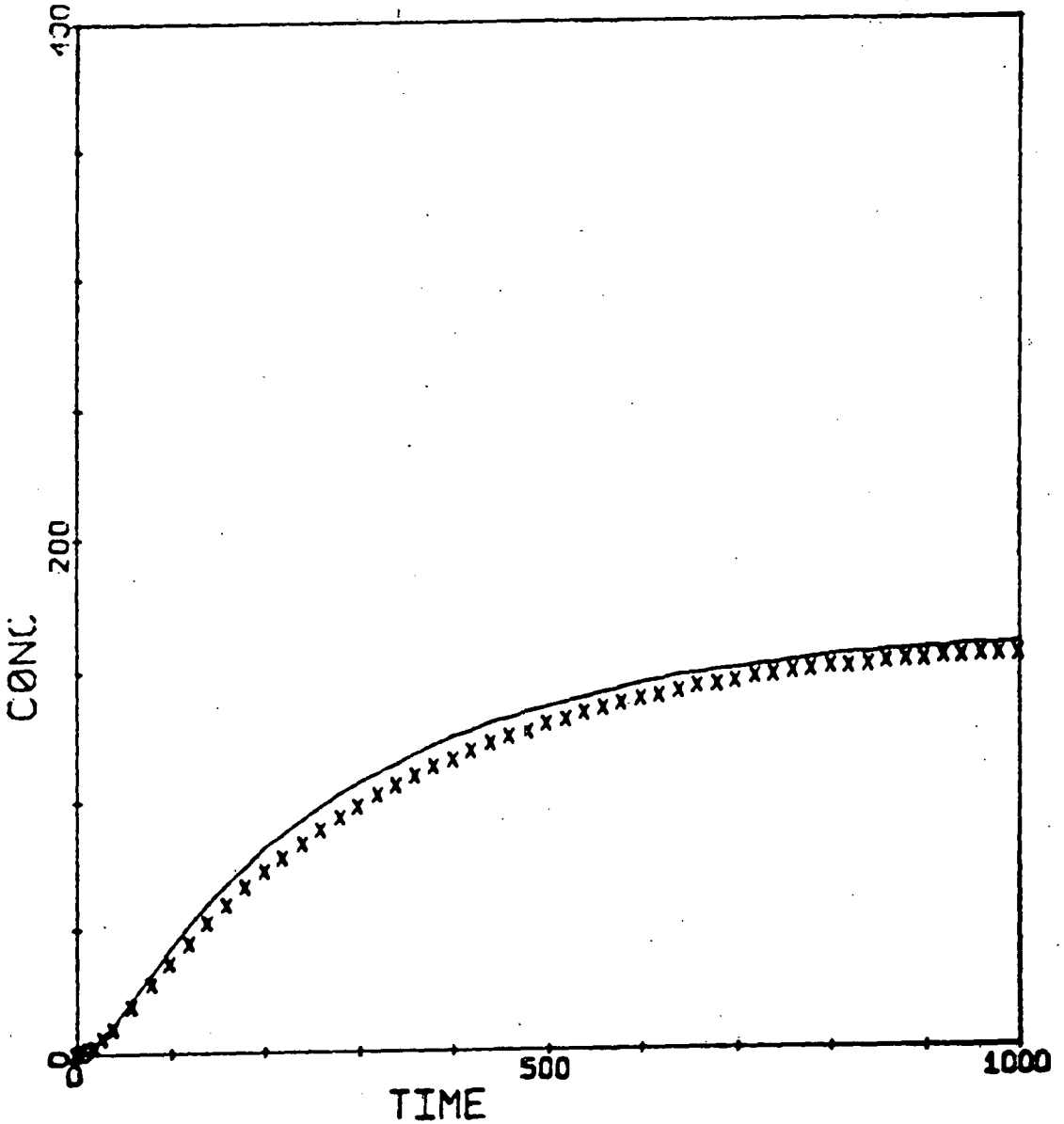

HC_{in}

C_7

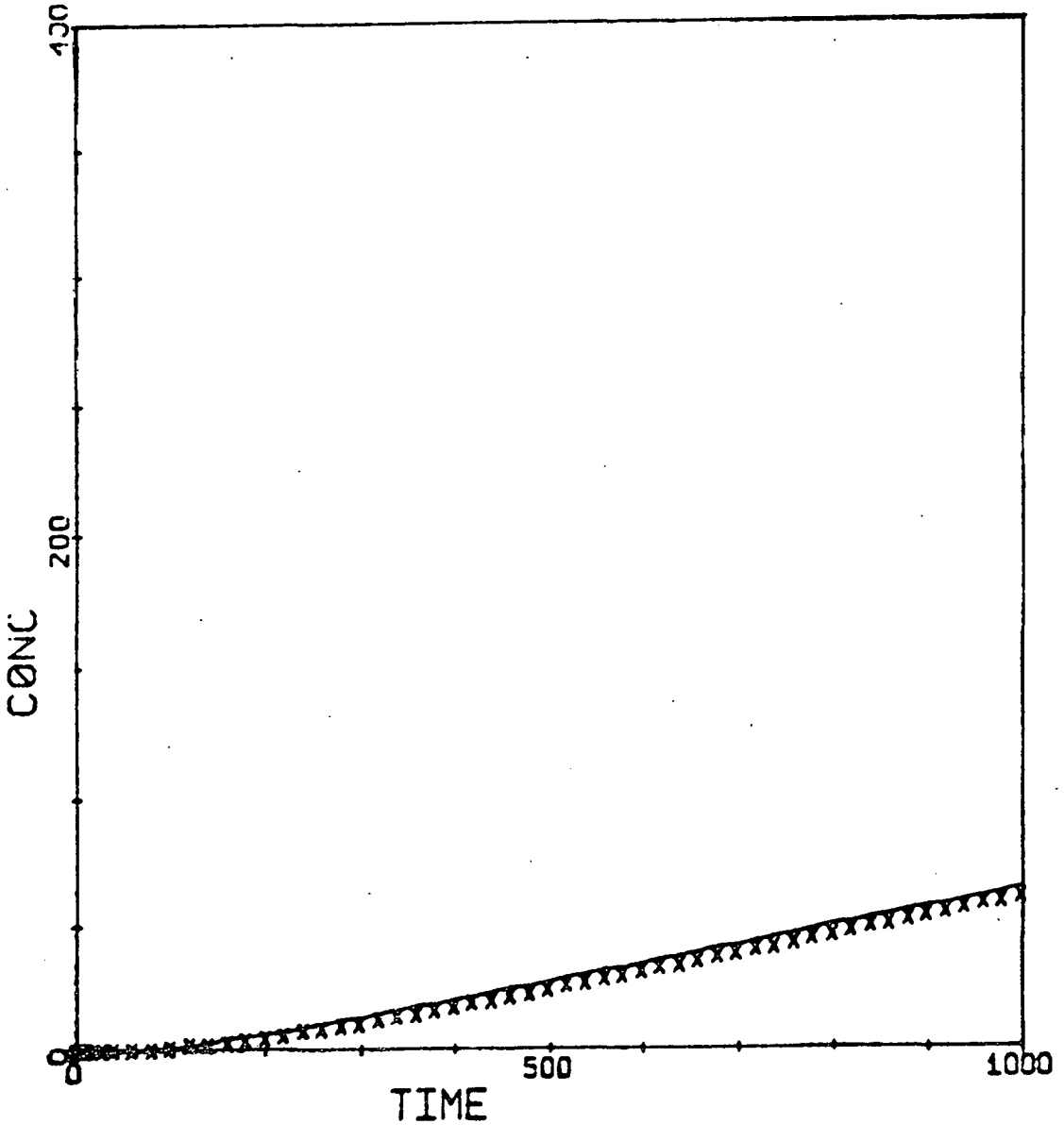

V. PUBLICATIONS

1. Stanulonis, J. J., B. C. Gates, and J. H. Olson, "Catalyst Aging in a Process for Liquefaction and Hydrodesulfurization of Coal," A.I.Ch.E. Journal 19, 417 (1976).

2. Eliezer, F., M. Bhinde, M. Houalla, D. Broderick, B. C. Gates, J. R. Katzer, and J. H. Olson, "A Flow Microreactor for Study of High-Pressure Catalytic Hydroprocessing Reactions," Ind. Eng. Chem. Fundam. 16, 380 (1977).

3. Houalla, M., D. Broderick, V. H. J. de Beer, B. C. Gates, and H. Kwart, Preprints, ACS Div. Petrol. Chem., 22 (3), 941 (1977).

4. Shih, S. S., J. R. Katzer, H. Kwart, and A. B. Stiles, Preprints, ACS Div. Petrol Chem. 22 (3), 919 (1977).

5. Broderick, D. H., G. C. A. Schuit, and B. C. Gates, "The Sulfided Co-Mo/γ-Al_2O_3 Catalyst: Evidence of Structural Changes During Hydrodesulfurization of Dibenzothiophene, J. Catal. 54, 94 (1978).

6. Houalla, M., N. K. Nag, A. V. Sapre, D. H. Broderick, and B. C. Gates, "Hydrodesulfurization of Dibenzothiophene Catalyzed by Sulfided CoO-MoO/γ-Al_2O_3: The Reaction Network," A.I.Ch.E. Journal, in press.

7. Shih, S. S., J. R. Katzer, H. Kwart, and A. B. Stiles, "Quinoline Hydrodenitrogenation: Reaction Network and Kinetics," submitted to J. Catal.

8. Zawadaski, R., S. S. Shih, J. R. Katzer, and H. Kwart, "Kinetics and Reaction Network for Acridine Hydrodenitrogenation," submitted to J. Catal.

9. Shih, S. S., E. Reiff, R. Zawadaski, J. R. Katzer, and A. B. Stiles, "Effect of Catalyst Composition on Quinoline and Acridine Hydrodenitrogenation," submitted to Ind. Eng. Chem. Prod. Res. Devel.

10. Nag, N. K., A. V. Sapre, D. H. Broderick, and B. C. Gates, "Hydrodesulfurization of Polycyclic Aromatics Catalyzed by Sulfided CoO-MoO_3/γ-Al_2O_3: The Relative Reactivities," J. Catal. accepted for publication.

11. Kwart, H., G. C. A. Schuit, and B. C. Gates, "Hydrodesulfurization of Thiophenic Compounds: The Reaction Mechanism," J. Catal., submitted for publication.

☆ U.S. GOVERNMENT PRINTING OFFICE: 1979—640-092/ 1305